Mechanical degradation and remodelling of cerebral arteries

Kindo, Temesgen Markos

Award date:
2006

TECHNISCHE UNIVERSITEIT EINDHOVEN

Department of Mathematics and Computing Science

MASTER'S THESIS

Mechanical Degradation and Remodelling of Cerebral Arteries

by

Temesgen Markos Kindo

Supervisors : dr. ir. A.A.F. van de Ven (TU/e)

dr. ir. P.M.J. Rongen (PMS)

Eindhoven, October 2006

Abstract

In the sense of blood vessels, aneurysms are focal dilatations that result from a local *weakening* of the arterial vessel walls. They can result from congenital malformations, infections, or hypertension. Rupture is the ultimate danger of this disease. Rupture can be fatal or disabling. The size and geometry of the aneurysm have been hypothesized to be indicators of the danger of rupture.

The size of an aneurysm was taken to be an indicator of rupture potential and the necessity of medical intervention; the larger the aneurysm the higher the risk of rupture. However, it was later observed that some large aneurysms stayed intact whereas smaller ones ruptured. It is currently believed that aneurysm growth/rupture is governed by mechanical quantities such as stretch and stress in the arterial tissue.

Elastin and collagen are two constituents of the artery which are responsible for much of its mechanical properties. Aneurysms are considered to result from weakening/degradation of elastin. It has been hypothesized, based on data from real aneurysms, that collagen *remodels* so as to avoid weakening of the tissue while maintaining a certain equilibrium value of stretch. In the current model remodelling by elongation and thickening is considered.

Using pressurized axisymmetric membrane models, material characterization was carried out to obtain which material models and material parameters best fit to experimental observations. Isotropic and anisotropic mixture models were considered. The large deformations observed necessitate the use of finite-deformation theories and the constitutive equations are, in general, highly non-linear.

Mathematical hypothesis for elastin degradation and collagen remodelling were incorporated into the model to obtain the complete set of equations. The stresses and stretches resulting from different material and remodelling equations and parameters were investigated and the combination resulting in a growth pattern which best conforms to clinical observation was selected. An isotropic material model with convex degradation functions for elastin with a constrained remodelling (limited thickening potential) was found to result in growth patterns in agreement with clinical observations. This model also potentially explains why some aneurysms grow excessively and rupture without any prior symptoms.

Finally, the crash in the numerical simulations in an ongoing project, which this work is part of, were found to be because of instabilities and not mesh distortions from large deformations as it was previously believed.

Acknowledgements

Thinking of the family God has given me, especially of mom, fills my heart with joy. I have no idea what my world would have been with out them. The unwavering support they provided throughout my studies deserves gratitude. I can't wait to go home and be with them once again.

Dr. Ir. A.A.F. van de Ven represents what it means to be a teacher and a mentor in the classic sense. It has been almost two years working with him on course work and research and it was a pleasure all along. I hope I can emulate him (except for the beer) and care for my future students the way he did for me. He provided invaluable advice, comments, and critically edited my reports. Thumbs up for Fons.

I would like to acknowledge Dr. Ir. Peter Rongen of Philips Medical Systems (PMS) for the useful discussions we had and the sometimes very insightful comments he provided while working as an intern, for this project, under him in PMS. Moreover, the jokes he used to email every morning used to pull smiles out of my sleepy morning faces. PMS supported this work. The company and the employees of the X-Ray Predevelopment group deserve a thank you. Niels Nielhof took care of the administrative and legal issues, which can be frustrating when an *allochotoon* is involved. Niels deserves appreciation.

Ihor Machyshyn was always ready to help. I would like to thank him for all the support and the help he provided, especially with the computational aspects of this work, and responding to my ever increasing questions and doubts. I owe him a lot and wish him success with his PhD work. I would also like to thank Dr. Ir. Peter Bovendeerd, Dr. Jos Maubach, Prof.dr.ir. F.N. van de Vosse all of TU/e, and Guus Segal of the Delft University of Technology who were kind enough to reply to my questions at one or more occasions.

I would not have been here with out the financial support of The Royal Dutch/Shell Centenary Scholarship Fund. They are doing a commendable job of helping many students from developing countries realize their dreams of getting a good education. I can only pay them back by helping others have better futures.

Being a student in a far away country I used to panick when things went wrong. Mareleen van Heusden of the International Office was subjected to a couple of SOS calls from me, all of which she took care of kindly and with reassuring smiles. Thanks a lot Mareleen.

The African students in Eindhoven, especially those from Kenya, Tanzania and Uganda, made me feel at home when I was the only Ethiopian in the university. They instilled pan Africanism in me. I hope I can make my plan of visiting those three countries a reality soon. Godwin Kakuba showed me African hospitality in my first days in Eindhoven and has been a shoulder to cry on whenever I was frustrated with this or that 'space'. *Ahsante.* Yeneneh Yalew Yimer, who started his PhD in TU/e when I was getting bored and extremely home sick, has been a real compatriot. *Galatomi Obo Yaaneene.*

My classmates have been superb. I had good laughs with them and I always knew they were there if I needed them. Marianne and Nanda deserve a special mention; I will miss you big time girls!

Most of all, I thank God who has always been good to me although I have been and still am a prodigal son.

Dedicated to **Dr. Berhanu Nega** who is unjustly imprisoned for preaching freedom and individual rights and who still teaches, from his prison cell, love and respect to everyone including his tormentors.

Contents

Chapter 1

Introduction

1.1 Problem Background and Motivation

Philips Medical Systems (PMS) is a global leader in diagnostic imaging systems, health care information technology solutions, and patient monitoring and cardiac devices. PMS is organized into Imaging Systems, Ultrasound and Monitoring, Health Care Informatics, New Ventures, and Global Sales and Services. Imaging Systems is further divided into X-Ray, Computed Tomography, Magnetic Resonance and Nuclear Medicine. At the X-Ray Predevelopment section within the X-Ray department, new devices and software for capturing and processing X-ray data are investigated. This work was carried out in collaboration with the X-Ray Predevelopment section.

An aneurysm is a localized dilation or ballooning of blood vessels. Aneurysms most commonly occur in arteries at the base of the brain (the circle of Willis) and in the aorta. Rupture and blood clotting are risks associated with aneurysms. Rupture leads to hemorrhage which can result in death or severe trauma. Details of the different types of aneurysms, their causes and hypothesized growth mechanisms are given is Sec. 2.3.

There are different methods of treating a ruptured aneurysm, if the bleeding had not already been fatal. For an unruptured aneurysm, however, there is no reliable method of intervention once it is discovered. For this reason doctors offer a variety of opinions on how to treat an intact aneurysm once it is discovered.

The size of the aneurysm was considered to be a critical indicator of the rupture potential and need of medical intervention. However, size is now not considered to be an accurate parameter as there have been incidents of small aneurysms rupturing and large one remaining intact. It is now believed that aneurysms rupture when the hemodynamically induced wall stress exceeds the wall strength. This necessitates a mechanical analysis, thus what this project is concerned with in the broadest sense.

In the current clinical practice, diagnosis and treatment for complex diseases of the vascular system highly depend on advanced three-dimensional imaging techniques and analysis of the resulting images by radiologists. Algorithms for image analysis and computer aided diagnosis provide an important aid to the radiologists to cope with the vast amount of data [31, p. 7].

Philips Medical Systems (PMS) wants to provide tools that support physicians in aneurysms diagnostics and treatment, i.e, tools that provide information to make decisions on whether medical intervention is necessary or not, what type of operation is preferred when necessary,

when the next surveillance should be done if intervention is not immediately required, and what the rupture potential of an intact aneurysm is. This can be done by coupling image processing and mechanical analysis.

The envisaged process of going from aneurysm detection to making decisions on the necessary medical intervention is schematically shown in Fig. 1.1. It involves medical imaging, construction of a computational mesh, numerical simulation of hemodynamics and vessel wall mechanics, and finally prediction of rupture potential and necessary medical intervention.

This work is concerned with mathematical modelling of aneurysm growth, i.e. part of step 3 in Fig. 1.1. To this end, different material and growth models will be considered. What remains to be done in step 3 is predicting rupture potential. This calls for the use of appropriate failure theories. The latter is beyond the scope of this work.

1.2 Problem Approach

In modelling aneurysms and other cardiovascular pathologies we will encounter the interplay of two phenomena: mechanics and biology. The first is concerned with hemodynamics and wall mechanics, and the latter describes the 'active' nature of the tissues. Whereas traditional engineering materials passively respond to a change in their environment, biological tissues adapt to their environment by changing their configuration and material properties.

Earlier studies considered the vessel walls to be rigid and passive, and investigated the fluid dynamical aspects. Among these are the works of Hermans [16], Ortega-Azurdy et al. [28] and Putter [30], all of which were conducted at PMS. The outcome was that the wall shear stresses are orders of magnitude less than the pressure, that the pressure is of the same order of magnitude in the healthy and aneurysmal vessels, and that the wall shear stresses in the aneurysmal vessel are several orders of magnitude less than the corresponding values in the parent vessel. However, these studies could not explain why aneurysms grow or rupture.

Hermans [17] analyzed the dilation of vessels under uniform pressure. Using a Neo-Hookean model for the wall, he showed that a neck-like geometry can be obtained by using a distribution of mechanical properties such that the wall is weak at the 'center' of the aneurysm but as stiff as the parent vessel near the boundary. He also suggested using a model which takes account of the different constitutive properties of the wall constituents, the hypothesized cause (degradation of elastin) and tissue response (remodelling). Machyshyn [23] implemented the degradation and remodelling following a remodelling law hypothesized for aortic abdominal aneurysms by Watton et al. [44]. The different constitutive properties of the mechanically relevant constituents of arterial walls were also incorporated into Machyshyn's model. A phenomenological constitutive relation for arterial walls suggested by Holzapfel [19] and later used by Van Oijen [26] was adopted by Machyshyn [23]. The deformations obtained were not as large as clinically observed and the numerical simulations carried out on the finite element package Sepran® crashed at some point.

One objective of the current project is to investigate the influence of constitutive relations, in particular isotropy versus anisotropy, and remodelling laws on growth (deformation) rates and patterns. The other objective is to investigate the cause of the crash in numerical simulations of Machyshyn [23] and rectify them.

In this work, we focus on the vessel wall mechanics and take the blood pressure as constant. Unless specified otherwise, this pressure is the systolic pressure. The vessel wall is modelled as a composite material containing two hyperelastic materials: elastin and collagen. We use

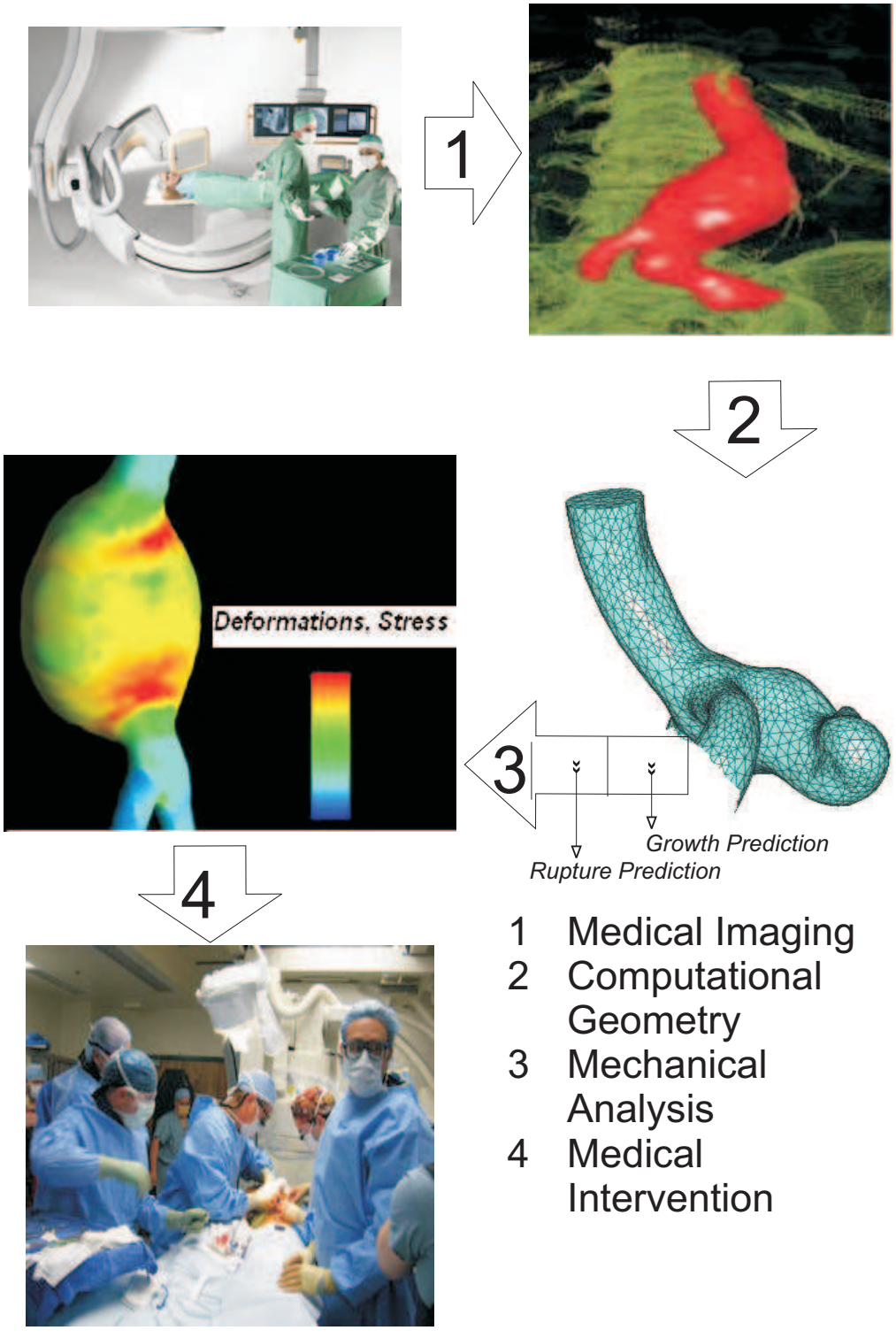

Figure 1.1: Overview of envisaged patient-specific aneurysm diagnosis and treatment

the mixture law to formulate the constitutive relation of the vessel. The aneurysm is assumed to be caused by a weakening of the elastin, called degradation. In reality, the elastin gets fragmented. As implementing the fragmentation requires the use of mass balance relations, we implemented it as a weakening (reduction of the appropriate strength modulus) of the tissue at a constant mass. We use degradation functions suggested by Watton et al. [44] and Machyshyn [23] to describe the weakening pattern in space and time. The collagen is hypothesized to respond in two ways: elongation and thickening. The elongation refers to changes in the reference configuration of the collagen so as to maintain some desired deformation state, and the thickening refers to calling upon passive collagen, which originally was not involved in load bearing. The evolution equations used for the remodelling are based on the work of Watton et al. [44].

The material parameters in the constitutive relations are obtained by fitting the pressure stretch relations in a membrane model to the experimental data of Scott et al. [34]. Axially symmetric, homogenous deformations of membrane models are analyzed using custom made Matlab® codes and more complicated cases are analyzed using the finite element package Sepran® .

Experimental data from the literature have been used to validate the models.

1.3 Results and Conclusions

Using axisymmetric membrane models we found out that isotropic material models are at least as good as anisotropic ones, that growth can be stable or unstable depending on the degradation and remodelling parameters, and that to conform to clinically observed concave patterns of stable cerebral aneurysms the elastin degradation should be convex in time. In addition, we infer from the numerical simulations that to predict the asymptomatic growth and rupture sometimes observed in practice, the capacity of the tissue to mitigate the effect of degradation via thickening should be constrained.

In the case of the numerical failures observed in Sepran [23], we found out that the problem was not mesh distortion from large deformations which can be taken care of by remeshing, but an instability which at this point we believe to be material instability.

1.4 Outline of the Report

The second chapter deals with a general overview of cardiovascular mechanics and aneurysms, and relevant experimental results. It qualitatively provides the motivation and justification for the mathematical models which we present in Chapter 3. In Chapter 3 we describe the mechanical equations (kinematic, equilibrium and constitutive relations), remodelling laws, initial and boundary conditions culminating in the initial boundary value problem (IVBP). We also quantify material parameters for the various constitutive laws using experimental results from Scott et al [34]. Starting with the general problem formulated in the third chapter, we consider numerical simulations of specific cases in Chapters 4 and 5. Chapter 4 treats the numerical simulations of axisymmetric deformations of cylindrical membranes and spherically symmetric deformations of spherical membranes. We use custom made Matlab® codes for the numerical implementation. In Chapter 5 we briefly discuss the causes and remedies of the crash in the numerical simulations in Sepran [23]. Conclusions and recommendations for future research are given in Chapter 6. A list of symbols used, their units and descriptions is

given in Appendix A. We have used a couple of biomedical terms with out defining them. In Appendix B, we have provided a glossary of biomedical and related terms used in this report.

Chapter 2

Mechanical Properties Arteries

In this chapter, we provide an overview of the anatomy, physiology and mechanical properties of healthy and aneurysmal blood vessels. We also present relevant experimental results. The discussion in this chapter will provide some insight for the mathematical modelling in Chapter 3.

Biological tissues are roughly divided into *hard tissues* like bone and tooth, and *soft tissues* such as skin, muscle, blood vessel, and lung. Soft tissues are very deformable especially in some pathological states such us aneurysms and hypertension. This necessitates the use of finite-deformation theories in the mechanical analysis of soft tissues.

2.1 Anatomy and Physiology

Biological soft tissues are composed mainly of cells and intercellular substances, the latter consisting of connective tissues such as collagen and elastin, and ground substance (hydrophilic gel). Collagen and elastin are considered to be the main load bearers. Collagen is crimped in the unstrained and low-strain states.

The microstructure of the arterial wall varies with location along the vascular tree, age, local adaptations, disease etc. Nonetheless, arteries can be categorized according to two general types: *elastic* and *muscular*. Elastic arteries, which include the aorta, main pulmonary artery, common carotids and common iliacs are located closer to the heart and tend to be larger in diameter. Muscular arteries, which include the coronaries, cerebrals, femorals, and renals are located closer to the arterioles and have smaller diameters. Transitional arteries exhibit some characteristics of the elastic and muscular types [21, 22].

Regardless of type, all arteries consist of three layers: the inner layer *intima*, the middle layer *media* and the outer layer *adventitia*.

The intima consists of a single layer of endothelial cells lining the arterial wall and resting on a thin basal membrane. The endothelial cell monolayer prevents blood from adhering to the lumenal surface. In healthy young individuals the intima is very thin and makes an insignificant contribution to the solid mechanical properties of the arterial wall. However, it thickens and stiffens with age. This may result in a disease called *arteriosclerosis*. The mechanical properties of arteriosclerotic arteries differ significantly from that of healthy arteries [19].

The media makes up the greatest volume of the artery and consists of a complex three-dimensional network of smooth muscle cells, elastin and collagen fibrils. Elastic laminae

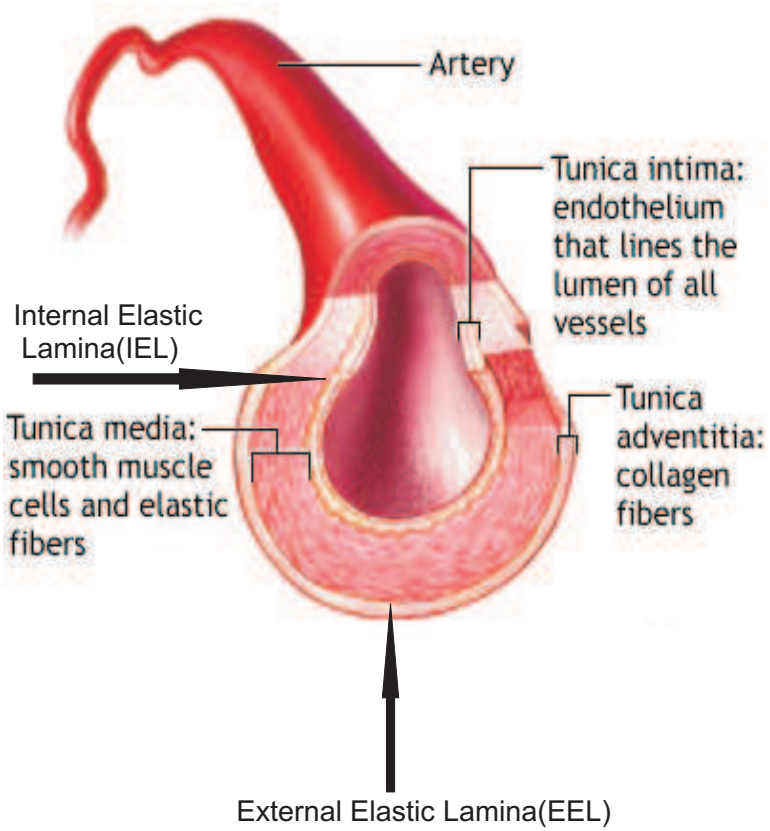

Figure 2.1: Cross-section of a healthy artery (from *Illustrated Health Encyclopedia* [48])

separate the media into a varying number of well-defined fiber-reinforced layers. The number of elastic laminae decreases away from the heart so that elastic laminae are hardly present in the muscular arteries. From a mechanical perspective, the media is the most significant layer in a healthy artery. Due to the high content of smooth muscle cells, it is the media that is believed to be mainly responsible for the viscoelastic behavior of an arterial segment [18].

The adventitia consists mainly of fibroblasts and fibrocytes (cells that produce collagen and elastin), histological ground substance and thick bundles of collagen fibrils forming a fibrous tissue. The wavy collagen fibrils are arranged in helical structures and serve to reinforce the wall. The thickness of the adventitia depends strongly on the type, physiological function and topographical site of the blood vessel. For example, in cerebral blood vessels there is virtually no adventitia [19].

The *internal elastic lamina (IEL)* separates the intima and the media, whereas the *external elastic lamina (EEL)* separates the media and the adventitia.

2.2 Mechanical Properties

In addition to nonlinearity, stress-strain tests on biological tissues show hysteresis, which is typical of viscoelastic materials. As far as arteries are concerned, proximal arteries may be regarded as (perfectly) elastic and distal arteries may be considered to be viscoelastic [19].

In the 1970's, Y.C. Fung showed that after several cycles of loading and unloading at the same rate the stress-strain curves for the viscoelastic tissues become repeatable. In addition, the response is relatively insensitive to loading rate. To describe this behavior, Fung et al. suggested that the tissue can be treated as two separate elastic materials - one during the loading and another during unloading, i.e. the tissue is *pseudoelastic*. Such an approach is very useful in arterial mechanics, because arteries are subjected to cyclic hemodynamic loads. Separate loading and unloading constitutive relations are seldom used in practice. Rather, most researchers use either viscoelasticity theory or simply assume that the material is elastic with the constitutive relation based only on the loading curve [40]. This is the approach we use in this work.

Tensile tests on collagen-rich and elastin-rich tissues revealed that elastin has much less strength but more flexibility than collagen. Also, elastin-rich tissues showed much less hysteresis and lesser nonlinearity [13]. An interesting tension-extension test was conducted by Roach and Burton on fresh human external iliac artery [33] (see also [13]). When the artery was digested with trypsin to selectively remove elastin from the tissue, its tension-extension curve shifted towards the left and the slope of the curve in the region of high tension became very similar to that of the non-treated tissue. On the other hand, the curve shifted towards the axis of the extension ratio after the selective removal of collagen with formic acid. Moreover, the slope of the curve became similar to that of the non-treated tissue in the region of small tension. Such a behavior is expected because of the initially crimped configuration of collagen, which leaves the elastin to carry all the load at lower values of the load (or equivalently stretch) and the considerably larger stiffness of collagen in the strained state. A schematic description of an elastic soft tissue is shown in Fig. 2.2.

Elastin and collagen are contained in different proportions in the layers of the arterial walls. In cerebral arteries, collagen fibers are mainly concentrated in the adventitia [46]. The orientation of the collagen fibers also differs; it is almost circumferential in the media. The preferential orientation and "tension-only" nature of collagen contribute to the general anisotropic behavior of arterial walls.

As mentioned in Section 2.1, the arteries are layered and thus not materially homogenous. Because of constituent regularity within each of the three layers, some investigators assume that mechanical properties are homogenous within each layer and thus only vary from layer to layer. This could simplify quantification, though it results in jumps in stresses across layers. With the intima considered not making significant contribution in the mechanical behavior, constitutive relations based on homogeneity of the entire wall are rationalized in cases where either the media or the adventitia is very thin compared to the other.

Although biological soft tissues are not truly incompressible, due in part to stress-induced movement of water in and out of the wall, they appear to experience nearly isochoric motion under many loading conditions of interest involving isothermal, near-physiologic loading. The incompressibility assumption has been confirmed experimentally in the arterial wall [13].

An artery excised from a body contracts in length and opens up when radially cut. This indicates the presence of axial and circumferential residual stresses. In general, even the open sector is not stress free since the opening angles of circumferentially separated layers are different. It has been suggested in the literature that the physiological state of a healthy artery has an essentially constant circumferential stress in each layer of its wall. This can only be the case if there is an inhomogeneous residual stress distribution [27].

Summing up, in the physiological state arterial walls may be considered to be heterogeneous (through the wall and along their length), anisotropic, incompressible, nonlinearly

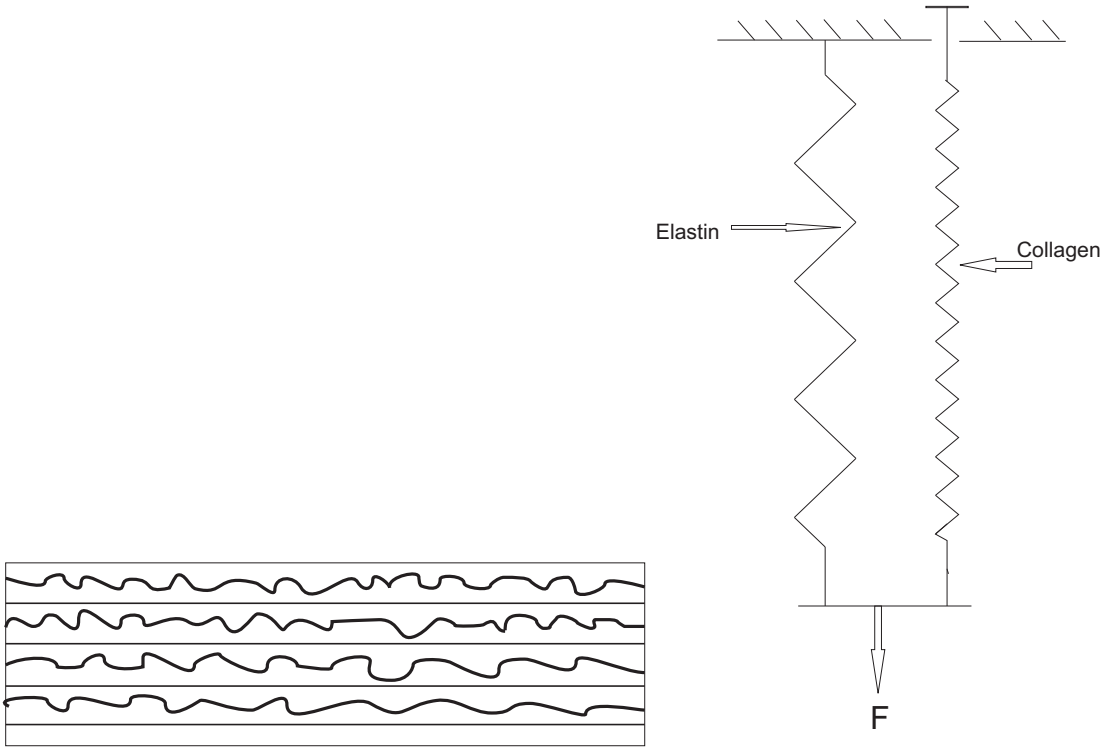

(a) Straight elastin and crimped collagen at low stretches

(b) A model of elastic soft tissue (adapted from Hayashi's [13] viscoelastic model)

Figure 2.2: Soft tissue

(visco)elastic subjected to an inhomogeneous residual stress. Details of how this is taken care of in the constitutive formulation and simplifying assumptions are provided in Chapter 3.

2.3 Aneurysms

In the sense of blood vessels, aneurysms are focal dilatations that result from a local "weakening" of the vessel walls. They can be either *true aneurysms* or *false aneurysms (pseudoaneurysms)*. A true aneurysm involves an outpouching of all three layers of a blood vessel and can be due to congenital malformations, infections, or hypertension. A pseudoaneurysm involves an outpouching of only the adventitia and it can be due to trauma involving the intima. From this point on, unless specified otherwise, by aneurysms we mean true arterial aneurysms.

Rupture and blood clotting are the risks involved with aneurysms. Rupture leads to drop in blood pressure, rapid heart rate, and lightheadedness; it has a high risk of death. Blood clots can block the passage of blood and suffocate tissue. It is generally thought that rupture occurs when hemodynamically induced wall stress exceeds wall strength [22].

Aneurysms commonly occur in the abdominal aorta, basilar artery and at the apex of a bifurcation in or near the circle of Willis. The first two have spindle-like shapes and belong to a class of aneurysms called *fusiform* and the last one has a sac-like nearly spherical shape; hence the name *saccular*. Fusiform aneurysms are symptomatic, in contrast to saccular

aneurysms which often remain asymptomatic until they rupture [22]. Rupture of fusiform cerebral aneurysms is rare [46]. Depending on their location, aneurysms are also classified as *intracranial* or *extracranial*, the latter one usually being the abdominal aortic aneurysm (AAA).

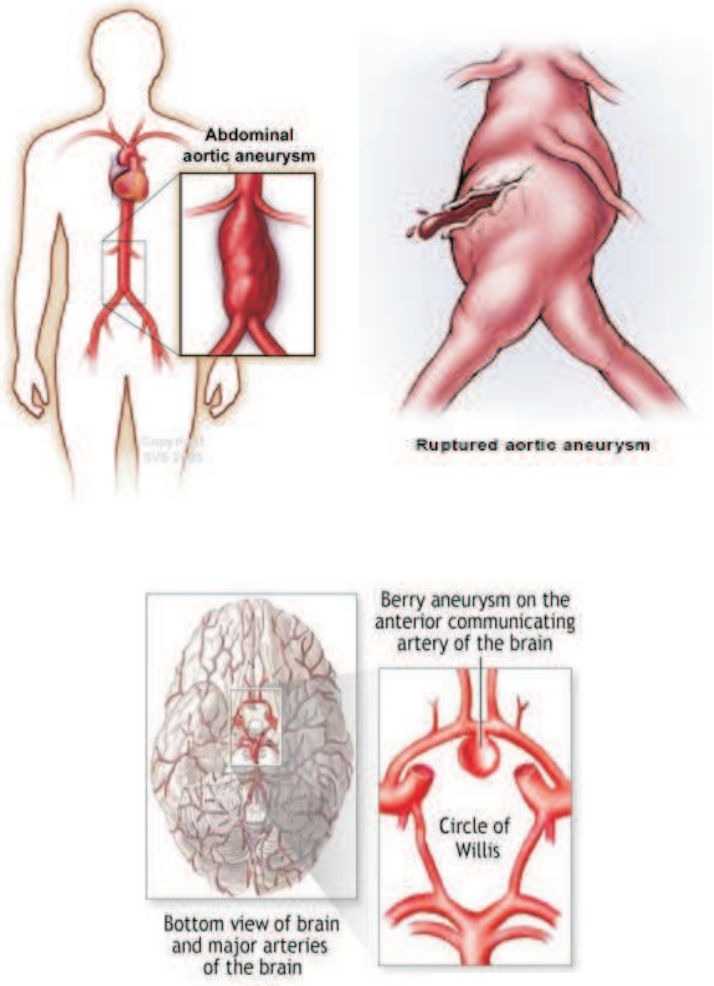

Figure 2.3: Aortic and Cerebral Aneurysms (from *Illustrated Health Encyclopedia* [48])

2.3.1 Intracranial (Cerebral) Saccular Aneurysms

There is no unanimous agreement over the initiation of saccular aneurysms [22], but it is hypothesized that the structural features of healthy cerebral arterial walls predispose cerebral arteries to the formation of saccular aneurysms [39] (see also [22, 46]). The external elastic lamina, which separates the media and adventitia, is absent in cerebral arterial walls [35](also [22]). Cerebral arteries have thinner media and adventitia than extracranial arteries with similar diameter [4, 36]. They have sparse medial elastin [22, 38], lack supporting perivascular

tissue, and appear to have irregularities at the apex of their bifurcation [10, 22]. The internal elastic lamina and muscular media must become markedly fragmented or disappear for a saccular aneurysm to form [22]. It has been reported that the media slightly extends into the neck region and is completely absent away from the neck of an aneurysmal wall [46]. A general finding is that the aneurysmal wall consists primarily of collagen, with small patches of smooth muscle [20].

Little is known about the mechanism driving the growth of saccular aneurysms. A hypothesis suggesting structural instabilities are responsible for enlargement was shown to be unlikely, at least for some classes of lesions [22]. The majority of aneurysms are less than 10 mm in diameter. Giant aneurysms may enlarge to over 30 mm in diameter [22, 46].

Rupture can occur either at the fundus, side or neck of aneurysms. The greatest occurrence (64 to 84%) is at the fundus [4]. Why rupture occurs at the fundus (and not the neck, which has a thinner wall) appears to be paradoxical. Although based on incomplete data, Humphrey and Canham's biomechanical analysis suggests that the stresses will be the greatest at the fundus if the material behavior is either isotropic or meridionally stiffer [20].

Small uncomplicated aneurysms have a tendency to assume a spherical shape as they enlarge [38]. For large neck to height ratios, this requires less stiffness in the meridional direction; for small neck to height ratios, the tissue should be meridionally stiffer. If the initial geometry was a sphere, isotropy would be required. This suggests that aneurysmal tissues can respond either isotropically or anisotropically as the situation demands.

Angiographic and clinical evidence seems to suggest that, whereas some aneurysms may increase in size over several years, others may enlarge considerably in hours to weeks, may decrease in size, or may spontaneously obliterate [45]. Based on the data obtained from the International Study of Unruptured Intracranial Aneurysms (ISUIA)† [25], Chang [8] carried out a statistical simulation and concluded that the diameter of unruptured saccular intracranial aneurysms is proportional to the cubic root of the aneurysm age. According to Chang any growth function with a negative second derivative, such as the logarithmic function, would have served the purpose. The objection against a function with a positive second derivative was that such a function would predict unrealistically higher rupture rates than observed in clinical practice [8].

The type, volume fraction, cross-link density and orientation of collagen contribute significantly to the overall mechanical properties of a lesion. Canham et al [5, 6, 7] reported that aneurysmal collagen has little waviness when perfusion-fixed at physiologic pressures, that it follows great circle trajectories, and that it is organized into seven to eight distinctive layers, each of which consists of nearly parallel fibers. In general, layer-to-layer orientation changes abruptly, not continuously, often to an opposite direction. In the region of the fundus of a small spherical lesion, for example, they reported that taken together, collagen from all layers spanned the full range of azimuthal angles; this implies in-plane isotropic response near the fundus; see also [22, p. 392, 393]. A morphology study by Finlay et al. [10] shows that the collagen fibers at the apex of bifurcations of cerebral arteries, the most common region for saccular aneurysms, are arranged in a complex net that possesses no specific fiber orientation; see also [46, p. 32]. The above results, taken together, suggest that the healthy state and ultimate pathological state in cerebral aneurysms can be approximated by an isotropic model. This does not necessarily mean that the lesions remain isotropic through out their history as

†The ISUIA is an ongoing international consortium on the clinical study of cerebral aneurysms which published a landmark data in 1998.

fiber reorganizations in time can not be ruled out.

Uniaxial extension tests carried out by Steiger et al. [37] on thin strips of tissue excised from human saccular lesions showed that lesion behavior differed at the fundus and neck; tearing occurring at $\lambda = 1.37, \sigma_c = 0.5$MPa in the fundus and $\lambda = 1.57, \sigma_c = 1.21$MPa in the neck. Toth et al [41] reported similar uniaxial data with specimen from the fundus tearing at stretches of 1.23, whereas those from the neck requiring tearing stretches of 1.55. That strain, not stress, was a more consistent measure of failure is consistent with results on the failure of normal vessels. Nevertheless, the above results have limited use as the data were inappropriately reduced using linearized measures of strain given the large strains reported [22, p. 394-395].

Although not sufficient for detailed quantification of multiaxial behavior, the best available data on human lesions are from Scott et al [34]. Scott et al. [34] performed *in vitro* inflation tests on four intact anterior cerebral arteries (ACA) segments. Three samples were loaded upto 200 mm Hg and one control sample was loaded up to 100 mm Hg. It was reported that after three cycles of loading that produced consistent distensibility curves similar to those of the control sample, the distensibility curves of the three test samples exhibited a measurable shifting. The post shifting curves displayed a larger unloaded radius implying that some form of permanent deformation had occurred. The typical toe region[†] is not pronounced in the shifted curves. Scott et al. [34] hypothesized that the shift of the curves was due to elastin breakage, however, they never performed a morphology study to investigate the fragments of elastin. They also found that the new distensibility curves were more similar in shape to those from distensibility tests of aneurysm segments. Based on those similarities, they hypothesized that mechanical breakage of elastin may play a significant role in aneurysm formation; see also [46, p. p. 68-91]. The procedure of these experiments and relevant results are provided in detail in Section 3.8.

2.3.2 Abdominal Aortic Aneurysms

Atherosclerosis has been strongly hypothesized to be responsible for the initiation of AAA [46]. In fact, 90% of AAA's are atherosclerotic [22, p. 446]. It is not clear why atherosclerosis sometimes results in occlusive lesions that are characterized by a proliferative response, whereas at other times it results in aneurysms that are characterized by wall deterioration and dilatation. The aneurysmal wall is devoid of normally organized elastin and smooth muscle [14]. This suggests that elastin degradation may be responsible for AAA formation. Elastin degrades to 10-20% of its original value [44].

There is not much evidence as to why and how AAA's grow and rupture. Freestone et al [11] suggest that as the media becomes thinner and the aorta dilates, the adventitia may experience a thickening due to the deposition of new collagen that occurs as a sort of compensatory mechanism to reinforce the wall. Although it is thicker, the wall may nonetheless be weaker if the collagen is not fully cross-linked [11].

Vardulaki [42] (see also [44]) reported an exponential growth in time of AAA's with an average growth rate of 4 mm/year. A more recent study [29], which surveyed 1743 patients in the US and UK, reported that the average growth rate is 2.6 mm/year, that exponential growth does not fit well with the observed data and that quadratic interpolation yielded better correlation. In both cases, however, it was established that AAA growth rates increase

[†]The 'toe' refers to the initial relatively flat part of the pressure-stretch curve as opposed to the steep curve at higher stretches.

with the diameter. Powell et al [29] observed that AAA expansion was not associated with age or sex, but was strongly associated with diameter at baseline, reflecting the tendency of AAA expansion to accelerate with time.

It appears that the initiation, growth mechanisms and rates, and mechanical properties of intracranial aneurysms and abdominal aortic aneurysms differ.

2.4 Vascular Adaptation

Biological tissues are not passive materials like engineering materials are. They respond to a sustained change in their environment by changing their state, properties or internal structure. This phenomena is called adaptation or remodelling. In the case of aneurysms, the highly nonlinear tensile nature of the collagen implies that collagen remodelling is necessary to account for the large dilations observed. Without remodelling, even if all the elastin is degraded, the strains in the collagen, and thus the dilation of the wall, would not have to increase significantly for the total load to be borne [44].

The details of some hypotheses for remodelling and the one considered in this project are outlined in Section 3.3. There is an acute shortage of clinical information that can be used to check the hypotheses, however.

One subtle consequence of remodelling, important in constitutive formulation and stress analyses of soft tissues is the unlikelihood of having a single "natural" configuration as that found in engineering materials. The best we can have is a sequence of natural configurations each of which may be useful in different analyses [22].

Chapter 3

Mathematical Modeling

In the first sections of this chapter, the equations governing arterial wall mechanics will be described. The tissue, the wall is made of, consists of an elastin matrix and collagen fibers. Two models for collagen, an isotropic and an anisotropic, are considered. Equations hypothesized for elastin degradation and collagen remodelling will be treated next. The initial-boundary value problem governing the whole process will be formulated.

The later sections of this chapter will be devoted to material characterization. Using experimental results and membrane models, we carry out a regression analysis to quantify the material parameters for the different constitutive laws. We also discuss how far each constitutive law fits with the experimental results.

3.1 Mechanical Equations

3.1.1 Kinematics and Deformations

Let the tissue be represented by a continuous material body $\mathcal{B}$ occupying a three-dimensional region of the Euclidean space $\mathbb{R}^3$, the configuration of $\mathcal{B}$. We denote the undeformed reference configuration by $\mathcal{G}_R$, and the position of a material point $\mathcal{P}$ in this reference configuration by $\mathbf{X}$. During its motion, the body continuously occupies a time-dependent deformed configuration $\mathcal{G} = \mathcal{G}(t)$. The position of points in the deformed configuration is given by $\mathbf{x} = \mathbf{x}(\mathbf{X}, t)$. The deformation can be expressed by the deformation gradient

$$\mathcal{F} = \frac{\partial \mathbf{x}}{\partial \mathbf{X}}. \tag{3.1}$$

Let $\mathbf{e}_0$ be an arbitrary unit vector in the tissue in the undeformed configuration. Then the tissue stretch $\lambda = \lambda(\mathbf{x}, t)$ in the direction of $\mathbf{e}_0(\mathbf{X})$ is given by

$$\lambda^2 = \mathcal{F}\mathbf{e}_0 \cdot \mathcal{F}\mathbf{e}_0 = \mathbf{e}_0 \cdot \mathcal{C}\mathbf{e}_0. \tag{3.2}$$

where $\mathcal{C} = \mathcal{F}^T\mathcal{F}$ is the right Cauchy-Green deformation tensor.

A unit vector $\mathbf{e}_0$ in the undeformed configuration will be transformed into the unit vector $\mathbf{e}_c$ in the deformed configuration as

$$\mathbf{e}_c = \frac{\mathcal{F}\mathbf{e}_0}{\lambda}, \tag{3.3}$$

where λ is given by (3.2).

The deformation tensor $\mathcal{F}$ and tissue stretch λ given above apply to the elastin and to the tissue as a whole. We assume that the elastin and collagen deform together, i.e. there is no relative motion between components at a given material point. The collagen is crimped in the reference configuration. It is also hypothesized that the collagen remodels to assume different reference configurations through time so as to preserve a certain preferred deformation state [23, 44, 46]. We refer to this remodelling as ***recruitment***. If the collagen is modelled as a fiber with preferential fiber orientation [23, 44], the collagen stretch can be expressed in terms of the tissue stretch in the direction of the fiber, λ, and a ***recruitment stretch*** λ_{rec}. Similarly, if the collagen is taken as an isotropic medium [46] the deformation tensor in the collagen can be expressed in terms of the tissue deformation tensor $\mathcal{F}$ and a ***recruitment deformation gradient*** $\mathcal{F}_{rec}$ as explained below.

Anisotropic Model

The artery is modelled as consisting of an isotropic elastin matrix and two families of helical collagen fibers making a certain angle with the circumferential direction. In a given layer of the artery, this angle is assumed to be constant for a given fiber family. In this work we consider a single layered artery.

At low strains, the collagen fibers are crimped and thus do not bear any load. As the tissue becomes stretched, a state will be reached at which the collagen fibers will become straight. The tissue stretch, i.e. elastin stretch, at which the collagen fibers are straightened is called the ***initial recruitment stretch***, $\lambda_{rec,0}$. Thus, the stretch in the collagen is defined with respect to the configuration in which it is first recruited, whereas the stretch in the elastin is always defined with respect to the initial reference configuration. This leads us to the following relationship between stretches,

$$\lambda_c(\mathbf{x},t) = \begin{cases} 1, & \lambda(\mathbf{x},t) \leq \lambda_{rec,0}(\mathbf{x},t), \\ \frac{\lambda(\mathbf{x},t)}{\lambda_{rec,0}(\mathbf{x},t)}, & \lambda(\mathbf{x},t) > \lambda_{rec,0}(\mathbf{x},t), \end{cases} \tag{3.4}$$

where λ and λ_c represent the tissue and collagen stretch, respectively; see Fig. 3.1

The above relation holds as long as λ_c is less than the ***attachment stretch*** λ_a, which the collagen wants to maintain. Once the collagen stretch is above the attachment stretch, the collagen remodels towards a stretch equal to the attachment stretch by changing the recruitment stretch. In this regime, the collagen stretch is given by

$$\lambda_c(\mathbf{x},t) = \frac{\lambda(\mathbf{x},t)}{\lambda_{rec}(\mathbf{x},t)}, \tag{3.5}$$

i.e. the stretch in the collagen is defined with respect to the current recruited configuration. How the recruitment stretch evolves is explained in Section 3.3.

Isotropic Model

If collagen fibers are randomly oriented with no preferred direction, the tissue can be assumed to be isotropic. In conformity with Wulandana and Robertson [47] both elastin and collagen will be assumed to be isotropic. In this case, the collagen deformation is described by a deformation tensor $\mathcal{F}_c$, a second-order tensor in $\mathbb{R}^3$, as opposed to a scalar stretch in the case of the anisotropic model. Here too, the collagen does not contribute to the tissue strength

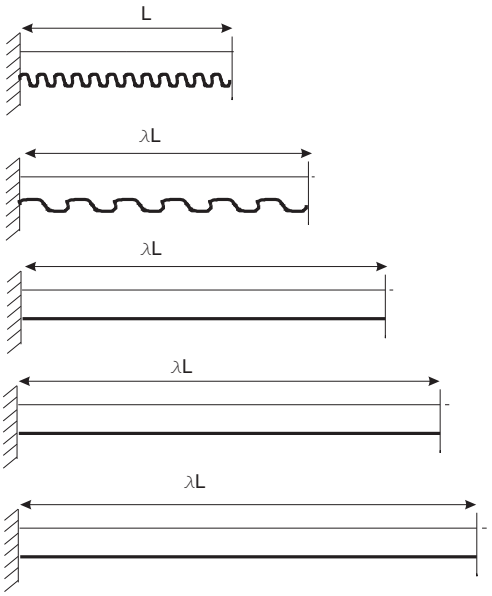

$\lambda = 1, \lambda_c = 1$
Undeformed state

$1 < \lambda < \lambda_{rec,0}, \lambda_c = 1$
Deformed but crimped collagen

$\lambda = \lambda_{rec,0}, \lambda_c = 1$
Collagen just stretched

$\lambda \leq \lambda_{rec,0}\lambda_a, \lambda_c = \frac{\lambda}{\lambda_{rec,0}} \leq \lambda_a$
Collagen stretched but no recruitment remodelling

$\lambda > \lambda_{rec,0}\lambda_a, \lambda_c = \frac{\lambda}{\lambda_{rec}}$
Recruitment remodelling

Figure 3.1: Schematic Representation of fiber stretches and recruitment (after Machyshyn [23])

until the elastin gets stretched enough to uncrimp the collagen. We will call the state at which the collagen becomes uncrimped as the ***initial recruitment state*** and denote the corresponding configuration by $\mathcal{G}_{rec,0}$. We denote the position of a material point $\mathcal{P}$ in the initial recruitment configuration by $\mathbf{X}_{rec,0}$; see Fig. 3.2. The deformation gradient for the motion of $\mathcal{P}$ from $\mathbf{X}$ to $\mathbf{X}_{rec,0}$ is $\mathcal{F}_{rec,0}$, with

$$\mathbf{dX}_{rec,0} = \mathcal{F}_{rec,0}\mathbf{dX}. \tag{3.6}$$

Stretching the tissue further, we come to a regime in which both elastin and collagen deform. The tissue is now in a deformed state $\mathcal{G}$, in which the position of $\mathcal{P}$ is denoted by $\mathbf{x}$. However, the collagen does not deform with respect to the reference state G_R, as the elastin does, but with respect to the initial recruitment state $\mathcal{G}_{rec,0}$. This means that the collagen deformation gradient is given by

$$\mathbf{dx} = \mathcal{F}_c\mathbf{dX}_{rec,0}. \tag{3.7}$$

From (3.6) and (3.7) we get a relation between the different deformation gradients

$$\mathcal{F} = \mathcal{F}_c\mathcal{F}_{rec,0} \tag{3.8}$$

To specify the recruitment criterion, we have to introduce a scalar function of $\mathcal{F}$; following Wulandana and Robertson [47], we call this function $s(\mathcal{F})$ and we say that initial recruitment occurs when s becomes equal to $s_{rec,0}$. Here, $s(\mathcal{F})$ can only be a function of the invariants of $\mathcal{F}$ and the critical value $s_{rec,0}$ is a material parameter. As will be discussed in Chapter 4, one possible form of s is the first invariant of $\mathcal{F}$.

The initial recruitment state is attained when

$$s(\mathcal{F}) = s_{rec,0}. \tag{3.9}$$

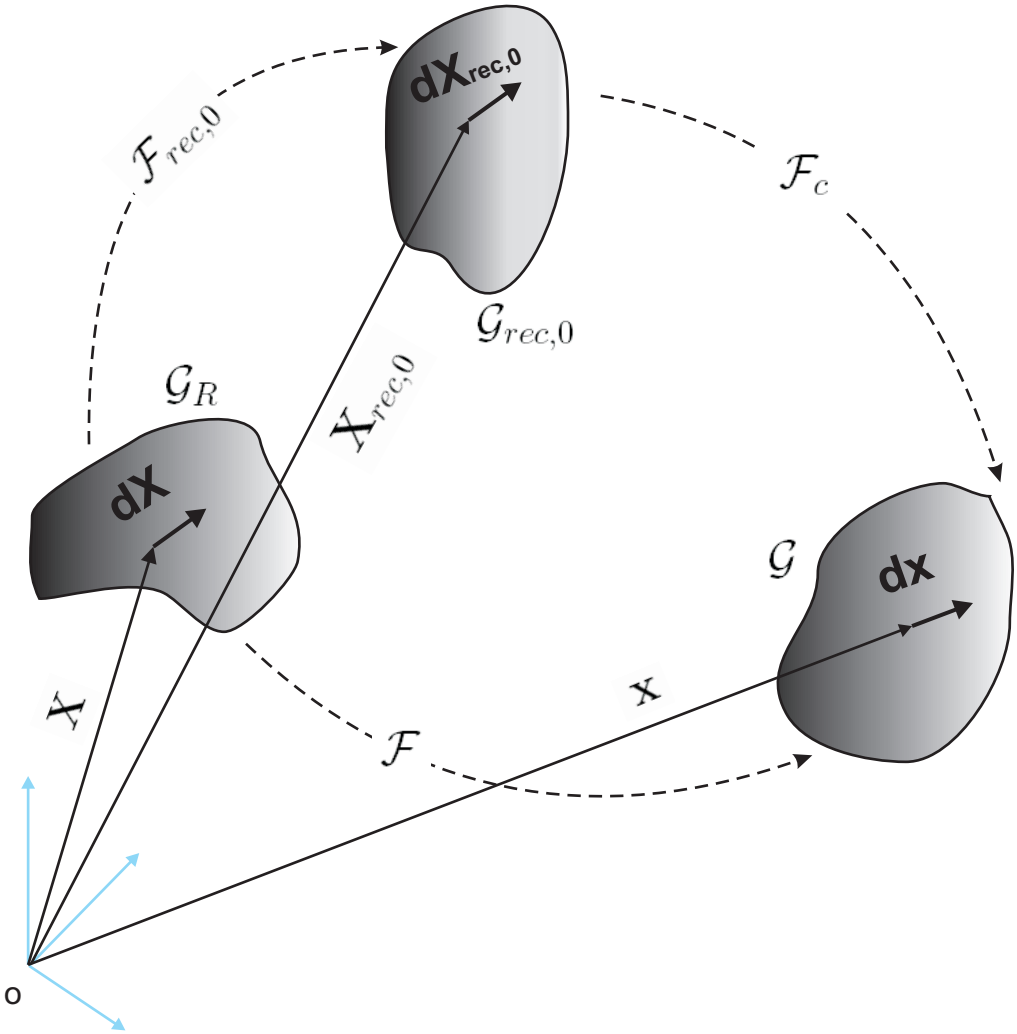

Figure 3.2: Schematic representation of different difformation gradients (after Wulandana and Robertson [47])

In a similar fashion, the attachment state is identified by an equilibrium value for the scalar function $s(\mathcal{F}_c)$ as

$$s(\mathcal{F}_c) = s_a. \tag{3.10}$$

Note that the parameter s_a for the isotropic collagen is not numerically the same as the attachment stretch λ_a for the anisotropic collagen. In Chapter 4 we will see that $s_a \approx 3\lambda_a$, with λ_a the attachment stretch for the anisotropic collagen, taken in the direction of the fibers.

Analogous to the anisotropic case, the collagen remodels to maintain the attachment state. The evolution equations for the remodelling are given in Section 3.3.

Incompressibility

As mentioned in Section 2.2, the arterial wall is considered virtually incompressible. The incompressibility condition can be enforced by

$$\det \mathcal{F} = 1. \tag{3.11}$$

In the case of an isotropic collagen, we also have

$$\det \mathcal{F}_c = 1, \tag{3.12}$$

which combined with (3.8) leads to

$$\det \mathcal{F}_{rec} = 1. \tag{3.13}$$

3.1.2 Equilibrium Equation

Disregarding body forces, the quasi-stationary equilibrium equation is given by

$$\mathrm{div}\mathcal{T} = \mathbf{0}. \tag{3.14}$$

Although the arteries are subjected to time-varying haemodynamic pressure, quasi-stationary analysis is reasonably accurate [22].

3.1.3 Constitutive Relations

The arterial wall is composed of an isotropic matrix material (elastin) and containing collagen fibers. The collagen fibers are modeled as a one-dimensional material having non-zero stress response only to extension (not to compression) in the direction of the fibers. In the sequel, we will consider two different models for the collagen:

1. An isotropic model in which the collagen fibers are assumed to be distributed within the elastin matrix in the undeformed state in a 3-dimensional isotropic way;

2. An anisotropic model in which the collagen fibers are modelled as two discrete families of helical fibers.

Using mixture theory, the stress is given by

$$\mathcal{T} = -p\mathcal{I} + n_e\mathcal{T}_e + n_c\mathcal{T}_c, \tag{3.15}$$

where $p = p(\mathbf{x}, t)$ is the hydrostatic pressure, $n_e = n_e(\mathbf{x}, t)$ and $n_c = n_c(\mathbf{x}, t)$ represent the volume fractions of elastin and "active" collagen, respectively, and $\mathcal{T}_e$ and $\mathcal{T}_c$ stand for the stress tensors for elastin and collagen, respectively. Active collagen refers to collagen that is involved in the load carrying; see Section 3.4 for details. For a healthy tissue, the volume fractions are uniform throughout. For a remodelling tissue, however, they can be non-homogenous if the deformations are non-homogenous as the remodelling is dependent on the deformation; see Section 3.3 for details.

Assuming no interaction between elastin and collagen, the strain energy function W of one constituent will be dependent on the deformation in that constituent only.

Isotropic Collagen

In the case of isotropic elastin and collagen, the stress contributions are given by

$$\mathcal{T}_e = 2\frac{\partial W_e}{\partial I_e}(\mathcal{B}_e - \mathcal{I}), \qquad \mathcal{T}_c = 2\frac{\partial W_c}{\partial I_c}(\mathcal{B}_c - \mathcal{I}), \tag{3.16}$$

where $\mathcal{B} = \mathcal{F}\mathcal{F}^T$ is the left Cauchy-Green stretch tensor, I is its first invariant (trace) and $\mathcal{I}$ is the identity tensor.

Elastin is considered to be a Neo-Hookean material and its strain energy function is given by

$$W_e = \frac{C_e}{2}(I_e - 3), \tag{3.17}$$

where C_e is the shear modulus of elastin.

Collagen, on the other hand, is assumed to have an exponential strain energy function

$$W_c = \frac{k_1}{2k_2}(e^{[k_2(I_c-3)^2]} - 1), \tag{3.18}$$

where k_1 and k_2 are material constants.

From (3.15) - (3.18) we arrive at the following constitutive relation for a composite artery composed of elastin and collagen both of which are isotropic matrix materials.

$$\mathcal{T} = -p\mathcal{I} + n_e C_e(\mathcal{B}_e - \mathcal{I}) + 2n_c k_1(I_c - 3)e^{[k_2(I_c-3)^2]}(\mathcal{B}_c - \mathcal{I}). \tag{3.19}$$

Anisotropic Collagen

If collagen is taken as a discrete set of fibers with preferred directions, we have the following form for a single-layered wall reinforced by two families of fibers:

$$\mathcal{T} = -p\mathcal{I} + n_e\mathcal{T}_e + n_{c,1}\mathcal{T}_{c,1} + n_{c,2}\mathcal{T}_{c,2}, \tag{3.20}$$

where $\mathcal{T}_{c,i}$ is the stress contribution from a given fiber family.

Following Machyshyn [23] and Van Oijen [26], we take

$$\mathcal{T}_{c,i} = \tau_{f,i}\mathbf{e}_{c,i} \otimes \mathbf{e}_{c,i}, \tag{3.21}$$

where $\mathbf{e}_{c,i} = \mathbf{e}_{c,i}(\mathbf{x}, t)$ is the unit vector in the i^{th} fiber direction and $\tau_{f,i} = \tau_{f,i}(\lambda_{c,i}(\mathbf{x}, t))$ is

$$\tau_{f,i} = 2k_1\lambda_{c,i}^2(\lambda_{c,i}^2 - 1)e^{[k_2(\lambda_{c,i}^2-1)^2]}. \tag{3.22}$$

Given a fiber direction in the reference configuration, the current fiber direction $\mathbf{e}_{c,i}$ can be obtained via (3.3).

Note that (3.21) and (3.22) assume the two collagen fiber families to have the same material behavior, i.e. the same values of k_1 and k_2 are used.

3.2 Elastin Degradation

Estimates for the concentration of elastin in a developed aneurysm suggest that between 63 and 92% of the elastin is lost [14]. The loss of elastin can be incorporated in the model as a reduction of the shear modulus of elastin or as a reduction of the volume fraction of elastin and a corresponding increase in the collagen volume fraction. We follow the first approach. Note, however, that these two approaches are not exactly equivalent. That the dilation of the aorta is localized to a specific region would suggest that elastin is being lost principally in a confined region. Such an inhomogeneous degradation can be modeled by an axisymmetric Gaussian distribution. The elastin shear modulus, which now is space and time dependent, is then given by

$$C_e(\mathbf{x},t) = C_{e,0}\left[1-(1-c(t))\exp\left[-m\left(\frac{R_d-x_d}{R_d}\right)^2\right]\right], \tag{3.23}$$

where $C_{e,0}$ is the elastin shear modulus in a healthy artery, $c(t)$ is the ratio of the elastin shear modulus at the point of degradation at time t to the physiologic shear modulus, $m>0$ is a parameter that controls the degree of localization of the degradation, R_d is the radius of the region degradation and $x_d = |\mathbf{x}-\mathbf{x}_d|$ is the distance from the center of degradation $\mathbf{x}_d$. Note that $0 \le x_d \le R_d$. From now on, we will refer to $c(t)$ as the ***degradation function***.

For a homogenous degradation, the only one considered in this work, (3.23) reduces to

$$C_e(\mathbf{x},t) = C_e(t) = C_{e,0}c(t). \tag{3.24}$$

Watton et al. [44] considered a power function for the degradation given by

$$c(t) = c_{min}^{\frac{t}{t_{deg}}}, \qquad t\in(0,t_{deg}), \tag{3.25}$$

where c_{min} is the minimum value of the degradation function (0.08 to 0.37 according to He and Roach [14]), and t_{deg} is the time it takes for the degradation function to attain c_{min}.

Following Machyshyn [23], we also use a sigmoid degradation function given by

$$c(t) = c_{min} + \frac{1-c_{min}}{1+\exp\left(\frac{s(2t-T_0-t_0)}{T_0-t_0}\right)}, \qquad t\in[t_0,t_{deg}], \tag{3.26}$$

where $s>0$ is a constant that corresponds to the steepness of the sigmoid function (commonly $e^s \gg 1$), i.e. the rate of degradation of elastin, t_0 is the time for the commencement of degradation, and $T_0 = t_0 + (t_{deg}-t_0)/3$ is a characteristic time for the interval $[T_0, t_{deg}]$ where $c(t)$ slightly varies (i.e. $\mathcal{O}(e^{-s})$) from c_{min}.

The time scale of development of aneurysm, t_{deg}, may vary from person to person. Based on the average growth rate of aneurysms and the aneurysm size at which a medical decision to operate on an aneurysm, the time scale of the development is estimated to be of the order of ten years (approximately 3×10^8 sec.)[44].

3.3 Collagen Remodelling

In the physiological range of stretches, collagen contributes only partly to the load bearing of the arterial walls. As stretches in the arterial wall increase, collagen becomes the main

load bearer, and due to its highly nonlinear mechanical behavior it quickly prevents stretches from becoming excessive. Consequently, to account for large dilations observed in aneurysms, remodelling of collagen must be occurring. Without remodelling, even if all the elastin is degraded, the stretches in the collagen, and thus the dilation of the wall, would not increase significantly for the total load to be borne [44]. This brings us to the first hypothesis in the remodelling, called ***recruitment***. In this hypothesis, it is assumed that the collagen remodels to maintain the attachment stretch, λ_a, in its fibers. This is consistent with the fact that collagen fibers are in a continual state of degradation and deposition, and that fibers attach in a state of stretch [1, 44]. In recruitment, the collagen fibers change their reference configuration(from $\lambda_{rec,0}$ to $\lambda_{rec} = \lambda_{rec}(\mathbf{x}, t)$) so as to maintain a stretch of λ_a. For a progressively increasing stretch, this would mean that the collagen fibers elongate. We will at times refer to recruitment as ***elongation***. Following Watton et al [44], we take the attachment stretch to be the stretch in the collagen at systole. Moreover, we use the same evolution equation for recruitment as in [23], viz.

$$\frac{\partial \lambda_{rec}}{\partial t} = \alpha(\lambda_c - \lambda_a), \qquad \lambda_{rec}(\mathbf{x}, 0) = \lambda_{rec,0}, \tag{3.27}$$

where α is a rate constant for recruitment, and $t = 0$ is the time for the initial attachment. For a non-homogenous deformation with respect to the unloaded configuration, the attachment stretch may not, in general, be attained simultaneously over the whole tissue unless the tissue is subjected to non-homogenous pre-stretches.

Apart from recruitment, the collagen can thicken (i.e. increase in cross-sectional area) to restore its stretch to λ_a. This is consistent with the fact that an increase in the collagen content is observed in aneurysms [14]. This may be seen as a desirable remodelling response for it limits the rate and extent of the dilation. We model the ***thickening*** as a change in the collagen volume fraction, n_c. The evolution equation for thickening is given by, according to [23],

$$\frac{\partial n_c}{\partial t} = \beta(\lambda_c - \lambda_a), \qquad n_c(\mathbf{x}, 0) = n_{c,0}, \tag{3.28}$$

where β is a rate constant for thickening, and $n_{c,0}$ is the initial collagen volume fraction.

The remodelling process described above refers to collagen modeled as fibers. In the case of isotropic 3-dimensional collagen, we propose parallel remodelling laws for elongation and thickening given below

$$\frac{\partial s_{rec}(\mathbf{x}, t)}{\partial t} = \alpha(s(\mathcal{F}_c) - s_a), \qquad s_{rec}(\mathbf{x}, 0) = s_{rec,0}, \tag{3.29}$$

$$\frac{\partial n_c(\mathbf{x}, t)}{\partial t} = \beta(s(\mathcal{F}_c) - s_a), \qquad n_c(\mathbf{x}, 0) = n_{c,0}, \tag{3.30}$$

where $s(\mathcal{F}_c) = s(\mathcal{F}_c(\mathbf{x}, t))$ is the deformation state criterium defined in Section 3.1.1.

Note that in the case of isotropic collagen every material point has one set of remodelling equations, whereas in the case of anisotropic collagen there are, in general, two sets of remodelling equations at a given material point - one for each fiber direction.

3.4 Degradation and Remodelling in Retrospect

In the constitutive relations discussed in Section 3.1.3, the elastin and collagen volume fractions are involved. It is not so clear whether the elastin is losing strength as assumed in

Section 3.2 or getting fragmented and leaving the tissue in the aneurysmal stage.

It has been suggested that arterial collagen exists in two forms: free collagen molecules (procollagen), and collagen fibrils (jointed or cross-linked). Being separate molecules, procollagen have no resistance to deformation of the artery, whereas collagen fibers do act against it, trying to restore their attachment configuration. In response to different stimuli, including mechanical ones, the arterial wall regulates the amount of cross-linked collagen in order to increase the wall compliance. In this case, the absolute amount of collagen, consisting of both procollagen and cross-linked collagen, is assumed to be constant. Thickening, according to this hypothesis, is realized by creating cross-links between procollagen, while the absolute volume of collagen remains fixed.

It is not certain whether in response to the weakening or fragmentation of elastin the artery responds by producing new collagen, or calling up on the inactive preexisting procollagen. It may also be the case that new collagen fibers are laid, but they take some time to mature and be fully active [22]. In this section, we will explain how each of the above hypotheses will affect the constitutive relation and remodelling laws. With two hypotheses each for elastin degradation and collagen thickening, we will have four possible scenarios.

Case 1

In this case, we assume that elastin weakens (reduced shear strength) and collagen thickens by cross-linking procollagen. The volume fractions are thus

$$n_e(\mathbf{x},t) = n_{e,0}, \qquad n_c(\mathbf{x},t) \geq n_{c,0}, \qquad n_p(\mathbf{x},t) \leq n_{p,0}, \tag{3.31}$$

where n_p is the volume fraction of procollagen. In addition, we have the constraint

$$n = n_c + n_p = \text{constant} = 1 - n_{e,0} = n_{c,0} + n_{p,0}. \tag{3.32}$$

This constraint will affect the evolution equation for collagen thickening, as the collagen volume fraction n_c can not go beyond n. To incorporate this we suggest using a logistic type thickening equation given by

$$\frac{\partial n_c}{\partial t} = \beta(\lambda_c - \lambda_a)(n - n_c), \tag{3.33}$$

$$\frac{\partial n_c}{\partial t} = \beta\left(s(\mathcal{F}_c) - s_a\right)(n - n_c), \tag{3.34}$$

for anisotropic and isotropic collagen, respectively; or simply stopping further thickening for $n_c > n$, i.e.

$$\frac{\partial n_c}{\partial t} = 0, \qquad \text{for } n_c > n. \tag{3.35}$$

He and Roach [14] (see also [22]) reported that the composition by dry weight of elastin, smooth muscle and collagen in a healthy aorta is 22.7%, 22.6%, and 54.8%, respectively and 2.4%, 2.2% and 96.5%[†] in an aneurysmal aorta. This indicates that either elastin is lost, or new collagen is produced or both elastin loss and collagen production occur in the aneurysmal tissue. If Case 1 holds, then such changes in weight fractions should not be observed in such a histological experiment. These numbers suggest that absolute weight changes of the wall

[†]The second set of numbers adds up to 101.1%

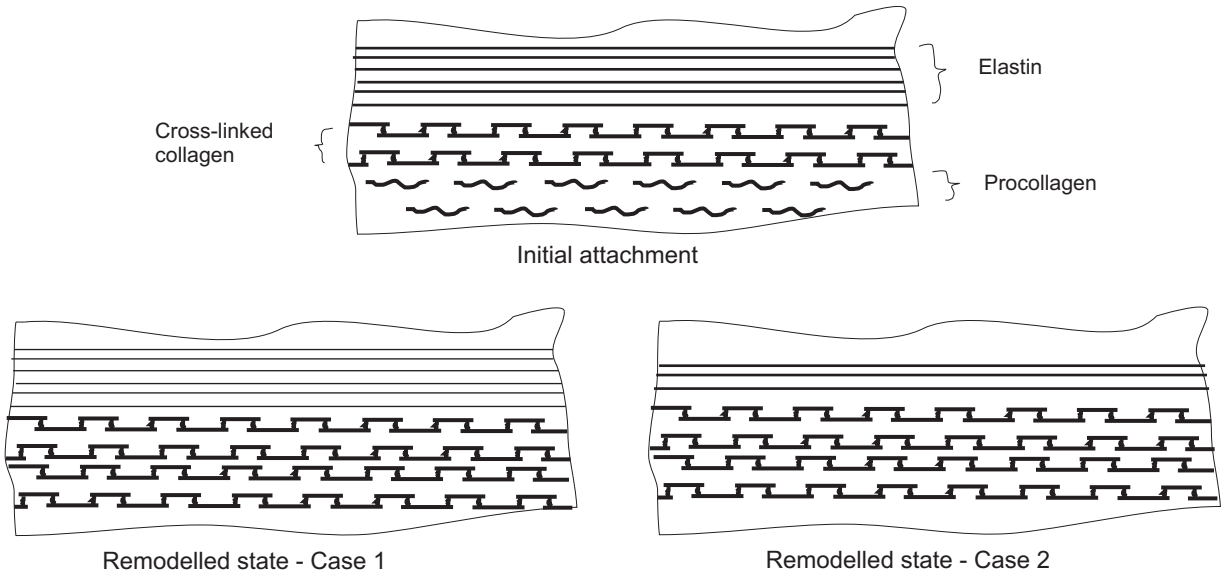

Figure 3.3: Thickening by cross-linking procollagen, strength represented by boldness

constituents are involved. Note, however, that weight fraction changes do not necessarily mean volume fraction changes although it is highly probable that one will translate into the other.

If we do not impose an upper bound on n_c, then the resulting process might be interpreted as producing more cross-links even among the active collagen so as to become more stiff. In a way this is equivalent to increasing k_1.

Case 2

Here we assume the absolute volume of elastin decreases while the shear modulus of the remaining elastin is maintained. Collagen is assumed to thicken by cross-linking. Here, the degradation function $c(t)$ in Section 3.2 expresses the ratio of the absolute volume of elastin at time t to the initial elastin volume. Note that the absolute reduction in elastin volume results in changes in the volume fractions of all constituents. If we introduce an auxiliary variable $f = f(t)$ such that the absolute volume of collagen is given by

$$V_c = f(V_{c,0} + V_{p,0}), \qquad \frac{n_{c,0}}{n_{c,0} + n_{p,0}} \leq f \leq 1, \tag{3.36}$$

we obtain relations for volume fractions as

$$n_e(t) = \frac{c(t)n_{e,0}}{c(t)n_{e,0} + n_{c,0} + n_{p,0}}, \qquad n_c(t) = f(t)\frac{n_{c,0} + n_{p,0}}{c(t)n_{e,0} + n_{c,0} + n_{p,0}}. \tag{3.37}$$

Note that, in this case, the thickening rule should be recast as an evolution equation for f.

Case 3

In this case, the elastin weakens by reducing the shear modulus while the collagen thickens by laying new fibers. The equations will be more manageable if we introduce a "growth"

parameter $g = g(t)$ such that the volume of collagen (in absolute terms) is given by

$$V_c = g(t)V_{c,0}, \qquad g(0) = 1. \tag{3.38}$$

The thickening equations change accordingly to

$$\frac{\partial g}{\partial t} = \beta(\lambda_c - \lambda_a), \tag{3.39}$$

$$\frac{\partial g}{\partial t} = \beta\left(s(\mathcal{F}_c) - s_a\right). \tag{3.40}$$

This leads us to,

$$n_e(t) = \frac{n_{e,0}}{n_{e,0} + g(t)n_{c,0}}, \qquad n_c(t) = \frac{g(t)n_{c,0}}{n_{e,0} + g(t)n_{c,0}}. \tag{3.41}$$

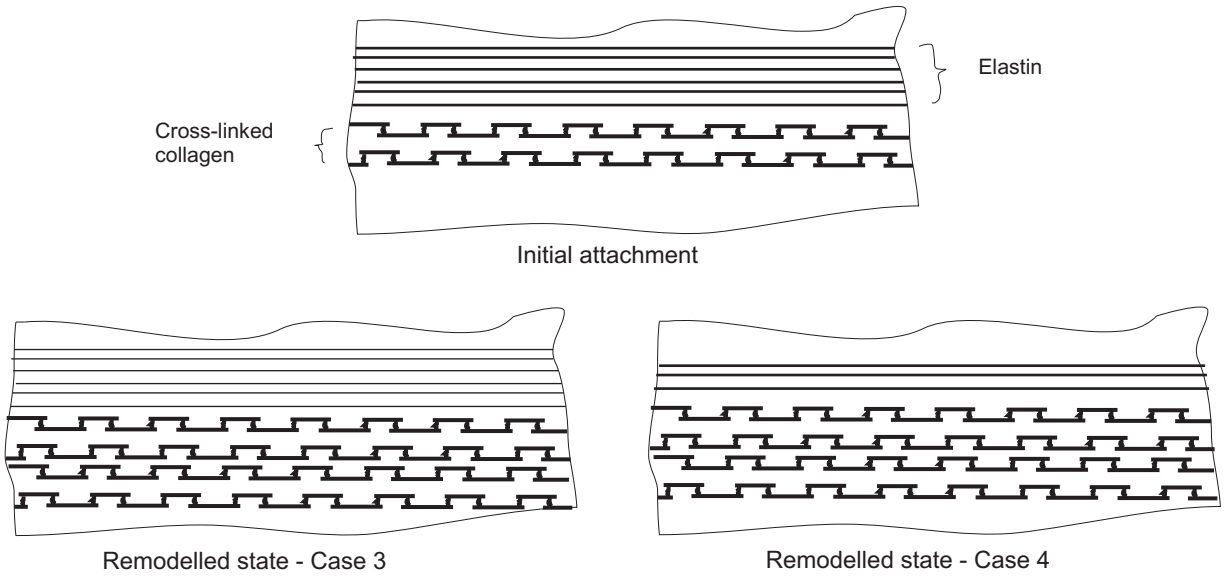

Figure 3.4: Thickening by producing new collagen fibers, strength represented by boldness

Case 4

Here, elastin fragments at constant shear modulus and the tissue produces more collagen. Following what we did for the third case and incorporating the effect of the degradation function $c(t)$, we have the following form for the volume fractions,

$$n_e(t) = \frac{c(t)n_{e,0}}{c(t)n_{e,0} + g(t)n_{c,0}}, \qquad n_c(t) = \frac{g(t)n_{c,0}}{c(t)n_{e,0} + g(t)n_{c,0}}. \tag{3.42}$$

It can be seen that in cases 3 and 4 we have assumed $n_p(t) = 0, \forall t$.

Cases $2 - 4$ require introduction of mass balance equations, which we however do not consider in this work. They may be useful for future models which incorporate absolute volume change during remodelling.

3.5 Initial Boundary Value Problem

The mechanical and biological equations involved in our model are explained in the preceding sections. In this section, we will point out which equations are involved in the physiologic stage, initiation and growth of aneurysms in the pathologic stage, and the initial and boundary conditions involved.

3.5.1 Healthy State

$\lambda \leq \lambda_{rec,0}$ **or** $s(\mathcal{F}) \leq s_{rec,0}$

If the pre-stresses are not considered, the arterial wall is stress free in the unloaded state. The blood pressure will gradually be increased. Until the tissue stretch reaches $\lambda_{rec,0}$, only elastin is involved in the load bearing. The equilibrium equation, incompressibility condition, and constitutive relation with the collagen contribution neglected will be used in the analysis. These equations will be supplemented by the natural boundary conditions:

$$\left(\mathcal{T}\mathbf{n}^i\right)|_{s^i} = -P\mathbf{n}^i, \tag{3.43}$$

$$\left(\mathcal{T}\mathbf{n}^o\right)|_{s^o} = \mathbf{0}, \tag{3.44}$$

where the $\mathbf{n}^i$ and $\mathbf{n}^o$ are the outward normals at the inner surface s^i and outer surface s^o of the vessel respectively, and $P = P(t)$ is the haemodynamic pressure, which at this stage is less than the systolic pressure.

Note also that according to the geometry used and symmetry conditions invoked, additional essential (displacement) boundary condition will be necessary.

The outer surface of the vessel is neither traction free nor unconstrained in its displacements as the surrounding tissues and organs will constrain its motion in both healthy and aneurysmal states. However, the exact boundary conditions involved are not so easy to determine. We take the simplifying assumption that the outer surface is free of traction and can have unconstrained displacements.

$\lambda > \lambda_{rec,0}, \lambda_c \leq \lambda_a$ **or** $s(\mathcal{F}) > s_{rec,0}, s(\mathcal{F}_c) \leq s_a$

In this regime, the collagen is stretched, but to a level less than or equal to the attachment state. The blood pressure will be increased until $\lambda_c = \lambda_a$ or $s(\mathcal{F}_c) = s_a$. The equations used will be exactly the same as the ones mentioned above, except that the collagen will be involved in the load bearing. The collagen volume fraction is $n_c = n_{c,0}$.

3.5.2 Aneurysmal or Degraded State

Once the collagen attains the attachment state, the pressure will be held constant (at the systolic pressure) and elastin will start to degrade in accordance with the equations given in Section 3.2. This will trigger collagen remodelling governed by the evolution equations and initial conditions in Section 3.3. Note here that the initial conditions refer to the time at which the elastin starts to degrade. In this regime, kinematic equations, incompressibility condition, the equilibrium equation, incompressibility condition, constitutive relations, the boundary conditions, recruitment equation with the initial condition, and thickening equation with the corresponding initial condition shall be solved simultaneously.

3.6 Pressure Stretch Relationships in Anisotropic Cylinders

In the case of cylinders and spheres in the initial configurations deforming into cylinders and spheres respectively, we can find single equations relating the applied pressure and membrane stretches. Because of the importance of these equations in the material characterization we take up after Section 3.8 and in the numerical analysis provided in Chapter 4, we derive them here. Equations for a spherical membrane and some relations in cylindrical membranes that are not required for the material characterization presented in this chapter are derived in Chapter 4 as required.

3.6.1 Kinematics

The reference configuration $\mathcal{G}_R$ is a cylindrical thin-walled tube of radius R and thickness H, with $H/R \ll 1$. In the thin-walled limit $H/R \to 0$, the tube is considered as a cylindrical surface of radius R, and mechanically modeled as a membrane. A material point $\mathbf{X}$ in the reference configuration is described by the cylindrical coordinates (R, Θ, Z), while in the deformed configuration it is described by (r, θ, z). The arterial wall consists of a single layer of elastin with two families of collagen making angles of γ with respect to the circumferential direction so that the unit vectors of the fiber directions in the reference configuration are given by

$$\mathbf{e}_{c,1,0} = \cos\gamma \mathbf{e}_\Theta + \sin\gamma \mathbf{e}_Z, \qquad \mathbf{e}_{c,2,0} = \cos\gamma \mathbf{e}_\Theta - \sin\gamma \mathbf{e}_Z. \tag{3.45}$$

We consider a homogenous deformation described by,

$$\theta = \Theta, \qquad z = Z, \qquad r = r(t). \tag{3.46}$$

This is an axially symmetric uniform inflation of the tube, in which the axial length of the tube is conserved.
Thus the basis vectors in the deformed configuration will be unaltered,

$$\mathbf{e}_r = \mathbf{e}_R, \qquad \mathbf{e}_\theta = \mathbf{e}_\Theta, \qquad \mathbf{e}_z = \mathbf{e}_Z. \tag{3.47}$$

The resulting tissue deformation gradient $\mathcal{F} = \mathcal{F}_e$ is

$$\mathcal{F} = \begin{pmatrix} \lambda_r & 0 & 0 \\ 0 & \lambda_\theta & 0 \\ 0 & 0 & 1 \end{pmatrix}, \tag{3.48}$$

where $\lambda_\theta = F_{\theta\theta} = r/R$ and $\lambda_r = F_{rr} = \frac{\partial r}{\partial R} = \lambda_\theta^{-1}$, because of incompressibility, requiring $\det(\mathcal{F}) = 1$.
In the sequel we will list only non-zero elements of tensors. In fact all the tensors to be encountered are diagonal tensors.
The left Cauchy-Green deformation tensor $\mathcal{B} = \mathcal{B}_e = \mathcal{F}\mathcal{F}^T$ is

$$\mathcal{B} = \begin{pmatrix} \lambda_\theta^{-2} & & \\ & \lambda_\theta^2 & \\ & & 1 \end{pmatrix}. \tag{3.49}$$

The stretch in the direction of a fiber is given by the Euclidian norm ($i = 1, 2$)

$$\lambda_{\gamma,i} = \|\mathcal{F}\mathbf{e}_{c,i,0}\|_2. \tag{3.50}$$

Using (3.45), we get the same stretch in both fiber directions (because of the symmetrical arrangement with respect to the circumferential direction) given by,

$$\lambda_{\gamma,1} = \lambda_{\gamma,2} = \lambda_\gamma = \sqrt{\lambda_\theta^2 \cos^2\gamma + \sin^2\gamma}. \tag{3.51}$$

The fiber directions in the deformed configuration can be obtained from (3.51) and (3.3) as

$$\mathbf{e}_{c,1} = \frac{\lambda_\theta}{\lambda_\gamma}\cos\gamma\mathbf{e}_\Theta + \frac{1}{\lambda_\gamma}\sin\gamma\mathbf{e}_Z, \tag{3.52}$$

$$\mathbf{e}_{c,2} = \frac{\lambda_\theta}{\lambda_\gamma}\cos\gamma\mathbf{e}_\Theta - \frac{1}{\lambda_\gamma}\sin\gamma\mathbf{e}_Z. \tag{3.53}$$

Note from (3.51) that for $\lambda_\theta > 1$, which is always the case if we inflate the cylinder, we have $\lambda_\gamma < \lambda_\theta$. This means that with increasing inflation the current fiber directions given by (3.52) and (3.53) become more and more circumferential resulting in a membrane which is stiffer circumferentially, than axially.

The collagen stretch is given by

$$\lambda_c = \begin{cases} 1, & \lambda_\gamma \le \lambda_{rec,0}, \\ \frac{\lambda_\gamma}{\lambda_{rec,0}}, & \lambda_{rec,0} < \lambda_\gamma \le \lambda_{rec,0}\lambda_a, \\ \frac{\lambda_\gamma}{\lambda_{rec}}, & \lambda_\gamma > \lambda_{rec,0}\lambda_a. \end{cases} \tag{3.54}$$

3.6.2 Stresses

We use the constitutive relation given in Section 3.1.3. We split the stress into hydrostatic pressure, elastin contribution and collagen contribution. The elastin contribution given componentwise is

$$t^e_{rr} = n_e C_e(\lambda_\theta^{-2} - 1), \qquad t^e_{\theta\theta} = n_e C_e(\lambda_\theta^2 - 1). \tag{3.55}$$

The longitudinal stress t_{zz} is not relevant here.

The collagen contributions are

$$t^{c,i}_{rr} = \mathbf{e}_r \cdot \mathcal{T}^{c,i}\mathbf{e}_r = \tau_{f,i}\mathbf{e}_r \cdot [\mathbf{e}_{c,i} \otimes \mathbf{e}_{c,i}]\mathbf{e}_r = 0, \qquad i = 1, 2, \tag{3.56}$$

$$t^{c,i}_{\theta\theta} = \mathbf{e}_\theta \cdot \mathcal{T}^{c,i}\mathbf{e}_\theta = \tau_{f,i}\mathbf{e}_\theta \cdot [\mathbf{e}_{c,i} \otimes \mathbf{e}_{c,i}]\mathbf{e}_\theta = \left(\frac{\lambda_\theta \cos\gamma}{\lambda_\gamma}\right)^2 \tau_{f,i}, \qquad i = 1, 2. \tag{3.57}$$

As the two collagen fibers are of the same material with stretch-stress relation given by (3.22) and the stretches in the two fiber directions are equal as shown by (3.51), we have

$$\tau_{f,1} = \tau_{f,2} = \tau_f = 2k_1\lambda_c^2(\lambda_c^2 - 1)e^{[k_2(\lambda_c^2-1)^2]}. \tag{3.58}$$

If we assume that $n_{c,1,0} = n_{c,2,0} = n_{c,0}/2$, the remodelling will result in the same recruitment and thickening along both fiber directions. In such a case, which is what we will pursue further, (3.58) holds in all stages of the physiological and aneurysmal conditions.

Summing up, we have the following expressions for the stresses in the arterial wall

$$\begin{aligned} t_{rr} &= -p + n_e C_e(\lambda_\theta^{-2} - 1), \\ t_{\theta\theta} &= -p + n_e C_e(\lambda_\theta^2 - 1) + 2\left(\frac{\lambda_\theta \cos\gamma}{\lambda_\gamma}\right)^2 k_1\lambda_c^2(\lambda_c^2 - 1)e^{[k_2(\lambda_c^2-1)^2]}(n_{c,1} + n_{c,2}), \\ &= -p + n_e C_e(\lambda_\theta^2 - 1) + 2n_c k_1\left(\frac{\lambda_\theta \cos\gamma}{\lambda_\gamma}\right)^2 \lambda_c^2(\lambda_c^2 - 1)e^{[k_2(\lambda_c^2-1)^2]}, \end{aligned} \tag{3.59}$$

where λ_γ and λ_c are obtained via (3.51) and (3.54), respectively. In addition, $t_{r\theta} = t_{rz} = t_{\theta z} = 0$ and t_{zz} is irrelevant[†].

3.6.3 Equilibrium Equations

The thin-walled tube is inflated by an internal pressure P. In a membrane approximation, the radial stress t_{rr} is $\mathcal{O}(H/R)$ compared to $t_{\theta\theta}$, so approximately zero, while the tangential or hoop stress $t_{\theta\theta}$ is related to P according to the Laplace formula, yielding,

$$t_{rr} = 0, \qquad t_{\theta\theta} = \frac{Pr}{h}, \tag{3.60}$$

where the current radius r and thickness h can be obtained from the kinematic relations as

$$r = \lambda_\theta R, \quad h = \lambda_r H = \frac{H}{\lambda_\theta}, \tag{3.61}$$

resulting in

$$t_{\theta\theta} = \frac{PR}{H}\lambda_\theta^2. \tag{3.62}$$

From (3.59) and (3.62), we obtain

$$-p + n_e C_e(\lambda_\theta^{-2} - 1) = 0, \tag{3.63}$$

$$-p + n_e C_e(\lambda_\theta^2 - 1) + 2n_c k_1 \left(\frac{\lambda_\theta \cos\gamma}{\lambda_\gamma}\right)^2 \lambda_c^2(\lambda_c^2 - 1)e^{[k_2(\lambda_c^2-1)^2]} = \frac{PR}{H}\lambda_\theta^2. \tag{3.64}$$

Eliminating the hydrostatic pressure p from (3.64) by means of (3.63) we arrive at,

$$n_e C_e(\lambda_\theta^2 - \lambda_\theta^{-2}) + 2n_c k_1 \left(\frac{\lambda_\theta \cos\gamma}{\lambda_\gamma}\right)^2 \lambda_c^2(\lambda_c^2 - 1)e^{[k_2(\lambda_c^2-1)^2]} = \frac{PR}{H}\lambda_\theta^2. \tag{3.65}$$

The longitudinal stress t_{zz} can be obtained from $t_{zz} = \mathbf{e}_z \cdot \mathcal{T}\mathbf{e}_z$ and is given by

$$t_{zz} = n_e C_e(1 - \lambda_\theta^{-2}) + 2n_c k_1 \lambda_c^2(\lambda_c^2 - 1)e^{[k_2(\lambda_c^2-1)^2]} \left(\frac{\sin\gamma}{\lambda_\gamma}\right)^2. \tag{3.66}$$

Membrane approximations are commonly used in arterial wall mechanics; see [22, 44, 46, 47].

[†]By irrelevant, we mean that explicit calculation of t_{zz} is not necessary in the material characterization and growth prediction of the axisymmetric uniform deformations considered here.

3.7 Pressure Stretch Relationships in Isotropic Cylinders

In this section we consider the inflation of a thin-walled cylinder where the collagen is assumed to be isotropic with the exponential material law given by (3.18). The remodelling equations will now be given in terms of the three-dimensional version given by (3.29) and (3.30). The attachment/recruitment criterium $s(\mathcal{F})$ should be a function of an invariant of $\mathcal{F}$. We consider it to be a function of the first invariant only. When the collagen is taken to be isotropic, as we have it in this section,the process of initial recruitment, initial attachment, and remodelling should be interpreted as follows:

- collagen is inactive until a certain deformation state given by a initial recruitment state $s_{\mathcal{F}}(\mathbf{x}) = s_{rec,0}$ is reached;
- collagen has a certain deformation state $s_{\mathcal{F}_c}(\mathbf{x}) = s_a$ which it tries to maintain by remodelling;
- the remodelling is realized by thickening and recruitment, i.e. by assuming a different undeformed configuration, which is described by $s_{rec}(\mathbf{x}, t)$.

Wulandana and Robertson [47] have considered a "dual-mechanism" model in which the collagen is inactive for $s(\mathcal{F}) < s_1$, elastin and collagen act together for $s_1 < s(\mathcal{F}) < s_2$ and elastin completely breaks down when $s(\mathcal{F}) = s_2$, leaving only collagen to contribute for the load carrying thereafter. We adopted their approach of using a stretch invariant as a recruitment criterium, but incorporated a gradual degradation of elastin accompanied by collagen remodelling.

3.7.1 Kinematics

The reference configuration and tissue deformation is the same as that of the fiber-reinforced wall discussed in Section 3.6.1. The difference is in the collagen deformation which should now be described by a second-order tensor. Enforcing incompressibility, the elastin and collagen deformation gradients are:

$$\mathcal{F}_e = \mathcal{F} = \begin{pmatrix} \lambda_\theta^{-1} & & \\ & \lambda_\theta & \\ & & 1 \end{pmatrix}, \qquad \mathcal{F}_c = \begin{pmatrix} \lambda_c^{-1} & & \\ & \lambda_c & \\ & & 1 \end{pmatrix}, \tag{3.67}$$

where λ_θ and λ_c are the circumferential stretch in elastin and collagen, respectively.

The left Cauchy-Green deformation tensors are similarly given by

$$\mathcal{B}_e = \mathcal{B} = \begin{pmatrix} \lambda_\theta^{-2} & & \\ & \lambda_\theta^{2} & \\ & & 1 \end{pmatrix}, \qquad \mathcal{B}_c = \begin{pmatrix} \lambda_c^{-2} & & \\ & \lambda_c^{2} & \\ & & 1 \end{pmatrix}. \tag{3.68}$$

Following (3.8) and noticing that the collagen is "undeformed" before the tissue stretch is such that $s(\mathcal{F}) = s_{rec,0}$ we have

$$\mathcal{F}_c(\mathbf{x}, t) = \begin{cases} \mathcal{I}, & s(\mathcal{F}) = I_{\mathcal{F}} \leq s_{rec,0}, \\ \mathcal{F}\mathcal{F}_{rec,0}^{-1}, & s_{rec,0} < s(\mathcal{F}) \leq s_{rec,0} s_a, \\ \mathcal{F}\mathcal{F}_{rec}^{-1}, & s_(\mathcal{F}) > s_{rec,0} s_a \end{cases} \tag{3.69}$$

For the deformation we are considering here, the incompressibility requirement and the expression for the first invariant provide sufficient equations to determine the recruitment deformation gradient tensor from its first invariant. For an arbitrary three-dimensional deformation, however, additional relations/constraints should be provided to uniquely determine the recruitment deformation tensor and thus the collagen deformation tensor.

There are no shear deformations in the case we are considering in this chapter. This results in a diagonal matrix for the recruitment deformation tensor. For the inflating cylinder, the elastin and collagen stretch in the longitudinal direction are both unity (unstretched). This yields $F^{rec}_{33} = 1$. Requiring incompressibility, we have

$$\mathcal{F}_{rec} = \begin{pmatrix} \lambda_{rec}^{-1} & & \\ & \lambda_{rec} & \\ & & 1 \end{pmatrix}, \tag{3.70}$$

where λ_{rec} is the recruitment variable in the circumferential direction. Finally, using $s = \mathrm{tr}(\mathcal{F})$, we arrive at

$$s(\mathcal{F}_{rec}) = \lambda_{rec} + \lambda_{rec}^{-1} + 1. \tag{3.71}$$

For a given value of s, (3.71) gives two values of λ_{rec}: one greater than unity and the other less than unity. As we defined λ_{rec} to be $F^{rec}_{\theta\theta}$, we take the value greater than one. Moreover, the two results are reciprocals of each other and thus we can take each one to be F^{rec}_{rr} and the other to be $F^{rec}_{\theta\theta}$.

3.7.2 Constitutive and Equilibrium Equations

Keeping the isotropic neo-Hookean constitutive relation for elastin, we consider collagen also to be isotropic. The isotropic material law for collagen is given by (3.18). The stress tensor given by (3.19), duplicated here for ease of reference, is

$$\mathcal{T} = -p\mathcal{I} + n_e C_e(\mathcal{B}_e - \mathcal{I}) + 2n_c k_1 (I_c - 3) e^{[k_2(I_c-3)^2]} (\mathcal{B}_c - \mathcal{I}). \tag{3.72}$$

Expressed in terms of the circumferential stretches λ_θ and λ_c, the stress tensor is

$$\begin{aligned} \mathcal{T} = \quad & -p\mathcal{I} + n_e C_e \begin{pmatrix} \lambda_\theta^{-2} - 1 & & \\ & \lambda_\theta^2 - 1 & \\ & & 0 \end{pmatrix} \\ & + 2n_c k_1 (\lambda_c^2 + \lambda_c^{-2} - 2) e^{[k_2(\lambda_c^2 + \lambda_c^{-2} - 2)^2]} \begin{pmatrix} \lambda_c^{-2} - 1 & & \\ & \lambda_c^2 - 1 & \\ & & 0 \end{pmatrix}. \end{aligned} \tag{3.73}$$

The equilibrium equation remains the same as what we had in Section 3.6.3, i.e.

$$t_{\theta\theta} = \frac{PR}{H}\lambda_\theta^2, \qquad t_{rr} = 0. \tag{3.74}$$

We eliminate the hydrostatic pressure p from the stress tensor using (3.74). By so doing we get the following expressions for the circumferential stress:

$$t_{\theta\theta} = n_e C_e(\lambda_\theta^2 - \lambda_\theta^{-2}) + 2n_c k_1 (\lambda_c^2 + \lambda_c^{-2} - 2) e^{[k_2(\lambda_c^2 + \lambda_c^{-2} - 2)^2]} (\lambda_c^2 - \lambda_c^{-2}). \tag{3.75}$$

Here too, $t_{r\theta} = t_{rz} = t_{\theta z} = 0$ and t_{zz} is irrelevant.

Using (3.75) and the circumferential stress from (3.74), we arrive at

$$n_e C_e(\lambda_\theta^2 - \lambda_\theta^{-2}) + 2n_c k_1(\lambda_c^2 + \lambda_c^{-2} - 2)e^{[k_2(\lambda_c^2+\lambda_c^{-2}-2)^2]}(\lambda_c^2 - \lambda_c^{-2}) = \frac{PR}{H}\lambda_\theta^2. \tag{3.76}$$

This resulting equilibrium equation for isotropic collagen is the equivalent of equation (3.65) for anisotropic collagen. In Chapter 4 we will compare the results of these two equations with each other.
Finally, we have the longitudinal stress t_{zz} given by

$$t_{zz} = n_e C_e(1 - \lambda_\theta^{-2}) + 2n_c k_1(\lambda_c^2 + \lambda_c^{-2} - 2)e^{[k_2(\lambda_c^2+\lambda_c^{-2}-2)^2]}(1 - \lambda_c^{-2}). \tag{3.77}$$

3.8 Material Characterization

In the remaining sections of this chapter, we present experimental data for characterizing cerebral arteries and carry out regression analysis to obtain the material parameters. We consider various constitutive relations for elastin and collagen and compare the results.

Scott et al. [34] performed inflation tests on intact segments anterior cerebral arteries (ACA). During the experiment, pressure and the corresponding luminal volume of the segment were recorded. Changes in the segment's inner diameter were calculated from the measured luminal volumetric changes. Care was taken to avoid variation of radius along the segment.

Four ACA segments were subjected to slow cycles of loading and unloading though only results from the loading procedure were reported. Three samples were loaded up to 200 mmHg and one control sample was loaded up to 100 mmHg. The control segment was reported to show consistent curves of tension versus strain after six repetitions of loading and unloading, whereas the other three segments behaved differently from the control. After three cycles of loading that produced three consistent distensibility curves similar to those of the control sample, the final six curves exhibited a measurable shifting. The post-shifting curves were also reproducible. The post-shifting series displayed a larger unloaded radius, implying that some form of permanent deformation had occurred. Scott et al. [34] used the new reference radius to calculate the strains after shifting. They hypothesized that the shift of the curves and the absence of the 'toe region' in the post-shifting curves was due to elastin breakage. However, they never performed a morphology study.

Scott et al. reported that the undeformed wall thickness of the segments was in the range from 100 to 200 μm, but they did not report the exact value. We follow Wulandana [46] and use a wall thickness of 125 μm.

3.8.1 Fitting Experimental Data to Constitutive Relations

In order to extract data points for the statistical analysis, Wulandana [46] scanned the 'tension'-strain curve and provided the numerical values; see [46, p. 174]. We note here that Scott et al. [34] refer to the product of the net pressure and the current radius as 'tension'.

In Table 3.1 we provide the tension-stretch data for the post-Shifting curve and include pressure in the pre-Shifting data.
The pressure P is calculated from the tension T and the stretch λ_θ by the formula

$$P = \frac{T}{R\lambda_\theta}, \tag{3.78}$$

where R is the pre-shifting undeformed radius, which was 0.33mm [46, p. 80].

In Figure 3.5 the pressure-stretch curve for the pre-shifting data is shown. Note the nearly linear pressure-stretch relation at lower stretches, and the increasing stiffness at higher stretches.

From the figures provided by Scott et al. [34], Wulandana [46, p. 80] found that the post-shifting zero tension radius is 0.58 mm whereas the pre-shifting undeformed radius is 0.33 mm[†]. From these two reference configurations, he computes the circumferential stretch

[†]Wulandana reports the above numbers in cm in [46]. Calculations with those values in later section of this work suggested that this sizes are too large. Actually this should be a typing error in [46] as Wulandana reports the same numbers in mm in [47]. We did not have access to the original paper by Scott et al. [34].

Table 3.1: Experimental data from Scott et al. [34], adapted from Wulandana [46, p. 174]

Before Shifting			After Shifting	
Stretch	Tension (N/m)	Pressure (KPa)	Stretch	Tension
1.00	0.0	0	1.0	0.0
1.10	0.1	0.275	1.08	0.6
1.20	0.3	0.758	1.11	1.0
1.30	0.5	1.166	1.17	1.6
1.40	0.7	1.515	1.20	2.0
1.50	0.95	1.919	1.22	3.0
1.51	1.0	2.007	1.26	4.0
1.60	1.5	2.840	1.30	5.0
1.66	2.0	3.651	1.31	6.0
1.72	3.0	5.285	1.37	8.0
1.80	4.0	6.734	1.40	10.0
1.90	6.0	9.569	1.45	13.0
2.00	8.0	12.121	1.48	15.0
2.05	10.0	14.782	1.50	17.9
2.10	12.0	17.316	1.52	20.0
2.18	13.9	19.322		
2.21	15.9	21.802		
2.25	18.0	24.242		
2.30	20.0	26.351		

at which collagen is initially recruited, i.e, $\lambda_{rec,0} = \frac{0.58}{0.33} = 1.76$. An alternative for the circumferential tissue stretch at initial recruitment is $\lambda_{rec,0} = 1.2$ used by Machyshyn [23] and Watton et al. [44].

Wulandana [46] uses a multi-mechanism model where the elastin is completely lost at some deformation state. He thus uses the post-shifting curve to characterize the collagen. We will not use the post-shifting curve for quantifying material parameters. We will use only the pre-shifting curve to characterize both materials. By considering an idealized thin-walled cylinder of infinite length with uniform axisymmetric deformations, for different constitutive models, we will try to find the constitutive model which best fits to this data set. In so doing we find not only the 'best' values for the material parameters, but also the 'best' material model. So, in fact, we fit the data to constitutive relations.

Scott et al. [34] did not report the rate of loading. However, based on the interval of the data points, Wulandana [46, p. 78] estimates pressure increments of 20 mmHg. Typical data measurements are done in the interval of at least 20 seconds [46, p. 78]. In any case, we can assume that the complete experiment would be carried out in the order of one day; hence a time scale smaller than the collagen turnover time (half life) of 3 to 90 days[‡]. So we do not consider any remodelling, implying that we are characterizing a healthy artery here.

Table 3.1 shows that the circumferential stretch at systolic pressure (12 KPa)is between

[‡]Humphrey [22] (see also [44]) suggested that a collagen turn over time (half life) of 3 to 90 day, although acknowledging that it may be longer. Note that the half life $t_{1/2}$ and mean life time τ are related by $t_{1/2} = \tau \ln 2$.

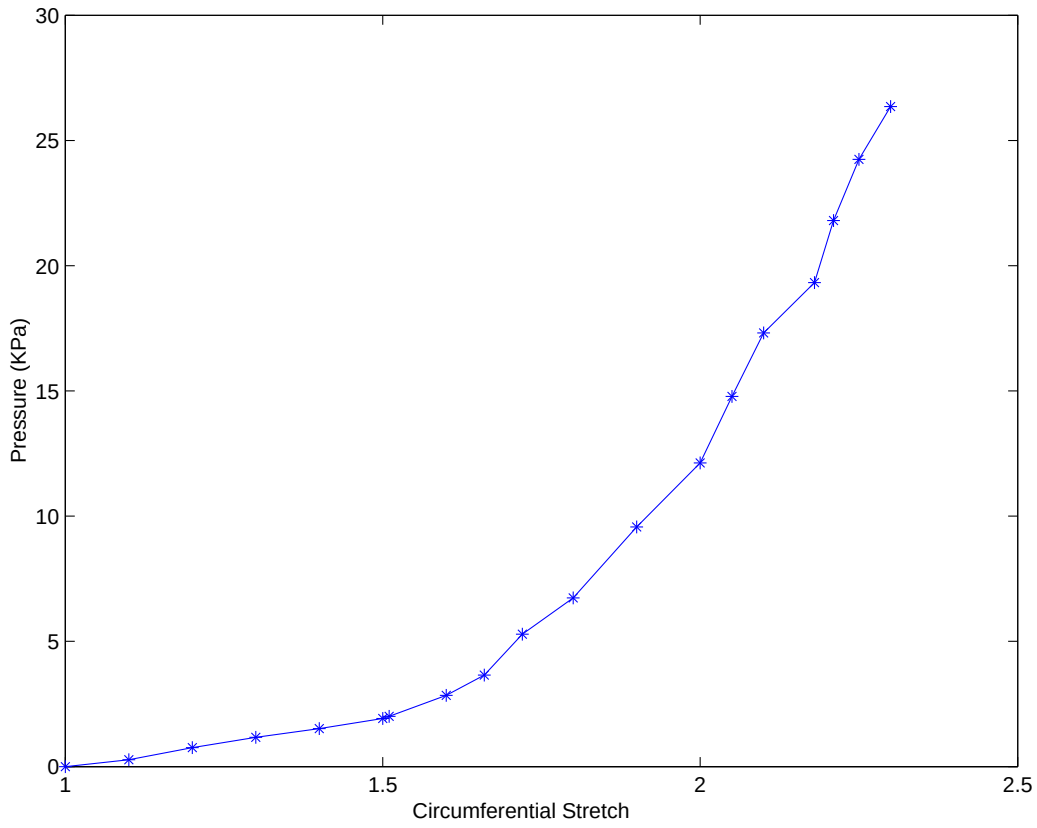

Figure 3.5: Pressure-Stretch Curve, after [34] and [46]

1.9 and 2.0 for cerebral arteries. Note that this is in a striking contrast to a circumferential stretch of 1.3 reported for abdominal arteries by Watton et al. [44] at the systolic pressure of 16 KPa[§].

For nonlinear regression, the Levenberg-Marquardt algorithm is preferred [15, p. 287]; see also [22]. It is a variant of the Newton method. Mathematica® has a built in nonlinear regression function where this algorithm is the default choice. We used Mathematica® to estimate the material parameters.

We consider two constitutive models for elastin: the neo-Hookean and an exponential relation used by Wulandana and Robertson [47], based on the strain energy functions

$$W_e = \frac{C_e}{2}(I_e - 3), \tag{3.79}$$

and

$$W_e = \frac{k_1}{2k_2}(e^{k_2(I_e-3)} - 1), \tag{3.80}$$

respectively, where I is the first invariant of $\mathcal{B} = \mathcal{F}^T\mathcal{F}$.

[§]Arterial pressure drops as we go further from the heart.

For isotropic collagen we additionally use the exponential model we introduced in Section 3.1.3, with

$$W_c = \frac{k_1}{2k_2}(e^{[k_2(I_c-3)^2]} - 1). \tag{3.81}$$

For anisotropic collagen, we choose the constitutive equation used by Van Oijen [26] and Machyshyn [23], which we described in Section 3.1.3. We provide it here for ease of reference,

$$\mathcal{T}_{c,i} = \tau_{f,i}\mathbf{e}_{c,i} \otimes \mathbf{e}_{c,i}, \tag{3.82}$$

with

$$\tau_{f,i} = 2k_1\lambda_{c,i}^2(\lambda_{c,i}^2 - 1)e^{[k_2(\lambda_{c,i}^2-1)^2]}, \tag{3.83}$$

where $\mathbf{e}_{c,i} = \mathbf{e}_{c,i}(\mathbf{x}, t)$ is the unit vector in the fiber direction.

For the anisotropic case, we use both the 'traditional' and 'modified' mixture rules. Using the mixture rule in all directions, according to the traditional mixture rule, introduces an artificial weakening of the tissue in the direction perpendicular to the fibers. To avoid this, Van Oijen [26] suggests modifying the mixture rule so that it holds only in the direction of the fibers.

3.8.2 Isotropic Models

The elastin and collagen deformation gradients are given by,

$$\mathcal{F}_e = \mathcal{F} = \begin{pmatrix} \lambda_\theta^{-1} & & \\ & \lambda_\theta & \\ & & 1 \end{pmatrix}, \qquad \mathcal{F}_c = \begin{pmatrix} \lambda_c^{-1} & & \\ & \lambda_c & \\ & & 1 \end{pmatrix}, \tag{3.84}$$

where λ_θ and λ_c are the circumferential stretch in elastin and collagen, respectively.

Neo-Hookean Elastin

Using (3.79) for the constitutive response of elastin and (3.81) for collagen, we get the stress tensor for the arterial wall as

$$\mathcal{T} = -p\mathcal{I} + n_e C_e(\mathcal{B}_e - \mathcal{I}) + 2n_{c,0}k_1(I_c - 3)e^{[k_2(I_c-3)^2]}(\mathcal{B}_c - \mathcal{I}). \tag{3.85}$$

Note that this is what we had in (3.19).
We then have the pressure stretch relationship from (3.76):

$$n_e C_e(\lambda_\theta^2 - \lambda_\theta^{-2}) + 2n_{c,0}k_1(\lambda_c^2 + \lambda_c^{-2} - 2)e^{[k_2(\lambda_c^2+\lambda_c^{-2}-2)^2]}(\lambda_c^2 - \lambda_c^{-2}) = \frac{PR}{H}\lambda_\theta^2. \tag{3.86}$$

We replace the product of the pressure and radius, i.e. $Pr = PR\lambda_\theta$ by the tension T. The products n_eC_e and $n_{c,0}k_1$ can be used as single independent variables in the regression analysis; in fact we do not have histological experiments to find n_e and $n_{c,0}$ from. If in the numerical simulation of a healthy or aneurysmal wall changing the initial volume fractions of elastin and collagen is required, then we have to simultaneously change the strength parameters C_e and k_1 so as to keep the above products constant. The collagen stretch will be $\lambda_c = \lambda_\theta/\lambda_{rec,0}$, where the initial recruitment parameter $\lambda_{rec,0}$ can either be considered to be one of the unknowns in the least squares regression or taken equal to 1.76 as discussed above. Following Machyshyn [23], we also consider the case of $\lambda_{rec,0} = 1.2$.

Finally, we have the following equation to be fitted to the experimental data of Table 3.1:

$$T = \frac{H}{\lambda_\theta}\left[n_e C_e(\lambda_\theta^2 - \lambda_\theta^{-2}) + 2n_{c,0}k_1(\lambda_c^2 + \lambda_c^{-2} - 2)e^{[k_2(\lambda_c^2+\lambda_c^{-2}-2)^2]}(\lambda_c^2 - \lambda_c^{-2})\right], \quad (3.87)$$

$$\lambda_c = \max(1, \frac{\lambda_\theta}{\lambda_{rec,0}}). \quad (3.88)$$

where $H = 0.125$mm, and where n_eC_e, $n_{c,0}k_1$, k_2, and possibly $\lambda_{rec,0}$ must be determined from the statistical analysis.

The quality of the curve fitting is measured by the R^2-value given by:

$$R^2 = 1 - \frac{\|T_{data} - T_{theoretical}\|_2^2}{\|T_{data} - T_{mean}\|_2^2}, \quad (3.89)$$

where T_{mean} is the mean value of the measured data. For details of the statistical analysis, we refer to Brown [3].
The results of the regression analysis are presented in Table 3.2.

Table 3.2: Results of Regression Analysis for Neo-Hookean Elastin and Exponential Collagen

	$\lambda_{rec,0} = 1.2$	$\lambda_{rec,0} = 1.76$
$\lambda_{rec,0}$	1.2	1.76
n_eC_e(Pa)	1668.11	14805.1
$n_{c,0}k_1$(Pa)	21339.7	783331.0
k_2	0.0675	-7.18555
R^2	0.9983	0.9749

Figure 3.6 shows a plot of the experimental and least-squares regression results. It can be seen from the plot and from the R^2-values in Table 3.2 that the case with $\lambda_{rec,0} = 1.2$ yields a better correlation between the experimental and theoretical results.

What now remains is finding the attachment deformation state. As discussed in Chapters 2 and 3, this is achieved when the pressure is equal to the systolic pressure, i.e, $P = 90$mmHg $= 12$KPa. Using the best fitting curve and (3.86), we find that at at $P = 12$KPa, $\lambda_\theta = 2$ for $\lambda_{rec,0} = 1.2$. This gives a circumferential attachment stretch of $2/1.2 = 1.67$.

Exponential Elastin

Next, we use the exponential constitutive relation based on (3.80) for elastin, keeping the same relation for collagen as before. The stress tensor in the arterial wall is then given by

$$\mathcal{T} = -p\mathcal{I} + n_e k_1^e\{e^{[k_2^e(I_e-3)]}\}(\mathcal{B}_e - \mathcal{I}) + 2n_{c,0}k_1^c(I_c - 3)\{e^{[k_2^c(I_c-3)^2]}\}(\mathcal{B}_c - \mathcal{I}). \quad (3.90)$$

Again using the Laplace formula for equilibrium and the zeroness of the radial stresses, we obtain the following pressure-stretch relationship as the analogous of (3.86):

$$n_e k_1^e\{e^{[k_2^e(\lambda_\theta^2+\lambda_\theta^{-2}-2)]}\}(\lambda_\theta^2 - \lambda_\theta^{-2}) + 2n_{c,0}k_1^c(\lambda_c^2 + \lambda_c^{-2} - 2)\{e^{[k_2^c(\lambda_c^2+\lambda_c^{-2}-2)^2]}\}(\lambda_c^2 - \lambda_c^{-2}) = \frac{PR}{H}\lambda_\theta^2. \quad (3.91)$$

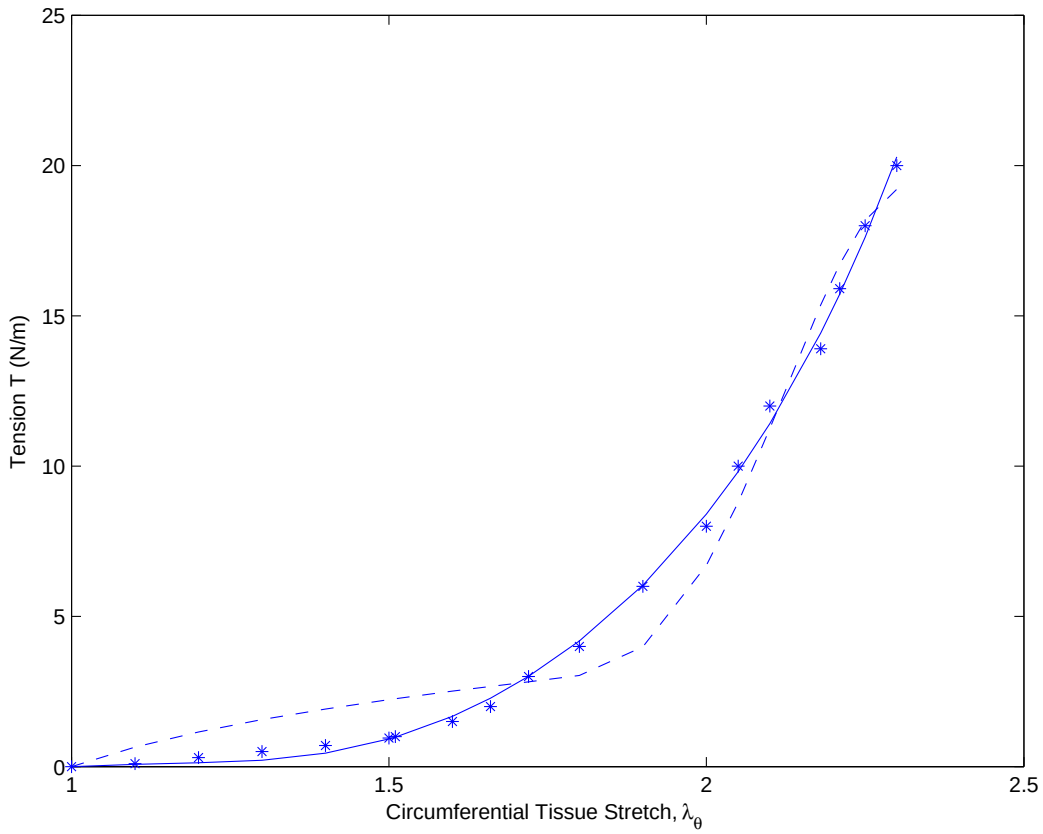

Figure 3.6: Tension-stretch curves for neo-Hookean elastin and isotropic collagen. The asterisks (*) indicate the experimental data, the full line (—) represents the 'best' fitting theoretical results for $\lambda_{rec,0} = 1.2$ and the dashed line (–) is for theoretical results for $\lambda_{rec,0} = 1.76$.

The tension $T = PR\lambda_\theta$ in terms of stretches then becomes

$$T = \frac{H}{\lambda_\theta}\left[n_e k_1^e\{e^{[k_2^e(\lambda_\theta^2+\lambda_\theta^{-2}-2)]}\}(\lambda_\theta^2-\lambda_\theta^{-2}) + 2n_{c,0}k_1^c(\lambda_c^2+\lambda_c^{-2}-2)\{e^{[k_2^c(\lambda_c^2+\lambda_c^{-2}-2)^2]}\}(\lambda_c^2-\lambda_c^{-2})\right]. \tag{3.92}$$

The relation between the elastin and collagen circumferential stretches , λ_θ and λ_c, remains the same as given by (3.88).

The results of the regression analysis show negative values of $\lambda_{rec,0}$ when this parameter is set free. This is not physical and therefore we exclude it. Values of $\lambda_{rec} = 1, 2$ and 1.76 result in negative strain energy functions for collagen, which still is not acceptable on physical grounds. We conclude that the exponential model based on different expressions for the elastic energy, i.e. (3.80) for W_e and (3.81) for W_c, does not yield an acceptable fit for the material parameters, and therefore should be rejected.

We thus took up the case of both constituents having the same form of strain energy function as given by (3.80). Note that this is also the form used by Wulandana and Robertson; see [46, 47]. In this case we have the tension-stretch relationship:

$$T = \frac{H}{\lambda_\theta}\left[n_e k_1^e\{e^{[k_2^e(\lambda_\theta^2+\lambda_\theta^{-2}-2)]}\}(\lambda_\theta^2-\lambda_\theta^{-2}) + n_{c,0}k_1^c\{e^{[k_2^c(\lambda_c^2+\lambda_c^{-2}-2)]}\}(\lambda_c^2-\lambda_c^{-2})\right]. \tag{3.93}$$

A value of 1.76 resulted in negative strain energy function, but the following parameters were obtained for $\lambda_{rec,0} = 1.2$:

$$n_e k_1^e = 861.44\text{Pa}, k_2^e = 1.1796, n_{c,0} k_1^c = 1861.68\text{Pa}, k_2^c = 1.71897. \tag{3.94}$$

The latter choice thus yields, in principle, an acceptable set of material parameters. Note here too that this result suggests that the collagen is stronger than the elastin, which is reasonable. The least-squares result has an R^2-correlation of 0.9026 with the experimental results and a comparison is provided in Figure 3.7. We observe that this result is not so bad, but by far not as good as the previous result in Figure 3.6 for the same value of $\lambda_{rec,0}$.

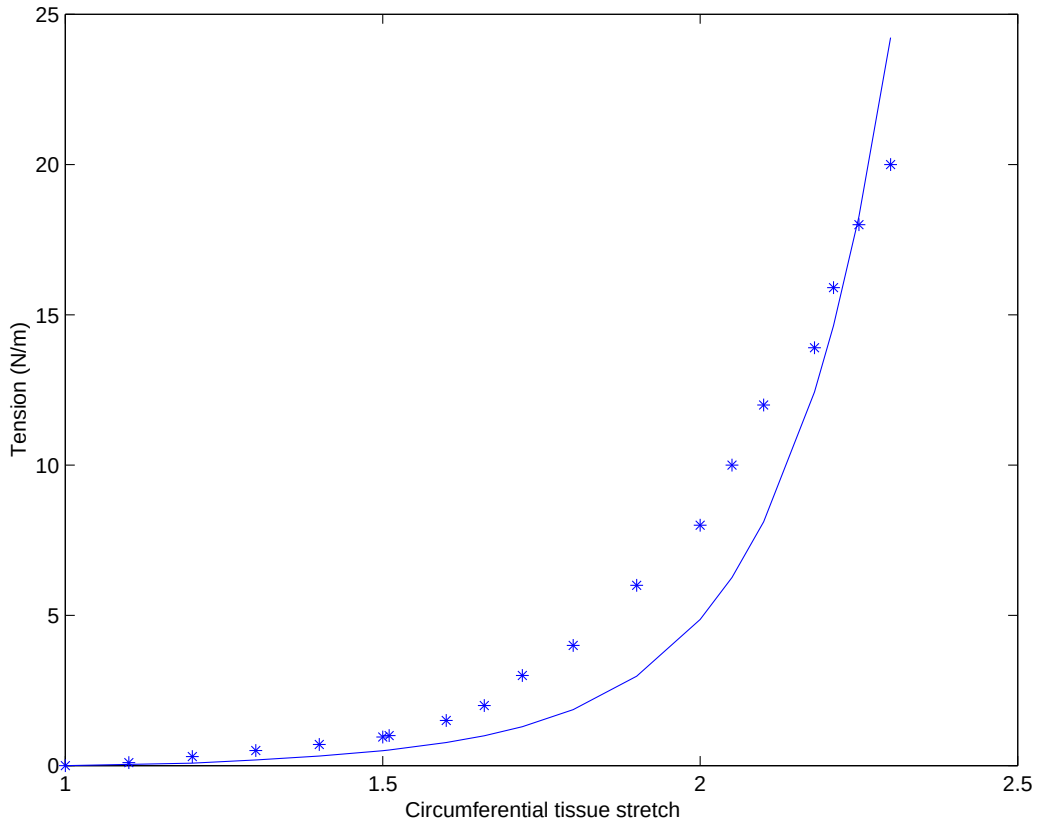

Figure 3.7: Tension-stretch curve for exponential elastin and isotropic collagen, based on (3.80). The asterisks (*) represent the experimental data and the solid line (—)is a theoretical result with $\lambda_{rec,0} = 1.2$

3.8.3 Anisotropic Models

Using the constitutive equations based on (3.79) and (3.82)-(3.83) for elastin and collagen, respectively, we will characterize two anisotropic models: the traditional mixture model and the modified mixture model.

Traditional Mixture Model

For the case of the traditional mixture model, the pressure-stretch relationship has been derived in Section 3.6 and the resulting relation is given by (3.65).

In this part, we have an additional unknown, namely γ, the collagen fiber angle. We can either take it to be an unknown in the regression analysis or give it a specific value from literature. In the latter case, we will follow Oijen [26] and take $\gamma = 36.5°$.

Using $\gamma = 36.5°$and $\lambda_{rec,0} = 1.2$ results in a set of best fit parameters with negative value for $n_e C_e$, which clearly is not justifiable. When the angle γ is taken to be a free parameter, the following results are obtained:

$$n_e C_e = 40036.5 \text{ Pa}, \quad n_c k_1 = 64.60 \text{ Pa}, \quad k_2 = 241.38, \quad \gamma = 78.19°. \tag{3.95}$$

The R^2 correlation for this set of parameters is 0.541, which is clearly not a good fit. Another point worth mentioning is that the angle γ obtained is so large that the maximum value of λ_γ for the circumferential stretches recorded in the experiment is 1.086, which is less than the initial recruitment parameter. Note that this means the collagen did not contribute to the load carrying throughout the whole experiment. The resulting tension-stretch curve in Figure 3.8 confirms the bad correlation of this model with the experimental data. The theoretical (least-square fit) curve in Figure 3.8 resembles that of a Neo-Hookean membrane, which is expected if the collagen remains 'crimped' throughout the loading history.

Modified Mixture Model

Applying the mixture rule only in the direction of the fibers [26, p. 14], we obtain the constitutive relation as:

$$\begin{aligned} \mathcal{T} = -p\mathcal{I} + \mathcal{T}_e \quad &+ \quad n_{c,1}\tau_{f,1}\left[\mathbf{e}_{c,1}\otimes\mathbf{e}_{c,1}\right] + (n_e-1)(\mathbf{e}_{c,1}\cdot\mathcal{T}_e\mathbf{e}_{c,1})\left[\mathbf{e}_{c,1}\otimes\mathbf{e}_{c,1}\right] \\ &+ \quad n_{c,2}\tau_{f,2}\left[\mathbf{e}_{c,2}\otimes\mathbf{e}_{c,2}\right] + (n_e-1)(\mathbf{e}_{c,2}\cdot\mathcal{T}_e\mathbf{e}_{c,2})\left[\mathbf{e}_{c,2}\otimes\mathbf{e}_{c,2}\right], \end{aligned} \tag{3.96}$$

where the $\tau_{f,i}$ and $\mathbf{e}_{c,i}$ are the fiber stress and unit vector in the direction of the collagen fiber, respectively, and $\mathcal{T}_e$ is the elastin stress tensor, which will be specified further on.

From (3.96), we obtain the radial and circumferential stresses in the tissue,

$$t_{rr} = \mathbf{e}_r\cdot\mathcal{T}\mathbf{e}_r = -p + T_{e,rr}, \tag{3.97}$$

and

$$\begin{aligned} t_{\theta\theta} &= \mathbf{e}_\theta\cdot\mathcal{T}\mathbf{e}_\theta \\ &= -p + T_{e,\theta\theta} + n_{c,1}\tau_{f,1}\mathbf{e}_\theta\cdot\left[\mathbf{e}_{c,1}\otimes\mathbf{e}_{c,1}\right]\mathbf{e}_\theta + (n_e-1)(\mathbf{e}_{c,1}\cdot\mathcal{T}_e\mathbf{e}_{c,1})\mathbf{e}_\theta\cdot\left[\mathbf{e}_{c,1}\otimes\mathbf{e}_{c,1}\right]\mathbf{e}_\theta \\ &+ n_{c,2}\tau_{f,2}\mathbf{e}_\theta\cdot\left[\mathbf{e}_{c,2}\otimes\mathbf{e}_{c,2}\right]\mathbf{e}_\theta + (n_e-1)(\mathbf{e}_{c,2}\cdot\mathcal{T}_e\mathbf{e}_{c,2})\mathbf{e}_\theta\cdot\left[\mathbf{e}_{c,2}\otimes\mathbf{e}_{c,2}\right]\mathbf{e}_\theta. \end{aligned} \tag{3.98}$$

Introducing the fiber angle γ by means of the relations (3.52)-(3.53) for $\mathbf{e}_{c,i}$ in (3.98), we obtain the following expression for the circumferential stress:

$$t_{\theta\theta} = -p + T_{e,\theta\theta} + (n_{c,1}\tau_{f,1} + n_{c,2}\tau_{f,2})\left(\frac{\lambda_\theta\cos\gamma}{\lambda_\gamma}\right)^2 + (n_e-1)\left(\frac{\lambda_\theta\cos\gamma}{\lambda_\gamma}\right)^2\left[\mathbf{e}_{c,1}\cdot\mathcal{T}_e\mathbf{e}_{c,1} + \mathbf{e}_{c,2}\cdot\mathcal{T}_e\mathbf{e}_{c,2}\right]. \tag{3.99}$$

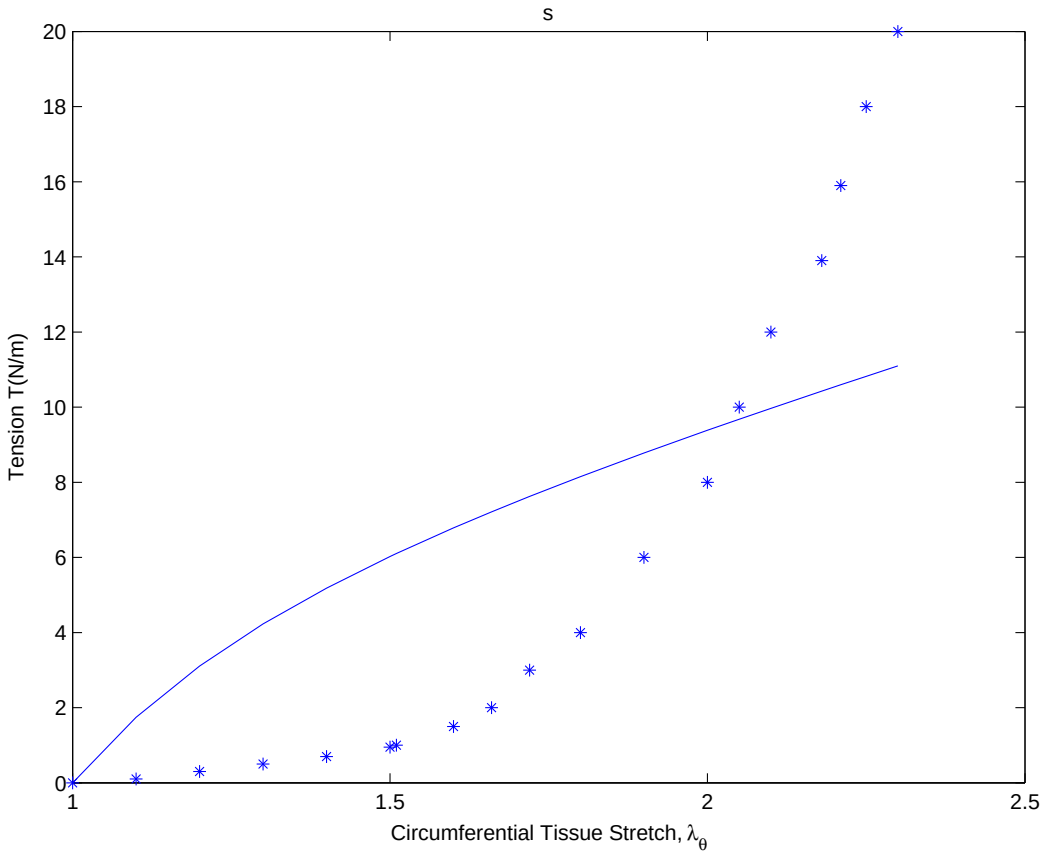

Figure 3.8: Tension-Stretch Curves for an Anisotropic Model with the Traditional Mixture Rule. The asterisks (*) represent the experimental data and the solid line (—) is a theoretical result.

With fiber stresses in the two directions being equal and an equal proportion of collagen fibers in the two direction, i.e $n_{c,1} = n_{c,2} = n_c/2$, the tangential stress becomes

$$t_{\theta\theta} = -p + T_{e,\theta\theta} + n_c \tau_f \left(\frac{\lambda_\theta \cos\gamma}{\lambda_\gamma}\right)^2 + 2(n_e - 1)\left(\frac{\lambda_\theta \cos\gamma}{\lambda_\gamma}\right)^2 \left[\left(\frac{\lambda_\theta \cos\gamma}{\lambda_\gamma}\right)^2 T_{e,\theta\theta} + \left(\frac{\sin\gamma}{\lambda_\gamma}\right)^2 T_{e,zz}\right]. \tag{3.100}$$

Note that (3.100) is independent of the constitutive equations used for elastin and the fiber stress. To find a final form suitable for the regression analysis, we substitute the neo-Hookean model for elastin, using (3.16) and (3.79). Setting the radial stress to zero to obtain the hydrostatic pressure term and substituting the result in the equation for circumferential stress, we arrive at

$$t_{\theta\theta} = C_e(\lambda_\theta^2 - \lambda_\theta^{-2}) + n_c \tau_f \left(\frac{\lambda_\theta \cos\gamma}{\lambda_\gamma}\right)^2 + 2C_e(n_e - 1)(\lambda_\theta^2 - 1)\left(\frac{\lambda_\theta \cos\gamma}{\lambda_\gamma}\right)^4. \tag{3.101}$$

From the circumferential stress, we can obtain the tension T, and the applied pressure P, and after that we go on with the nonlinear regression. A notable difference in the statistical analysis of the modified mixture rule from the traditional mixture rule is that in the former

the elastin volume fraction and its shear modulus can not be aggregated into a single parameter. We either have to obtain both of them independently from the regression analysis or assume a certain value for the elastin volume fraction of a healthy artery, preferably from a morphological experiment. We consider both cases here.

Setting all parameters $(C_e, n_e, n_c k_1, k_2, \lambda_{rec})$ free gives a result with negative recruitment stretch. On the other hand, assuming initial recruitment stretches of 1.2 and 1.76 and setting the remaining parameters free yields unphysical results in which n_e is greater than one. Prescribing an initial fiber angle of 36.5 degrees and setting the remaining parameters free gives a negative strain energy function, which is not physical either.

We obtain physically acceptable results only when the initial recruitment stretch is set to 1.2 and some values of elastin volume fraction. We invariably get poor correlation with least-square fit results similar to the one shown in Figure 3.8. In addition, the results show longitudinal fiber orientations, i.e $\gamma = 90^o$.

3.8.4 Conclusions

In this section we have considered different models for a cerebral arterial tissue, viz.

- isotropic models with
  - neo-Hookean elastin and exponential collagen (3.81);
  - exponential elastin (3.80) and exponential collagen(3.81);
  - exponential elastin (3.80) and exponential collagen (3.80).
- anisotropic models with
  - traditional mixture model;
  - modified mixture model.

We have tried to fit the material parameters of these models with a set of experimental data from Scott et al. [34] (see also [46]).
Based on the regression analysis presented here, we infer the following.

1. The isotropic models fit the experimental data evidently better than the anisotropic models do.

   This does not necessarily mean that cerebral arteries are definitely isotropic; there can be other anisotropic constitutive laws, which may better describe arterial response. However, it provides a strong case for the viability of isotropic constitutive relations for modelling cerebral arteries.

   Using bi-axial testing on canine aorta, Fung and Zhou [12] showed that the aorta is definitely anisotropic. For cerebral arteries, however, there is a lack of such a definitive mechanical experiment [47]. A morphology study at the apex of bifurcation of cerebral arteries [10] showed that collagen fibers have no specific fiber orientation; see Section 2.3.1 for details. Although not as compelling as a result from bi-axial or tri-axial mechanical analysis, this result can also be taken as an additional motivation for considering isotropic constitutive models for cerebral arteries.

   As the experimental data used in our statistical analysis is essentially uni-axial, nothing can be inferred from it about the bi-axial or tri-axial behavior of the wall. Hence, we

can not definitely conclude that the isotropic model is always a good model (especially for a 3-dimensional analysis), but we can say that the anisotropic models considered in this work are not adequate models for a cerebral arterial tissue.

2. Among the isotropic models considered, the model with neo-Hookean elastin and exponential (3.81) collagen, and an initial recruitment value $\lambda_{rec,0} = \lambda_\theta = 1.2$ gives the best correspondence with the experimental data. This correspondence is very good, as can be seen from Figure 3.6.

Recall that taking the initial recruitment stretch $\lambda_{rec,0}$ as a free parameter in our regression analysis did not yield satisfactory results. The best result was found for the ad hoc choice $\lambda_{rec,0} = 1.2$. We must admit that this is a bit in contrast with the experimentally predicted value of 1.76; see Section 3.8.1.

We have not used the post-shifting curve in this analysis. Wulandana and Robertson [47] use both the pre and post-shifting curves to carry out a joint regression analysis for the two mechanisms they consider. The post-shifting curve may be used to characterize arteries at the terminal stage of aneurysms.

For the anisotropic model with the traditional mixture rule, Machyshyn [23] uses the material parameters $n_e C_e = 5$KPa, $n_c k_1 = 2$KPa, $k_2 = 20$, a fiber angle of 30°, and circumferential tissue stretches of 1.2 and 1.4 at initial collagen recruitment and collagen attachment respectively. Using (3.51) this means stretches of 1.15 and 1.31 in the fiber directions at initial recruitment and attachment, respectively, thus an attachment collagen stretch of $1.31/1.15 = 1.14$. These material parameters result in a very stiff collagen where the pressure versus circumferential tissue stretch curve becomes almost vertical after a circumferential stretch of about 1.4. This is in sharp contrast to the experimental results from Scott et al. [34]. While the experimental data [34] shows that the systolic pressure is attained at circumferential stretch of 2, the material parameter set from Machyshyn [23] predicts pressure of the order 10^{19}KPa for a circumferential stretch of 2.

Chapter 4

Numerical Simulations - Thin Walled Membranes

4.1 Introduction

In this chapter, we consider numerical simulations of inflation due to degradation of elastin in thin-walled cylinders and spheres under internal pressure. Recall that arteries are thick in reality and our assumption of thin walls is used to simplify the analysis; membrane approximation of blood vessel walls is common in the relevant literature [22, 46, 47].

Anisotropic cylindrical vessels, isotropic cylindrical vessels and isotropic spherical membranes will be discussed in this order.

We first pressurize the cylinder or sphere until the initial attachment state is reached. After that, the pressure will be held constant and elastin degradation commences, which in turn triggers collagen remodelling.

The results for the different models will be discussed, and the influence of material parameters will be investigated, as will be the pattern of elastin degradation.

In the numerical simulation of cylindrical membranes the emphasis is on comparing isotropic and anisotropic material laws. As discussed in Chapter 3, the anisotropic models did not fit well to the experimental data from Scott et al. To compare isotropic and anisotropic models under aneurysmal conditions, we need material parameters such that the two models in some way respond similarly in the healthy state. During our statistical analysis, we observed that a good fit (or even a poor yet physically sound fit) between the pressure-stretch response of the isotropic and anisotropic models can not be obtained when circumferential stretches above 1.5 are taken into account. On the other hand, according to the pressure-stretch curve from Scott el al. [34, 46] (see a reproduced plot in Fig. 3.5) circumferential stretches of 2 are encountered at the systolic pressure ($\approx$12KPa in cerebral arteries). This makes it difficult to have material parameters for the isotropic and anisotropic models fitting reasonably to the experimental results of Scott et al. [34, 46] and at the same time complying with the assumption that the attachment state is reached at the systolic pressure. We thus used the material parameters for the anisotropic models from Machyshyn [23], which predict a circumferential tissue stretch λ_θ of 1.473[†] at systole, and carried out a regression analysis to obtain material parameters for the isotropic model, which result in a similar pressure-stretch

[†]We give this value with such precision because the pressure-stretch relationship has high derivatives in this range. A small change in the stretch requires a significant change in pressure.

curve for circumferential tissue stretches up to 1.5. We use the pressure-stretch relationships (3.65) and (3.76) for anisotropic and isotropic models, respectively. Note that we can use the term PR/H as the dependent variable and carry out the regression analysis without assigning specific numerical values for the undeformed radius and thickness. Our results show that the isotropic material parameters corresponding to $n_e C_e = 5$KPa, $n_c k_1 = 2$KPa and $k_2 = 20$ in the anisotropic model [23], are 5KPa, 36KPa, and 60, respectively. Figure 4.1 shows the pressure-stretch curves for the two models and the above material parameters. The fits yield a very good correspondence for stretches up to 1.5.

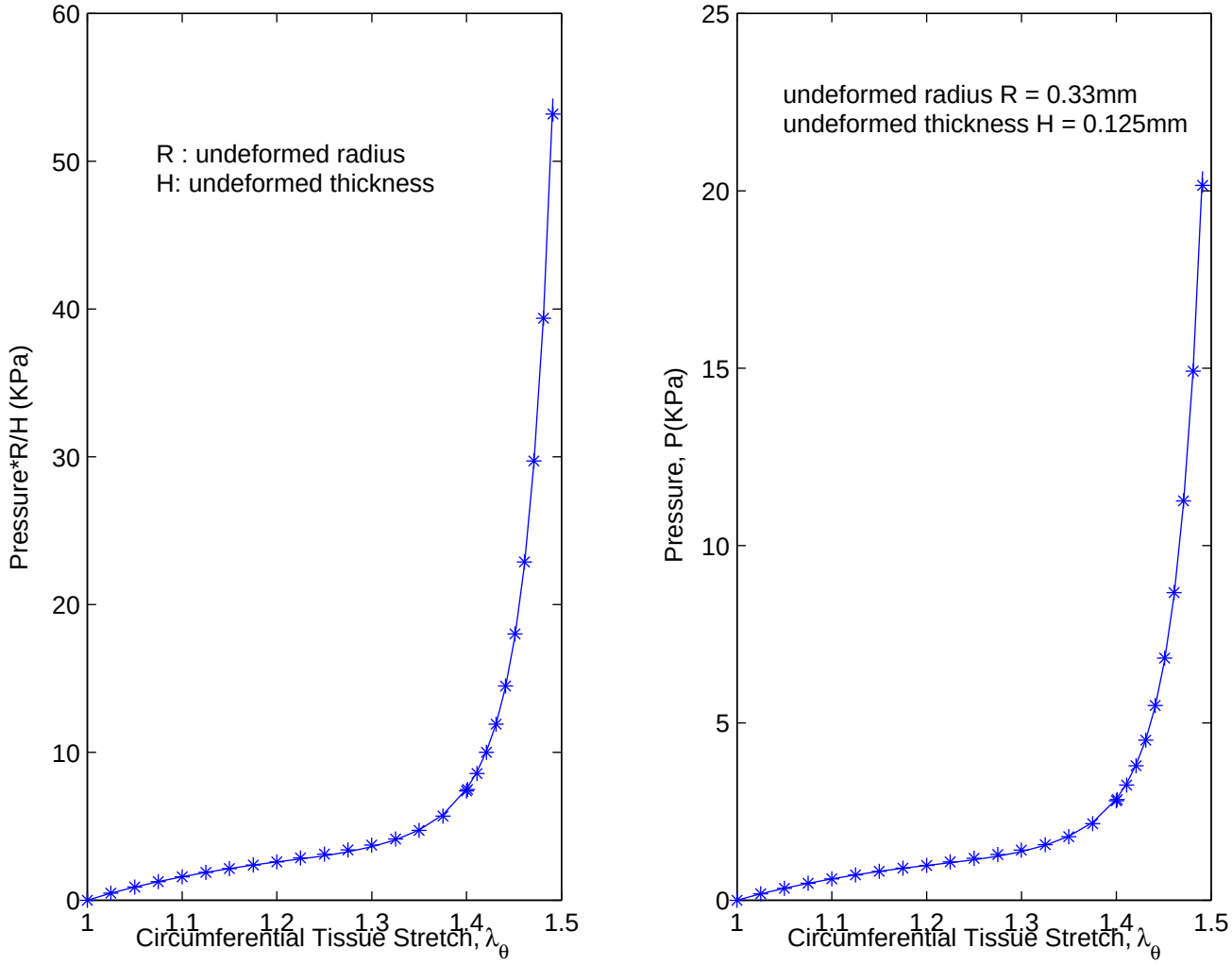

Figure 4.1: Pressure-Stretch Curves for Anisotropic Material Parameters from Machyshyn [23] (*) and Isotropic Material Parameters Obtained Via Least-Squares Fit (—); the figure on the left is the one used for the regression analysis. The figure on the right shows pressure-stretch relations for a specific case of radius and thickness which corresponds to the dimensions of a cerebral artery.

It is not known how much of the collagen content is cross-linked and active or not cross-linked and passive. We will consider different values of the initial volume fractions and study

their effects.

The equations involved in the numerical simulations, their discretized forms and a discussion on the results are given in each of the following sections on, successively, cylindrical vessels with anisotropic and isotropic collagen, and spherical vessels with isotropic collagen. Conclusions resulting from these discussions and additional relevant remarks are provided in the final section of this chapter.

4.2 Cylindrical Vessels with Anisotropic Collagen

In the early period of pressurization, where the tissue stretch in the direction of collagen fibers, λ_γ, is less than the initial recruitment stretch $\lambda_{rec,0}$, the second term in (3.65) is zero as $\lambda_c = 1$. In the intermediate stage, in which the collagen is involved in the load carrying but is not stretched to the attachment value, we have $\lambda_c = \lambda_\gamma/\lambda_{rec,0}$, $n_e = n_{e,0}$, and $n_c = n_{c,0}$. At the end of this stage, the collagen stretch is equal to the attachment stretch. Elastin degradation is assumed to happen after collagen is attached.

4.2.1 Degradation and Remodelling

Starting from the healthy state described by (3.65), we now proceed by considering a uniform degradation given by (3.24), recruitment equation (3.27), and thickening equation (3.28) or (3.33). With a uniform internal pressure, a uniform degradation will result in homogenous deformation and thus remodelling. Therefore, we replace the partial derivatives in the remodelling equations by simple derivatives with respect to time and list them below for easy reference:

$$\begin{aligned} &C_e(t) = C_{e,0}c(t), \\ &\frac{d\lambda_{rec}}{dt} = \alpha(\lambda_c - \lambda_a), \qquad \lambda_{rec}(0) = \lambda_{rec,0}, \\ &\frac{dn_c}{dt} = \beta(\lambda_c - \lambda_a), \qquad n_c(0) = n_{c,0}. \end{aligned} \tag{4.1}$$

The initial time $t = 0$ corresponds to the attachment state (systole) where elastin degradation starts.

4.2.2 Discretized Equations

We numerically solve the mechanical equations, stretch relations, and remodelling equations with the associated initial conditions. For ease of reference we list the concerned equations here:

$$\begin{aligned} &\lambda_\gamma = \sqrt{\lambda_\theta^2 \cos^2\gamma + \sin^2\gamma}, \\ &\lambda_c = \frac{\lambda_\gamma}{\lambda_{rec}}, \\ &n_e C_e(\lambda_\theta^2 - \lambda_\theta^{-2}) + 2n_c k_1 \left(\frac{\lambda_\theta \cos\gamma}{\lambda_\gamma}\right)^2 \lambda_c^2(\lambda_c^2 - 1)e^{[k_2(\lambda_c^2-1)^2]} = \frac{PR}{H}\lambda_\theta^2, \\ &\frac{d\lambda_{rec}}{dt} = \alpha(\lambda_c - \lambda_a), \qquad \lambda_{rec}(0) = \lambda_{rec,0}, \\ &\frac{dn_c}{dt} = \beta(\lambda_c - \lambda_a), \qquad n_c(0) = n_{c,0}. \end{aligned} \tag{4.2}$$

The above system of equations is a nonlinear system of differential algebraic equations (DAE's) for the unknown time-dependent variables $\lambda_\gamma(t), \lambda_c(t), \lambda_\theta(t), \lambda_{rec}(t)$ and $n_c(t)$. We use the implicit Euler method for the time integration*. This results in the nonlinear system

*We will also use the explicit Euler method and compare the results. This comparison is important as the finite element implementation in Sepran® is based on explicit time integration, which can potentially suffer from numerical instabilities at large time steps.

of algebraic equations:

$$\begin{aligned}
&\lambda_{\gamma,i} = \sqrt{\lambda_{\theta,i}^2 \cos^2\gamma + \sin^2\gamma},\\
&\lambda_{c,i} = \frac{\lambda_{\gamma,i}}{\lambda_{rec,i}},\\
&n_e C_{e,i}(\lambda_{\theta,i}^2 - \lambda_{\theta,i}^{-2}) + 2n_{c,i}k_1\left(\frac{\lambda_{\theta,i}\cos\gamma}{\lambda_{\gamma,i}}\right)^2 \lambda_{c,i}^2(\lambda_{c,i}^2-1)e^{[k_2(\lambda_{c,i}^2-1)^2]} = \frac{P_i R}{H}\lambda_{\theta,i}^2, \quad (4.3)\\
&\frac{\lambda_{rec,i} - \lambda_{rec,i-1}}{\Delta t} = \alpha(\lambda_{c,i} - \lambda_a),\\
&\frac{n_{c,i} - n_{c,i-1}}{\Delta t} = \beta(\lambda_{c,i} - \lambda_a),
\end{aligned}$$

where $i = 1, 2, 3..., \lambda_{\theta,i} = \lambda_\theta(t_i), \lambda_{\gamma,i} = \lambda_\gamma(t_i), \lambda_{rec,i} = \lambda_{rec}(t_i), \lambda_{c,i} = \lambda_c(t_i), n_{c,i} = n_c(t_i), C_{e,i} = C_{e,0}c(t_i)$, and $t_i = i\Delta t$. The discrete stage $i = 0$ refers to the beginning of elastin degradation.

If we use explicit time integration, we use forward difference approximations for the time derivatives and the last two equations in the above system of algebraic equations will be replaced by

$$\frac{\lambda_{rec,i+1} - \lambda_{rec,i}}{\Delta t} = \alpha(\lambda_{c,i} - \lambda_a), \quad (4.4)$$

$$\frac{n_{c,i+1} - n_{c,i}}{\Delta t} = \beta(\lambda_{c,i} - \lambda_a). \quad (4.5)$$

The default time integration method we are using is the implicit (forward) time integration. When we use explicit time integration, we will specify that.

Unless specified otherwise, the pressure P through out the aneurysmal state is constant and is equal to the systolic pressure[†].

If the logistic thickening rule is used, we have

$$\frac{n_{c,i} - n_{c,i-1}}{\Delta t} = \beta(\lambda_{c,i} - \lambda_a)(n_{max} - n_{c,i}), \quad (4.6)$$

instead of the last equation in (4.3).
The Newton-Raphson method is employed to solve the system of nonlinear algebraic equations (4.3) at each time step.

The applied pressure P, the material coefficient k_1 and the elastin shear modulus $C_e(t)$ are scaled on the maximum elastin shear modulus $C_{e,0}$. A characteristic time scale was taken to be the time it takes for the elastin to degrade from its maximum stiffness to the minimum one, i.e. T. The remodelling parameters α and β are scaled on T^{-1}.

Note that the value of $\lambda_{rec,0}$ should be so chosen that the tissue, which behaves as a neo-Hookean material prior to the initial recruitment, does not become unstable before collagen gets involved. In the case we are considering now this does not happens as can be seen from (3.65) by setting $\lambda_c = 1$: the pressure is a monotonously increasing function of λ_θ for $\lambda_\gamma \leq \lambda_{rec,0}$. However, such a phenomenon is possible in the case of a spherical membrane where a neo-Hookean material exhibits limit point instabilities.

In selecting the remodelling parameters α and β we follow the idea of Watton et al. [44], i.e determining α based on the half-life of collagen and choosing β so as to obtain physiologically

[†]The pressure can be increased to investigate the effect of hypertension on aneurysms.

consistent growth rates. Although the half-life of collagen is 3-90 days (it may also be longer), Watton et al. [44] reported that using $\alpha = 12$, which corresponds to a collagen half-life of 180 days, and $130 < \beta < 150$ resulted in physiologically consistent growth rates for aortic abdominal arteries. We will use $0 \leq \alpha \leq 60$ (corresponding to half-lives of 42 days and above) and $0 \leq \beta \leq 200$ and investigate their influence.
Unless specified otherwise, we use $R = 0.33$mm, $H = 0.125$mm, $\gamma = 30^\circ$, $\lambda_{\theta,rec,0} = 1.2$ ($\lambda_{rec,0} = 1.15$), $\lambda_{\theta,a} = 1.473$ ($\lambda_a = \lambda_{\gamma,a}/\lambda_{rec,0} = 1.19$), $n_e C_e = 5$KPa, $n_c k_1 = 2$KPa and $k_2 = 20$.

4.2.3 Results and Discussions

Degradation Functions

We considered convex, linear, concave, sigmoid and step degradation functions $c(t)$. As shown in Fig. 4.2[‡], linear and concave degradation functions result in collagen stretch λ_c, which does not show any tendency of abating to the attachment stretch λ_c during the degradation, $t \in [0, 1]$; this was true for all values of α and β we considered. This may be attributed to the progressively high rate of elastin degradation which is faster than collagen remodelling. For concave degradation functions, the growth pattern observed was always convex. For convex degradation functions, the growth was concave for those values of α and β which resulted in a stable growth; see Figure 4.2(b). By a stable growth, we refer to a scenario in which the tissue stretch λ_θ attains a steady state value within the degradation period or a 'reasonable' time span after elastin ceases to degrade. Only for a stable growth, the collagen stretch λ_c attends the attachment value λ_a after the degradation has stopped, i.e. for $t > 1$. In a process of unstable growth (Figure 4.2(a)), the latter is not true, and, moreover, the tissue stretches, e.g. λ_θ, seem to grow indefinitely, at least over a period of two times the degradation time ($t \leq 2$). For those cases in which the growth became stable, the final tissue stretch depends on the final value of the elastin stiffness *irrespective of the degradation pattern.*

Typical stable growths from step and sigmoid degradation functions are shown in Fig. 4.3. Here too we see that for given α and β the final size depends on the minimum value of the elastin shear modulus with higher loss of elastin inducing higher growth. Note also that where the degradation is sharp, the remodelling is sharp too, implying that the process is driven by elastin degradation.

Remodelling Parameters

Our numerical simulations reveal that the remodelling parameters α and β have pronounced effects on stretches and stresses. Both the ratio β/α and numerical values of the parameters are important. The effect of the remodelling parameters on stretches and stresses is depicted in Figs. 4.4-4.6.

For a given value of α, a higher value of β results in lower tissue stretches and stresses. The effect is best manifested in the circumferential stress $t_{\theta\theta}$, whereas there is no qualitative effect on the longitudinal stress t_{zz}; compare Fig 4.4, where $\alpha = 12, \beta = 10$ and Fig. 4.5, for $\alpha = 12, \beta = 200$. Similarly, for a given β, increasing α increases the stretches and stresses as

[‡]All figures from the numerical simulation are placed at the end of the chapter.
REMARK: In some of the figures we have serial numbers 'I' and 'II' following the word 'collagen'. Note that these are just tags for the figures and do not refer to Type I or Type II collagen.

shown in Figure 4.6. Note that the total longitudinal stress t_{zz} reduces in all cases, although its collagen part increases.

We observe further that $t_{\theta\theta}$ is almost a factor of 10 greater than t_{zz}, and also that the contribution of collagen to the total stress is about the same amount greater than that of elastin. Note in Fig. 4.4 and 4.5 that although the collagen stretch λ_c reduces after some time (part (a) of the figures), its contributions to the total circumferential stress $t_{\theta\theta}$ and longitudinal stress t_{zz} continue to increase (part (b)); this is due to thickening.

Values of β/α less than a certain critical value do not result in a steady-state tissue size, i.e. stable growth. For one set of material parameters we have found for this ratio a critical value around 3; see Fig. 4.7(a). Note however that this critical value is not independent of α. In Fig. 4.7(b), where $\alpha = 60$, we see that this critical value is about 2. For the range of remodelling parameters we considered, the ratio decreases with α. A plot of β versus α demarcating stable and unstable growth results in a curve which is initially concave and then becoming more or less affine for $\alpha > 30$; see Fig 4.8.

Machyshyn [24] carried out a perturbation analysis and found a condition $L = L(\lambda_\theta, \beta/\alpha) < \lambda_a$ for a stable recruitment which attenuates the collagen stretch.

The numerical observation that β/α is an important remodelling parameter can analytically be corroborated by dividing the recruitment (3.27) and thickening (3.28) equations by α and β, respectively, subtracting the resulting equations from one another and integrating with respect to time. By so doing, we arrive at

$$n_c(\mathbf{x}, t) = \frac{\beta}{\alpha}(\lambda_{rec}(\mathbf{x}, t) - \lambda_{rec,0}(\mathbf{X})) + n_{c,0}(\mathbf{X}). \tag{4.7}$$

For a uniform degradation with homogenous deformations all terms in (4.7) are functions of time only.

Implicit versus Explicit Time Integration

For linear transient problems implicit integrators are unconditionally stable[†]. The unconditional stability of implicit integrators has not been proven for all nonlinear problems, although specific results indicate that unconditional stability holds for certain classes of problems. Here we will compare solutions obtained using both implicit and explicit time integration using different time steps for an otherwise similar problem.

In Fig 4.9(a), results of numerical simulations using implicit time integration with time steps of 0.1, 0.04 and 0.004 for $\alpha = 12$ and $\beta = 200$ are presented. It can be seen that there is no significant difference between the solutions with the different time steps, especially between the two lesser values. On the other hand, Fig. 4.9(b) shows that the solution obtained with $\Delta t = 0.04$ shows numerical instabilities (oscillations) in the degradation period $t \in [0, 1]$. Note however that the steady-state solution does not oscillate. The explicit time integration solution with $\Delta t = 0.1$ is given in Fig. 4.10(a). Here, the solution oscillates wildly and eventually breaks down. We discovered that the reason of the break down is as a result of a singularity ∞/∞ in the calculation of the incremental stretch[‡]. We also observed out-of-

[†]Here we are referring to the stability of the numerical method used in the solution and not the stability of the physical system involved such as a limit point instability.

[‡]The incremental stretch at the i^{th} Newton-Raphson iteration in a given time step is given by $\Delta\lambda_{\theta,i} = -f(\lambda_{\theta,i})/f'(\lambda_{\theta,i})$ where $f(\lambda_\theta) = 0$ is the pressure-stretch relationship for that time step. Note that in the explicit time integration λ_{rec} and n_c are known by projecting from the previous time step and thus become parameters and not independent variables in the pressure-stretch relationship of the current time step.

balance stresses, i.e differences between the stresses calculated from the constitutive relations and those calculated from the equilibrium equations, becoming very high prior to breakdown of the computations.

The sensitivity of the explicit time integration solution to time steps depends on the problem parameters. For instance, it can be observed from Fig 4.10(b) that the oscillations in the numerical simulations increase with β. Note also that while the numerical solutions with explicit integration and $\Delta t = 0.04$ are stable in the post-degradation time, i.e $t > 1$, for $\alpha = 12, \beta = 200$ (Fig 4.9(b)), but the solutions with the same time step are unstable throughout the whole time span for another set of remodelling parameters (Fig 4.10(b)).

In the remaining sections of this work, we consider only implicit time integration.

Delayed Remodelling

When the elastin starts to degrade, remodelling may not immediately kick off. To somehow capture this we prevented remodelling for 40% of the characteristic time at the beginning, i.e. remodelling starting at $t = 0.4$. This value is chosen arbitrarily and we do not have any clinical evidence suggesting such a value.

Our numerical simulations suggest that for the same material parameters and degradation function the deformations and stresses for the delayed remodelling become the same as the non-delayed remodelling with time, provided the remodelling parameters are such that the growth stabilizes; see Fig 4.11. Note in the delayed response that although the collagen initially has relatively higher stretch λ_c, the tissue stresses do not change. This may be explained by the lower volume fraction of collagen in the initial stages of the delayed response.

For remodelling parameters, which do not result in a stable size at or in the vicinity of the end of elastin degradation, the delayed and non-delayed response result in different stretches and stresses throughout the time span we considered; a typical example is given in Fig 4.12. However, especially the differences in the stresses remain very small. Hence, we conclude that delaying the remodelling has only a minor effect on the ultimate results.

4.3 Cylindrical Vessels with Isotropic Collagen

In this section, we consider a cylindrical vessel made of an isotropic material. As described in Sections 3.3 and 3.7, the initial recruitment state is a function of the first invariant of the elastin deformation gradient, whereas the recruitment and thickening of collagen during remodelling are governed by the first invariant of collagen deformation. The elastin and collagen deformation gradients are related to each other through a recruitment deformation gradient as shown by (3.69). The pressure-stretch relationship is described by (3.76).

We use two sets of material parameters. For the purpose of comparing isotropic and anisotropic response we use the material parameters obtained in Section 4.1, which result in the same healthy state pressure-stretch curve as the anisotropic model for circumferential stretches upto 1.5. As discussed in Section 3.8 this set of material parameters results in a very stiff response as opposed to the experimental result from Scott et al. [34]. Therefore, we also carry out numerical simulations using material parameters that are in compliance with this experiment and compare the results with the first material parameter set.

4.3.1 Degradation and Remodelling

We consider a uniform elastin degradation given by (3.24). The remodelling equations are given by (3.29) and (3.30). With the homogenous degradation considered here, the evolution equations for remodelling reduce from a set of partial differential equations in space and time to a set of ordinary differential equations in time resulting in

$$\frac{ds_{rec}}{dt} = \alpha(s(\mathcal{F}_c) - s_a), \qquad s_{rec}(0) = s_{rec,0}, \tag{4.8}$$

$$\frac{dn_c}{dt} = \beta(s(\mathcal{F}_c) - s_a), \qquad n_c(0) = n_{c,0}, \tag{4.9}$$

where

$$s(\mathcal{F}_c) = \mathrm{tr}(\mathcal{F}_c) = \lambda_c + \lambda_c^{-1} + 1. \tag{4.10}$$

The attachment invariant s_a is the first invariant of the collagen deformation gradient at attachment, i.e $s_a = \mathrm{tr}(\mathcal{F}_c)|_{\lambda_c=\lambda_a}$. Analogously we have $s_{rec,0} = \mathrm{tr}(\mathcal{F}_e)|_{\lambda_\theta=\lambda_{rec,0}}$.
The same values are used for the remodelling parameters α and β as in the anisotropic model.

4.3.2 Discretized Equations

The set of differential algebraic equations that has to be solved is given by

$$\begin{aligned}
&C_e(t) = C_{e,0}c(t),\\
&\lambda_c = \frac{\lambda_\theta}{\lambda_{rec}},\\
&n_e C_e(\lambda_\theta^2 - \lambda_\theta^{-2}) + 2n_c k_1(\lambda_c^2 + \lambda_c^{-2} - 2)e^{[k_2(\lambda_c^2+\lambda_c^{-2}-2)^2]}(\lambda_c^2 - \lambda_c^{-2}) = \frac{PR}{H}\lambda_\theta^2,\\
&s(\mathcal{F}_{rec}) = \lambda_{rec} + \lambda_{rec}^{-1} + 1,\\
&s(\mathcal{F}_c) = \lambda_c + \lambda_c^{-1} + 1,\\
&\frac{ds_{rec}}{dt} = \alpha(s(\mathcal{F}_c) - s_a), \qquad s_{rec}(0) = s_{rec,0},\\
&\frac{dn_c}{dt} = \beta(s(\mathcal{F}_c) - s_a), \qquad n_c(0) = n_{c,0}.
\end{aligned} \tag{4.11}$$

Using Euler's implicit method for time integration, we have the following set of nonlinear algebraic equations to be solved at each discrete time step:

$$
\begin{aligned}
&C_{e,i} = C_{e,0} c_i, \\
&\lambda_{c,i} = \frac{\lambda_{\theta,i}}{\lambda_{rec,i}}, \\
&n_e C_{e,i}(\lambda_{\theta,i}^2 - \lambda_{\theta,i}^{-2}) + 2n_{c,i}k_1(\lambda_{c,i}^2 + \lambda_{c,i}^{-2} - 2)e^{[k_2(\lambda_{c,i}^2+\lambda_{c,i}^{-2}-2)^2]}(\lambda_{c,i}^2 - \lambda_{c,i}^{-2}) = \frac{P_i R}{H}\lambda_{\theta,i}^2, \\
&s(\mathcal{F}_{rec,i}) = \lambda_{rec,i} + \lambda_{rec,i}^{-1} + 1, \\
&s(\mathcal{F}_{c,i}) = \lambda_{c,i} + \lambda_{c,i}^{-1} + 1, \\
&\frac{s_{rec,i} - s_{rec,i-1}}{\Delta t} = \alpha(s(\mathcal{F}_{c,i}) - s_a), \\
&\frac{n_{c,i} - n_{c,i-1}}{\Delta t} = \beta(s(\mathcal{F}_{c,i}) - s_a).
\end{aligned}
\tag{4.12}
$$

Here too we employ the Newton-Raphson method to solve the system of nonlinear algebraic equations (4.12).

4.3.3 Results and Discussions

For isotropic cylindrical membranes, we consider two sets of material parameters. First we consider material parameters that result in the same healthy state pressure-stretch relationship as the anisotropic model considered in Section 4.2. It is to be recalled that we computed these parameters in Section 4.1; the numerical values so obtained being $n_e C_e = 5$KPa, $n_c k_1 = 36$KPa and $k_2 = 60$. The second set of material parameters to be considered comprises of $n_e C_e = 1.668$KPa, $n_c k_1 = 21.34$KPa and $k_2 = 0.0675$, which we obtained in Section 3.8 based on the experimental data of Scott et al. [34]. We use the same dimensions $R = 0.33$mm and $H = 0.125$mm. There is no notion of fiber angle in an isotropic model.

The essence of this section is on qualitative comparison of isotropic and anisotropic models, and among the two sets of material parameters for an isotropic tissue.

$\underline{n_e C_e = 5\text{KPa}, \; n_c k_1 = 36\text{KPa}, \; k_2 = 60}$

The influence of the degradation function is similar to that on the anisotropic model, i.e the terminal value of elastin shear modulus determines, to a large extent, how large the tissue will grow. As in the isotropic model, sharp degradations trigger fast remodelling.

Similarly, the relative proportion of the remodelling parameters affects the stresses and stretches. As in the case of the anisotropic model, a higher value of β/α results in low stretches and stresses; see Fig. 4.13 and Fig. 4.14*. The isotropic model has a smaller region in the $\alpha - \beta$ plane resulting in stable growth; compare Fig. 4.15(a) with the corresponding plot for the anisotropic model shown in Fig. 4.8. It can also be inferred from a comparison of these figures that the critical ratio of β/α for stable growth is larger for this isotropic model.

A comparison of growth rates and stresses of the isotropic and anisotropic models can be made using Fig. 4.13 for unstable growth and Fig. 4.14 for stable growth. The differences

*Note that in Fig. 4.13(a) and Fig. 4.14(a) different scales are used at the left (anisotropic) and right axes (isotropic).

in the deformation quantities are not significant. Stresses, however, show notable differences. Longitudinal tissue stresses always increase in isotropic models as opposed to the anisotropic model in which longitudinal stresses always reduce with degradation and remodelling. Circumferential stresses on the other hand differed only in cases of unstable growth. Circumferential stresses are the same in both models at the beginning of the degradation, i.e $t = 0$, whereas longitudinal stresses have different values at this time. This is due to the fact that we used the pressure-stretch relationship, which essentially is a circumferential stress-stretch relationship, for material characterization. Thus the two models will have the same circumferential stress-stretch relationship in the healthy state and generally different ones in longitudinal direction. In any case, we can draw the qualitative conclusion that longitudinal stresses increase with degradation and remodelling for isotropic models as opposed to anisotropic models where a drop is observed. Note that the qualitative change in circumferential stretch comes from a larger increase in the absolute contribution of collagen to the longitudinal tissue stress t_{zz}. Otherwise collagen stress increased and elastin stress decreased in both cases with degradation and remodelling. Apparently this difference in stress patterns is the most important difference between isotropic and anisotropic models.

$n_e C_e = 1.668\text{KPa}$, $n_c k_1 = 21.34\text{KPa}$, $k_2 = 0.0675$

We will now use the second set of material parameters. In this case, the experimental [34] result shows a circumferential tissue stretch at attachment of about 2. With that value, we obtain a stable growth with $\lambda_\theta \approx 3$ for $\alpha = 60$, $\beta = 50$. The value of β here is close to the critical value. Note from Fig. 4.16 that for $\beta = 45$ the growth becomes unstable. This can also be seen from Fig. 4.15(b).

Finding the $\alpha - \beta$ pair which results in a desired stable growth can only be done by trial and error. At a given α, reducing β increases the final size of the tissue. However, the reduction can not be carried on indefinitely as reducing β can result in an unstable growth. The same is true for keeping β constant and varying α. In this case too, going right in the $\alpha - \beta$ plane increases the final size until a critical value is reached where growth becomes unstable. A better strategy would be trying values just close to the critical value, i.e. at the border of the blue and red regions in Fig. 4.15(b), for example. A stable final circumferential tissue stretch λ_θ of 3 is the maximum we were able to get[†]. This is a 50% increase in size over the size at systole ($\lambda_{\theta,a} = 2$). We can infer from Fig. 4.15(a) and Fig. 4.15(b) that the critical ratio depends on both the material model and the material constants used.

We note that the maximum stable growth we have been able to achieve in the case of the first set of material parameters for the isotropic model and for the anisotropic model was $\lambda_\theta = 1.54$, which is only a 4.5% increase over the tissue stretch at attachment.

The fact that higher growth can be observed in the second set of material parameters and not in the first one can be attributed to the very high stiffness of the first material.

[†]We tried higher values of α with collagen half-lives as short as a week. The circumferential tissue stretch does not go beyond 3.

4.4 Spherical Membranes with Isotropic Collagen

In this section, we consider the inflation of thin-walled spherical membranes of isotropic elastin and collagen. Two sets of strain energy functions will be considered:

- neo-Hookean elastin (3.79) and exponential collagen (3.81);
- elastin and collagen with the same exponential strain energy function (3.80).

The initial recruitment, attachment and remodelling criteria are given by the first invariant of the relevant deformation gradient tensor.

We will first derive the pertinent mechanical and remodelling equations and then discretize them. We will also explain how the initial recruitment, attachment and remodelling criteria are determined. Finally, we will discuss the results of numerical simulations.

4.4.1 Kinematics

The reference configuration $\mathcal{G}_R$ is a thin-walled sphere of radius R and thickness H, with $H/R \ll 1$. In the thin-walled limit $H/R \to 0$, the sphere is considered as a cylindrical surface of radius R, and mechanically modeled as a membrane. A material point $\mathbf{X}$ in the reference configuration is described by the spherical coordinates (R, Θ, Φ), while in the deformed configuration it is described by (r, θ, ϕ). We consider a homogenous deformation given by

$$r = r(t) = \lambda(t)R, \qquad \theta = \Theta, \qquad \Phi = \phi. \tag{4.13}$$

The resulting elastin and collagen deformation gradient tensors are

$$\mathcal{F}_e = \mathcal{F} = \begin{pmatrix} \lambda^{-2} & & \\ & \lambda & \\ & & \lambda \end{pmatrix}, \qquad \mathcal{F}_c = \begin{pmatrix} \lambda_c^{-2} & & \\ & \lambda_c & \\ & & \lambda_c \end{pmatrix}, \tag{4.14}$$

where λ and λ_c are the in-plane stretches in elastin and collagen, respectively, and $F_{rr} = \lambda^{-2}$ is determined from the incompressibility condition $J = \det(\mathcal{F}) = 1$.

The left Cauchy-Green deformation tensors are similarly given by

$$\mathcal{B}_e = \mathcal{B} = \begin{pmatrix} \lambda^{-4} & & \\ & \lambda^2 & \\ & & \lambda^2 \end{pmatrix}, \qquad \mathcal{B}_c = \begin{pmatrix} \lambda_c^{-4} & & \\ & \lambda_c^2 & \\ & & \lambda_c^2 \end{pmatrix}. \tag{4.15}$$

The relation between tissue (elastin) deformation gradient and collagen deformation gradient is the same relation as in the case of the isotropic cylinder, i.e. (3.69). We have the recruitment deformation tensor as

$$\mathcal{F}_{rec} = \begin{pmatrix} \lambda_{rec}^{-2} & & \\ & \lambda_{rec} & \\ & & \lambda_{rec} \end{pmatrix}, \tag{4.16}$$

where λ_{rec} is the recruitment stretch in the in-plane directions. Note that $\lambda_c = \lambda/\lambda_{rec}$.

The trace of the recruitment deformation tensor which is a recruitment/remodelling criterium is

$$s_{rec} = \mathrm{tr}(\mathcal{F}_{rec}) = 2\lambda_{rec} + \lambda_{rec}^{-2}. \tag{4.17}$$

Analogous to the case of the cylinder, solving (4.17) for λ_{rec} results in two values: a value greater than one and another value between zero and one. We take the value greater than one as λ_{rec}.

4.4.2 Constitutive and Equilibrium Equations

We will first derive the stress-stretch relationships for an inflating sphere using a generic strain energy density function. We will then substitute specific forms of the strain energy function.

From (3.15) and (3.16), the stress tensor is given by

$$\mathcal{T} = -p\mathcal{I} + 2n_e\frac{\partial W_e}{\partial I_e}(\mathcal{B}_e - \mathcal{I}) + 2n_c\frac{\partial W_c}{\partial I_c}(\mathcal{B}_c - \mathcal{I}). \tag{4.18}$$

Substitution of the left Cauchy-Green stretch tensors from (4.15) into (4.18) results in

$$\mathcal{T} = -p\mathcal{I}+2n_e\frac{\partial W_e}{\partial I_e}\begin{pmatrix} \lambda^{-4}-1 & & \\ & \lambda^2-1 & \\ & & \lambda^2-1 \end{pmatrix}+2n_c\frac{\partial W_c}{\partial I_c}\begin{pmatrix} \lambda_c^{-4}-1 & & \\ & \lambda_c^2-1 & \\ & & \lambda_c^2-1 \end{pmatrix}. \tag{4.19}$$

From the membrane approximation that $t_{rr} = 0$, we obtain the hydrostatic pressure term p and using that we find the in-plane stresses, i.e $t_{\theta\theta} = t_{\phi\phi}$. Thus, we have

$$t_{\theta\theta} = t_{\phi\phi} = 2n_e\frac{\partial W_e}{\partial I_e}(\lambda^2 - \lambda^{-4}) + 2n_c\frac{\partial W_c}{\partial I_c}(\lambda_c^2 - \lambda_c^{-4}). \tag{4.20}$$

For the first set of strain energy functions, i.e (3.79) and (3.81), the in-plane stress is given by

$$\begin{aligned} t_{\theta\theta} = t_{\phi\phi} &= n_eC_e(\lambda^2 - \lambda^{-4}) + 2n_ck_1(I_c - 3)e^{k_2(I_c-3)^2}(\lambda_c^2 - \lambda_c^{-4}), &(4.21)\\ &= n_eC_e(\lambda^2 - \lambda^{-4}) + 2n_ck_1(2\lambda_c^2 + \lambda_c^{-4} - 3)(\lambda_c^2 - \lambda_c^{-4})e^{k_2(2\lambda_c^2+\lambda_c^{-4}-3)^2}. &(4.22)\end{aligned}$$

In a similar fashion, the in-plane stress for the second set of strain energy functions, i.e (3.80), leads us to

$$t_{\theta\theta} = t_{\phi\phi} = n_ek_1^e(\lambda^2 - \lambda^{-4})e^{k_2^e(2\lambda_e^2+\lambda_e^{-4}-3)} + n_ck_1^c(\lambda_c^2 - \lambda_c^{-4})e^{k_2^c(2\lambda_c^2+\lambda_c^{-4}-3)}. \tag{4.23}$$

The equilibrium equation, which in this case is the Laplace formula, is given by

$$t_{\theta\theta} = t_{\phi\phi} = \frac{Pr}{2h} = \frac{PR\lambda}{2H\lambda^{-2}} = \frac{PR}{2H}\lambda^3, \tag{4.24}$$

where $r = R\lambda$ and $h = H\lambda^{-2}$ are the current radius and wall thickness, respectively.

Finally, by equating the stresses obtained from the constitutive relations and this equilibrium equation, we obtain a single mechanical equation for each set of strain energy functions,

$$n_eC_e(\lambda^2 - \lambda^{-4}) + 2n_ck_1(2\lambda_c^2 + \lambda_c^{-4} - 3)(\lambda_c^2 - \lambda_c^{-4})e^{k_2(2\lambda_c^2+\lambda_c^{-4}-3)^2} = \frac{PR}{2H}\lambda^3, \tag{4.25}$$

and

$$n_ek_1^e(\lambda^2 - \lambda^{-4})e^{k_2^e(2\lambda_e^2+\lambda_e^{-4}-3)} + n_ck_1^c(\lambda_c^2 - \lambda_c^{-4})e^{k_2^c(2\lambda_c^2+\lambda_c^{-4}-3)} = \frac{PR}{2H}\lambda^3. \tag{4.26}$$

In the healthy state, the above two equations complemented by the relation between elastin and collagen stretches will be solved given the applied pressure, material parameters and geometric quantities (R and H). In the aneurysmal state, the remodelling equations

should be added to the set of equations, and unless specified otherwise the pressure P is kept constant. Note in general that a given deformation state is attained at different levels of applied pressure in the spherical and in the cylindrical membranes, both having the same material properties. It thus becomes an issue whether the level of internal pressure or the deformation state should be used to specify the attachment state. We take the deformation state as the governing parameter and keep the applied pressure constant at the value where the attachment state $S(\mathcal{F}_c) = s_a$ is reached.

To determine the initial recruitment state, we use the same value of the initial recruitment invariant $s_{rec,0}$ that we used in the case of cylindrical membranes, i.e.

$$s_{rec,0}^{sphere} = 2\lambda_{rec,0,sphere} + \lambda_{rec,0,sphere}^{-2} = s_{rec,0}^{cylinder} = \lambda_{rec,0,cylinder} + \lambda_{rec,0,cylinder}^{-1} + 1. \quad (4.27)$$

The attachment value s_a is determined in a similar fashion.

By so doing, we find that the initial recruitment state corresponding to a circumferential tissue stretch of 1.2 ($s_{rec} = 3.033$) in the cylinder corresponds to an in-plane tissue stretch of 1.113 in the sphere. Similarly, for a tissue stretch at attachment of 2 in the cylinder we have a circumferential collagen attachment stretch of 2/1.2, which gives $s_a = 3.267$. For this value, the in-plane collagen stretch in the sphere should be 1.365 and the tissue stretch 1.113×1.365 = 1.519. We do not have a reference spherical geometry in an artery. For our numerical simulations we use an adhoc value of $R/H = 5$. For the material parameters, we use the following values obtained from our material characterization. We have $n_e C_e = 1.668$KPa, $n_{c,0}k_1 = 21.34$KPa and $k_2 = 0.0675$ for neo-Hookean elastin with exponential collagen, and $n_e k_1^e = 861.44$Pa, $k_2^e = 1.1796$, $n_{c,0}k_1^c = 1861.68$Pa and $k_2^c = 1.71897$, where both elastin and collagen have exponential strain energy functions.

4.4.3 Discretized Equations

The degradation and remodelling equations are the same as those of the isotropic cylinder. In the case of exponential elastin, we have two material constants instead of one (C_e) for the neo-Hookean elastin. We consider the degradation to apply on k_1^e.
The equations discretized with the backward Euler (implicit) time integration are given below:

$$\begin{aligned}
&\begin{cases} C_{e,i} = C_{e,0}c_i, \\ \text{or} \\ k_{1,i}^e = k_{1,0}^e c_i, \end{cases} \\
&\lambda_{c,i} = \frac{\lambda_i}{\lambda_{rec,i}}, \\
&\frac{P_i R}{2H}\lambda_i^3 = \begin{cases} n_e C_{e,i}(\lambda_i^2 - \lambda_i^{-4}) + 2n_{c,i}k_1(2\lambda_{c,i}^2 + \lambda_{c,i}^{-4} - 3)(\lambda_{c,i}^2 - \lambda_{c,i}^{-4})e^{k_2(2\lambda_{c,i}^2+\lambda_{c,i}^{-4}-3)^2}, \\ \text{or} \\ n_e k_1^e(\lambda_i^2 - \lambda_i^{-4})e^{k_2^e(2\lambda_i^2+\lambda_i^{-4}-3)} + n_{c,i}k_1^c(\lambda_{c,i}^2 - \lambda_{c,i}^{-4})e^{k_2^c(2\lambda_{c,i}^2+\lambda_{c,i}^{-4}-3)}, \end{cases} \\
&s(\mathcal{F}_{rec,i}) = 2\lambda_{rec,i} + \lambda_{rec,i}^{-2}, \\
&s(\mathcal{F}_{c,i}) = 2\lambda_{c,i} + \lambda_{c,i}^{-2}, \\
&\frac{s_{rec,i} - s_{rec,i-1}}{\Delta t} = \alpha(s(\mathcal{F}_{c,i}) - s_a), \\
&\frac{n_{c,i} - n_{c,i-1}}{\Delta t} = \beta(s(\mathcal{F}_{c,i}) - s_a).
\end{aligned} \quad (4.28)$$

4.4.4 Results and Discussions

As in the case of cylinders, the shape of the growth function, $\lambda(t)$, depends on the degradation function. Linear and concave degradation functions result in convex growth, which begins to stabilize only after the end of the degradation period. A typical growth and remodelling pattern for spherical membranes with concave degradation functions is shown in Fig. 4.17. We observe a higher increase of the tissue stretch λ due to degradation for case (b), exponential elastin (about 10%) than for case (a), neo-Hookean elastin (about 1%); both cases have $\alpha = 20$ and $\beta = 60$. Note that the collagen stretch does not subside during the degradation, only after degradation it does. Further we see that all the stretches tend to a stationary value after degradation. In the ensuing discussion, we consider only convex degradation functions which result in concave stable growth. We shun concave degradation functions from further consideration because the resulting growth pattern does not go inline with clinical observations. The details of the clinical observation will be provided in Section 4.5.

The maximum stable growth obtained for the values of α andβ we considered ($\alpha \in [0, 60], \beta \in [0, 200]$) was $\lambda = 1.7$ for neo-Hookean elastin, Fig. 4.18(a)[‡] and $\lambda = 1.8$ for exponential elastin, Fig. 4.20(a), starting with an in-plane tissue stretch at attachment of 1.519. There is no considerable difference in the tissue growth attained with the two material laws except that they are obtained at different values of the remodelling parameters; maximum stable growth was found to occur for $\alpha = 50, \beta = 45$ in the case of neo-Hookean elastin, and for $\alpha = 56, \beta = 70$ in the case of exponential elastin. However, there is a difference in the growth pattern : we get a pronounced concave growth for neo-Hookean elastin, but an almost linear one for exponential elastin, compare Fig. 4.18(a) and Fig. 4.20(a) or Fig. 4.21(a).

In the case of stable growth with neo-Hookean elastin, the elastin contribution to the tissue stress is always small, and even decreases further with remodelling and degradation as shown by Fig. 4.18(b). For exponential elastin, on the other hand, the stress from elastin can either increase, Fig. 4.20(b), or decrease, Fig. 4.21, depending on the remodelling parameters, although for both the growth is ultimately stable.

Unstable growth is always convex, and results in increasingly high stretches and stresses. An example of unstable growth for neo-Hookean elastin is depicted in Fig. 4.19. Over a period of twice the degradation time, we observe stresses a thousand or more times higher than stresses observed in stable growth. This is true for all constitutive equations and geometries considered.

For a remodelling with $\alpha = 0$, i.e thickening only, the tissue retracts as in Fig. 4.22. This happens for cylinders also. Retraction of aneurysms was observed in some clinical records [45].

There is a significant difference between the two material laws regarding the values of α and β which result in stable growth. For neo-Hookean elastin we get a critical value of β/α below which the growth becomes unstable. Similar to what we saw for cylindrical membranes, this critical value decreases with α; see Fig. 4.23. For the exponential elastin however there is no such value. For some values of α, the growth is stable for all values of β; for others there is both a maximum as well as a minimum critical ratio. The region of stability in the $\alpha - \beta$ plane depends on the attachment stretch too. For the exponential elastin we show these values for an in-plane tissue stretch of 1.519; the same value used for the neo-Hookean elastin, in Fig. 4.24(a). The plot for a tissue stretch at attachment of 1.2 is given by Fig. 4.24(b).

[‡]In Fig. 4.18-4.21 we have 'collagen I' or 'collagen II' in the captions. Recall that the numbers here are simply serial numbers for the figures and do not refer to the different types of collagen.

Initial Volume Fractions and Degradation Rules

In the numerical simulations discussed thus far, we considered the linear thickening given by (3.30) and used adhoc values of 0.6 and 0.2 for the initial volume fractions of elastin and active collagen, respectively. With our assumption that procollagen, which initially was inactive, gets involved in load carrying during remodelling, the collagen volume fraction n_c should not exceed 0.4. In the stable growths, we observed that the collagen volume fraction indeed remained below 0.4. To investigate the effect of constrained thickening we will use the material law with neo-Hookean elastin, $n_e = 0.7$ and $n_{c,0} = 0.2$, where we find stable growth with the collagen volume fraction going above 0.3, i.e the maximum allowed for $n_e = 0.7$. We will compare linear thickening (3.30), constrained linear thickening (3.30)-(3.32), and logistic thickening (3.34).

The values of α and β, which result in stable growth with unconstrained linear thickening, are exactly the same as those for the first volume fractions considered, i.e $n_e = 0.6, n_c = 0.2$; for this we refer to Fig. 4.23. The constrained linear thickening has a slight difference as shown by Fig. 4.25(a). The difference is observed after $\alpha = 50$ where some values, which resulted in stable growth for linear thickening, result in unstable growth when the thickening is constrained. This is an indication that for these values of the remodelling parameters the unconstrained linear thickening resulted in n_c going above 0.3. We show the deformation, remodelling and stress patterns in Figs. 4.26 and 4.27; they are discussed in the next paragraph. The logistic thickening, on the other hand, has a significantly different scenario where a large part of the $\alpha - \beta$ plane results in unstable growth as shown by Fig. 4.25(b) with a higher critical value of β for a given α.

In Fig. 4.26 we show what happens if the thickening is constrained after the maximum value of n_c is reached, i.e all the reserve procollagen has been used up. We see that in the constrained thickening the membrane resorts to elongation only resulting in very high stretches and stresses. The complete degradation and remodelling path for the time span we consider, $t \in [0, 2]$, is shown in Fig. 4.27. If the wall is not capable of handling the high stresses, the constrained thickening model predicts a sudden bursting on depletion of procollagen for a vessel, which would have grown to a stable size had there been sufficient reserve of procollagen to be called into action.

4.5 Conclusions and Model Validation

In this chapter, we have investigated the effect of constitutive equations, remodelling laws and parameters, and degradation functions on tissue growth and remodelling. We have also touched up on some relevant numerical issues. The following are the main conclusions that can be inferred from the results and discussions in this chapter.

- Degradation functions are the driving force of remodelling and subsequent growth. Sharp degradation triggers fast remodelling. The final size of the tissue, if it becomes stable, is largely dependent on the minimum value of the elastin shear modulus. The shape of the growth function, on the other hand, is influenced by the pattern of degradation. Concave degradation results in convex growth and the growth begins to stabilize only after degradation has ceased. Convex degradations resulted in concave growth for models with neo-Hookean elastin and almost linear growth for the model with exponential elastin.

  Unstable growth can be convex or concave; the convex growth results in very fast increase in stretches and stress as opposed to concave unstable growth which is gradual.

  If the thickening is constrained to a maximum value, i.e. a limited amount of reserve procollagen, growth which was stabilizing prior to depletion of the procollagen will turn unstable and result in sharp increase in the size of the membrane and stresses. We hypothesize that this explains why some times asymptomatic growth and rupture occurs in reality.

- The numerical values and ratios of the remodelling parameters α and β play a significant role. Higher values of β/α result in low stretch and deformations and vice versa. For material models with neo-Hookean elastin and exponential collagen there is a critical value of this ratio, which depends on constitutive relations and degradation function among other things, below which the tissue growth will be unstable. The critical ratio decreases with α, but still a higher value of β is required for a higher α, i.e the curve demarcating stable and unstable regions in the $\alpha - \beta$ plane is an increasing function with a non-positive second derivative.

  In the case of models with exponential elastin and collagen, there is both a maximum and minimum critical value of β/α. For some values of α, the growth was stable for all values of β.

- In cylindrical membranes, the anisotropic model considered results in progressively decreasing longitudinal stress whereas in the isotropic models longitudinal stress increases with time. With the circumferential stress increasing, or at least not decreasing significantly, the anisotropic model may lead to a situation where the tissue is much stiffer circumferentially than it is longitudinally.

- The pattern and final size of tissue growth do not exhibit significant differences between isotropic and anisotropic models, provided the material parameters in the models are so selected that both models have the same pressure-stretch relationships in the healthy state.

- In the case of spherical membranes, the elastin contribution to the in-plane stress decreases with degradation and remodelling for the model with neo-Hookean elastin,

whereas for the model with exponential elastin this amount can either increase or decrease depending on the values of the remodelling parameters. The collagen stress increases in both cases and this increase is higher than the drop in elastin stress, resulting in an overall increase of in-plane stress. Generally, the level of collagen stresses is much higher than that of elastin stresses.

- For a stable growth, delayed remodelling has virtually no effect on the final state.
- Using explicit time integration introduces limitations on the size of the time step that can be taken. A large time step can result in numerically unstable solutions or a break down of the solution.

For the purpose of discriminating between the different material models and remodelling equations and to validate the selected model, we use the statistical results of the ISUIA study [8, 25] on unruptured aneurysms and the clinical observation that rupture of cerebral aneurysms is mostly asymptomatic.

Based on the statistical result of Chang [8] that unruptured aneurysms have a concave growth pattern, we conclude that the elastin degradation function should be predominantly convex. Among the degradation functions we considered, the power function (3.25) best fits criteria. The sigmoid function (3.26) with appropriately selected parameters so as to make it largely concave can serve the purpose too.

The model with exponential elastin and collagen did not show concave stable growth. Recall from Section 3.8 that this model showed a poorer fit to the experimental data than the isotropic model with neo-Hookean elastin in the healthy state. We infer from this that the material model with neo-Hookean elastin and exponential collagen better describes both the healthy and aneurysmal states.

With unconstrained thickening and convex degradation functions, our numerical simulations show growth, which can be concave and stable, convex and unstable, or concave and unstable with slow growth. This model can not predict an asymptomatic growth and rupture. The constrained growth, on the other hand, can predict this phenomena. We thus conclude that constrained thickening is the better model.

We therefore select *the isotropic model with neo-Hookean elastin and exponential collagen, convex degradation, and remodelling with constrained thickening* as our model of choice.

The growth pattern predicted by this model agrees with the clinically observed growth pattern for unruptured cerebral aneurysms [8]. Potentially it explains why a membrane which seems to be stabilizing may suddenly grow and rupture. However, making qualified statements about rupture needs a study on failure theories of composite materials, which is beyond the scope of this work.

As for the growth size, we can not make comparison with the clinical data on cerebral aneurysms. We considered cylindrical membranes growing into cylinders or spherical membranes growing into spheres, whereas saccular cerebral aneurysms for which we had access to the clinical data grow as outpouching from a vessel wall.

Figures: Anisotropic Cylindrical Membranes

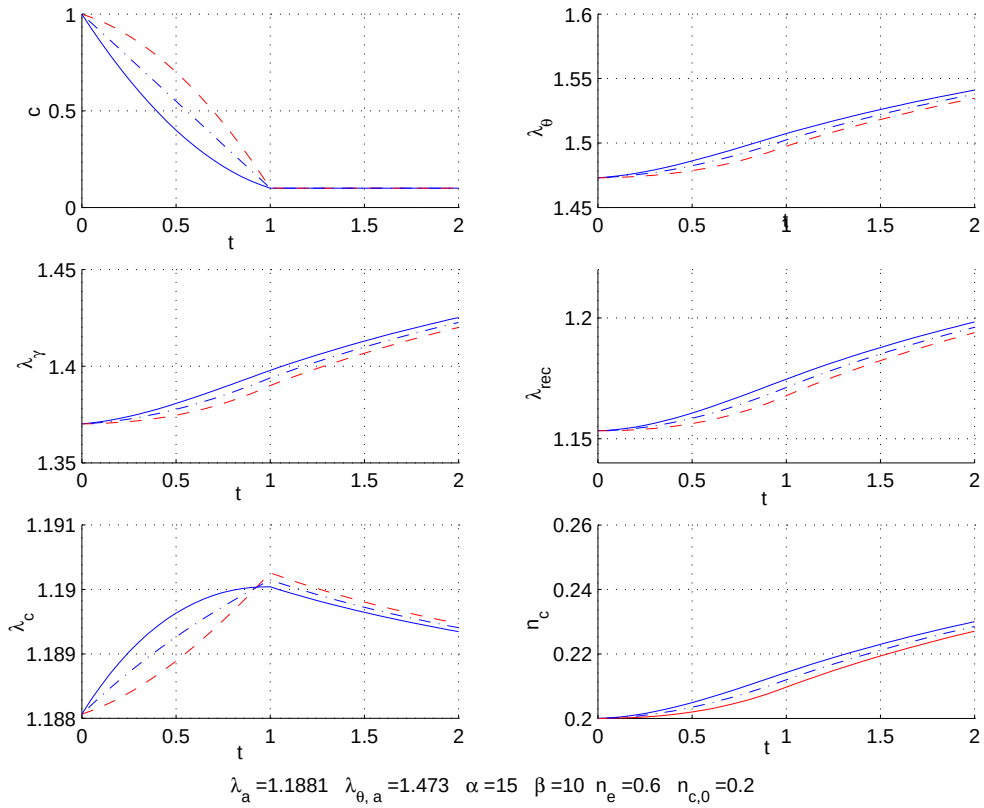

(a) Unstable Growth

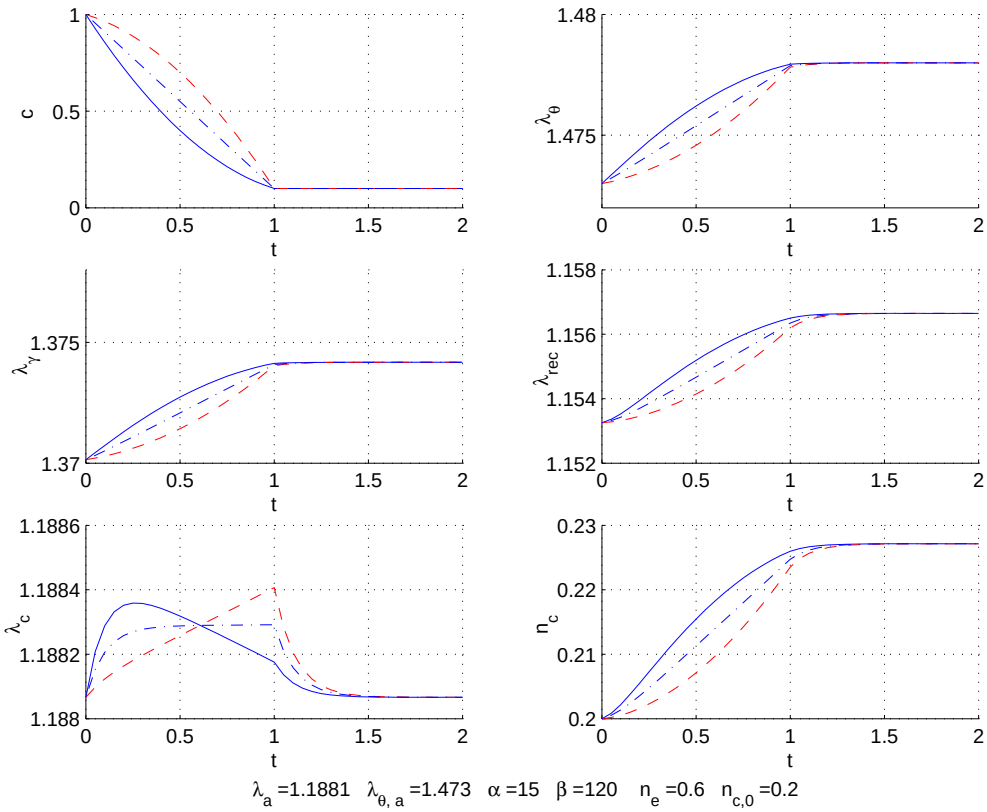

(b) Stable Growth

Figure 4.2: Effect of degradation functions I: concave(- - -), linear(-.-.-) and convex(—) degradation functions

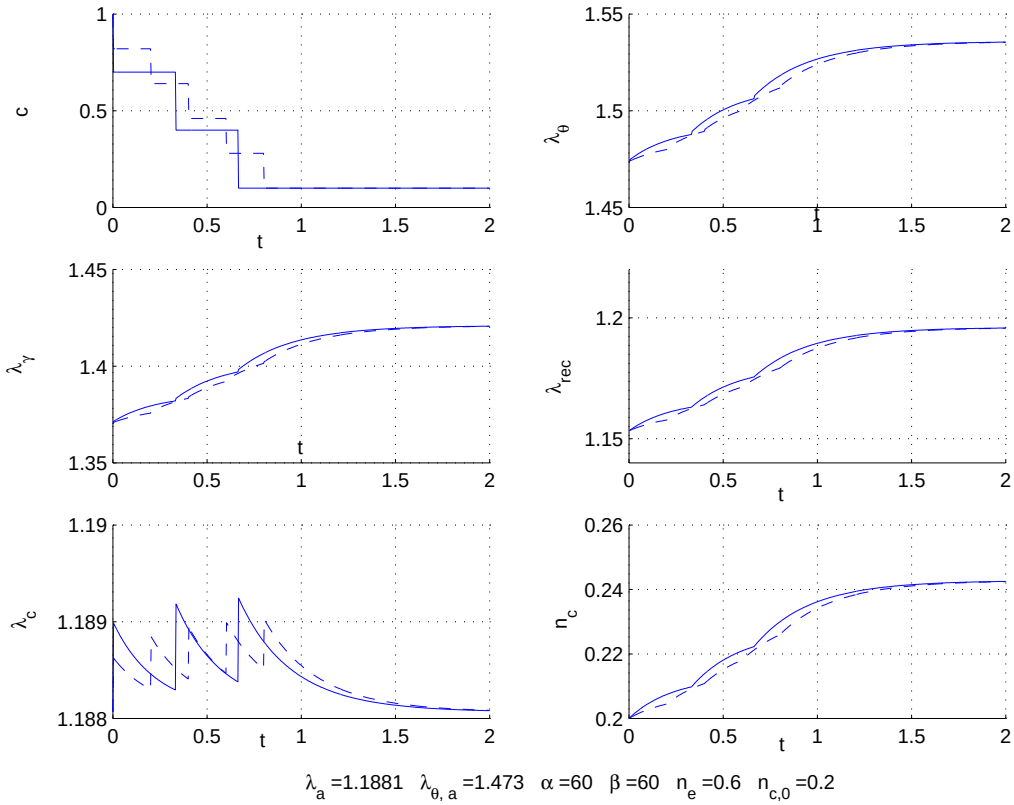

(a) Step-wise Degradation

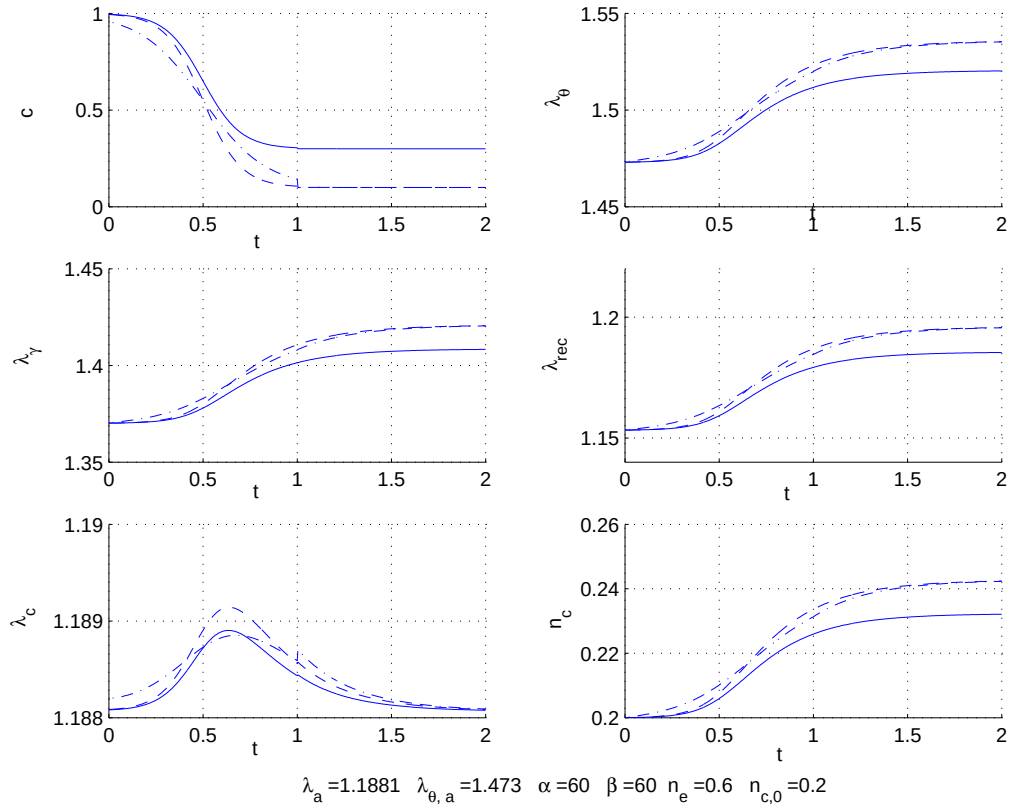

(b) Sigmoid Degradation

Figure 4.3: Effect of degradation functions II: step-wise(a) and sigmoid (b) degradation functions

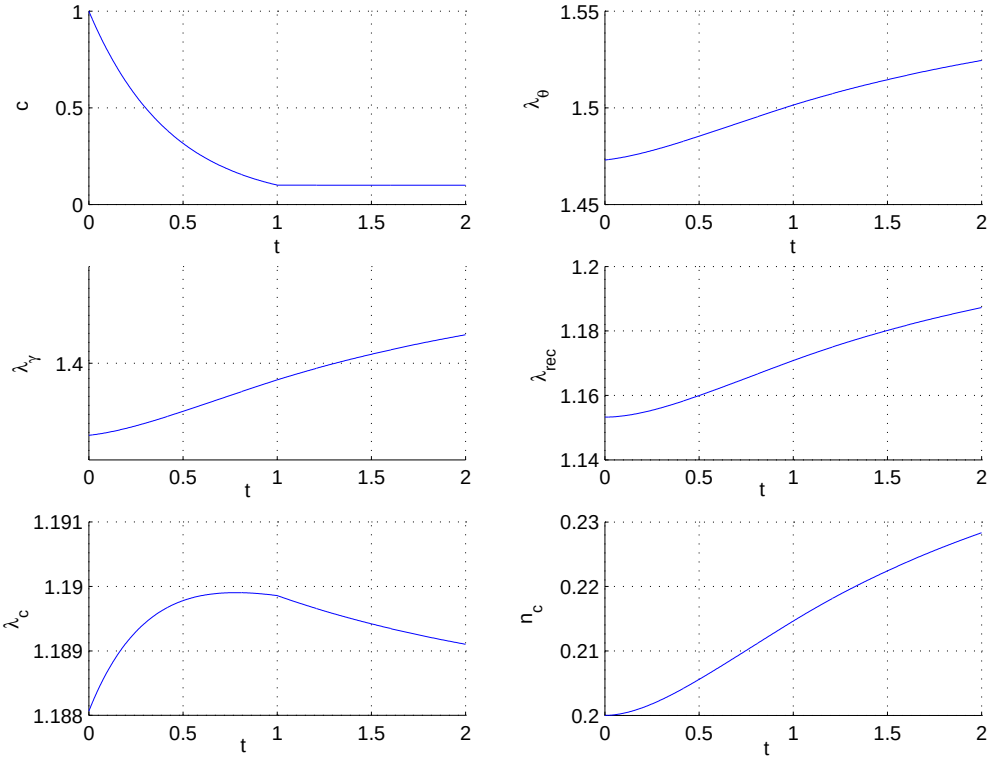

(a) Deformation

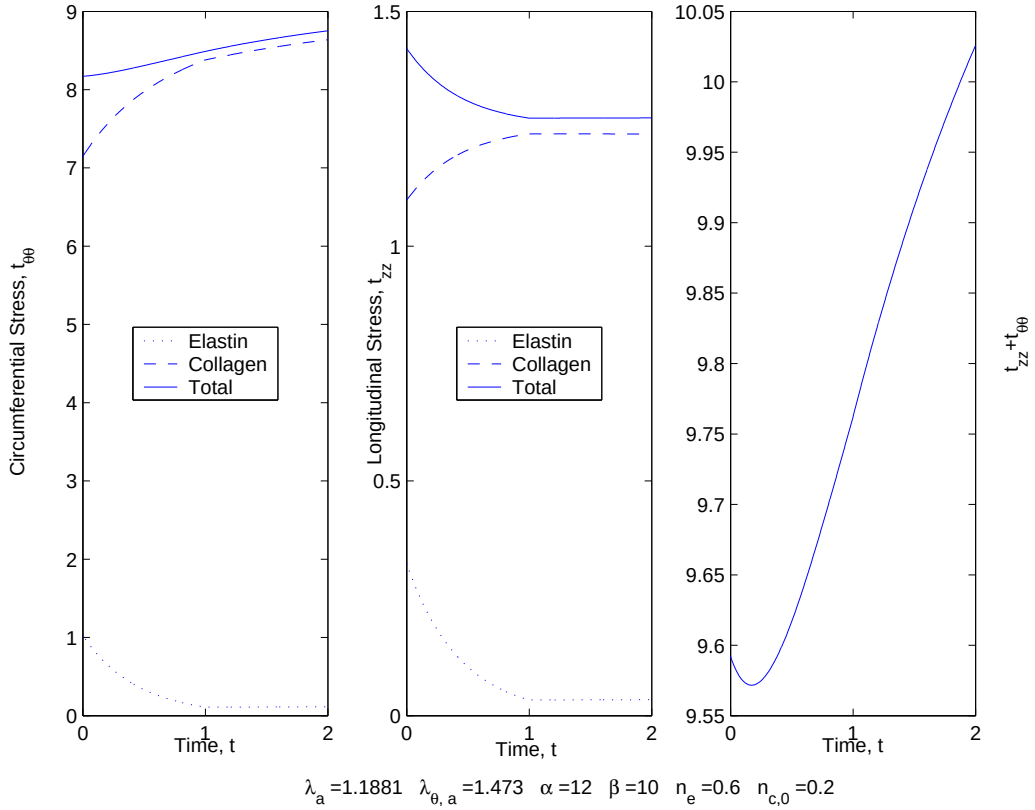

(b) Stresses scaled on C_e; total stress (—) is the sum of elastin stress(...) and collagen stress (- -).

Figure 4.4: Effect of remodelling parameters I: $\alpha = 12, \beta = 10$.

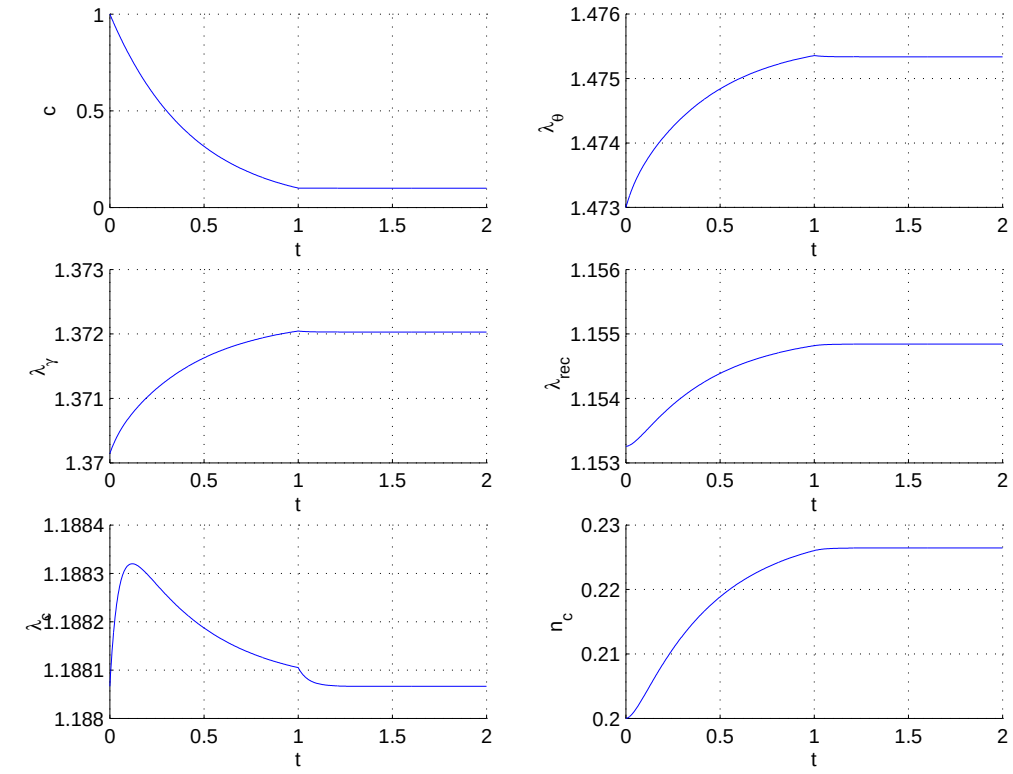

(a) Deformation

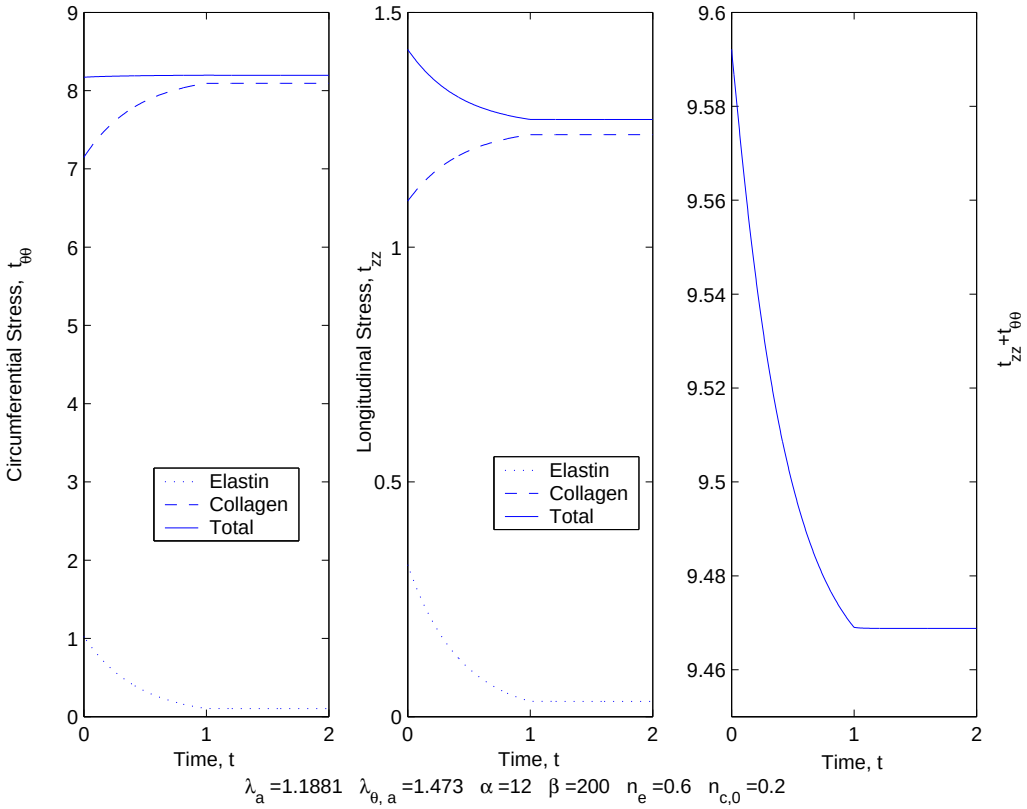

(b) Stresses scaled on C_e; total stress (—) is the sum of elastin stress(...) and collagen stress (- -).

Figure 4.5: Effect of remodelling parameters II: $\alpha = 12, \beta = 200$.

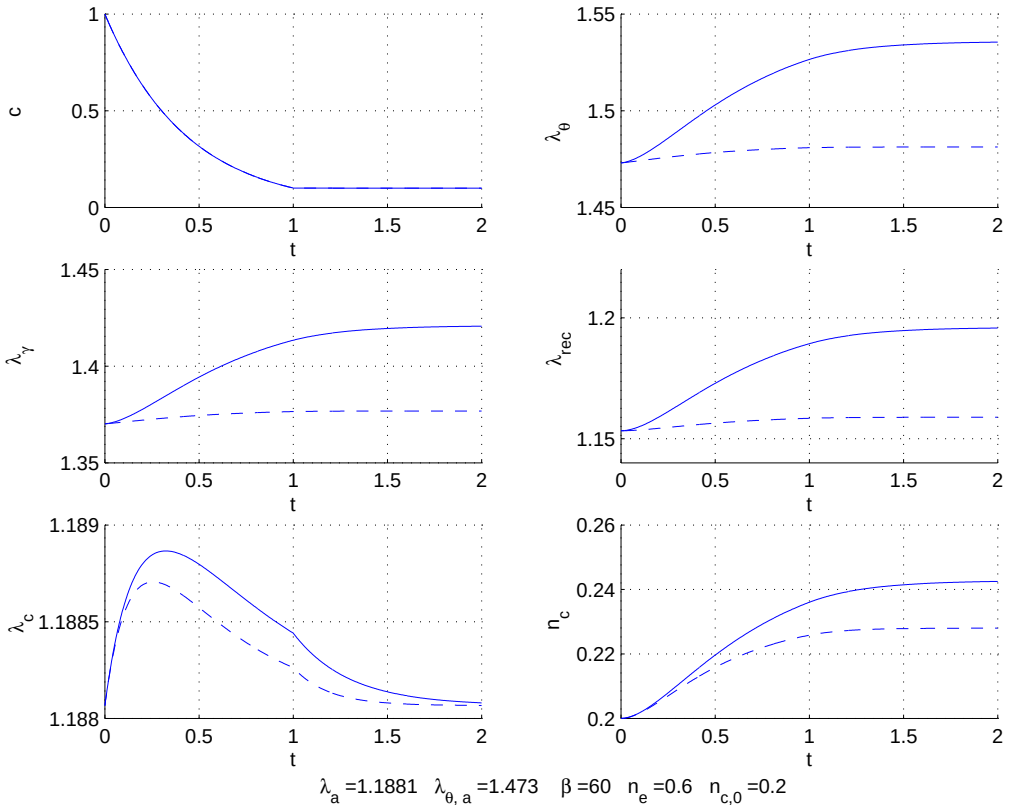

(a) Deformation

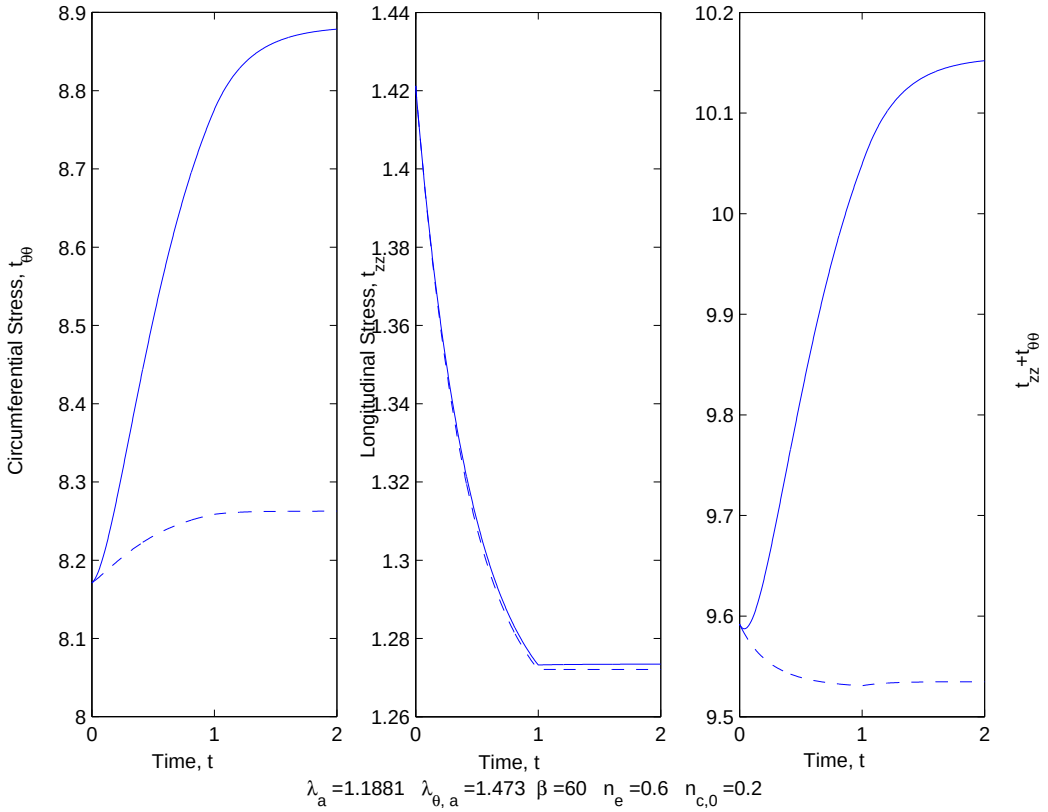

(b) Stresses scaled on C_e

Figure 4.6: Effect of remodelling parameters III: $\beta = 60$, $\alpha = 60$(—), $\alpha = 12$(- -).

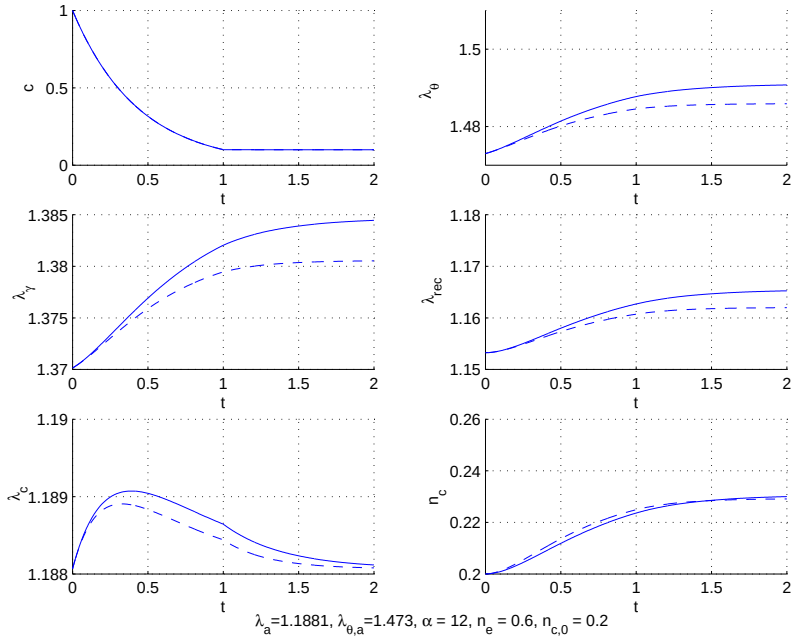

(a) $\alpha = 12$,solid line $\beta = 30$, dashed line $\beta = 40$

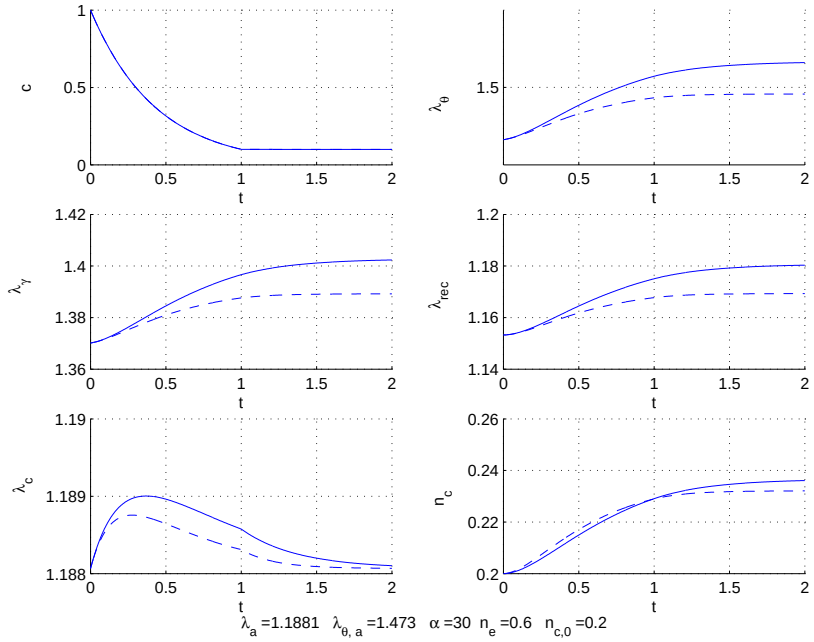

(b) $\alpha = 60, \beta = 120$

Figure 4.7: Critical ratio of remodelling parameters

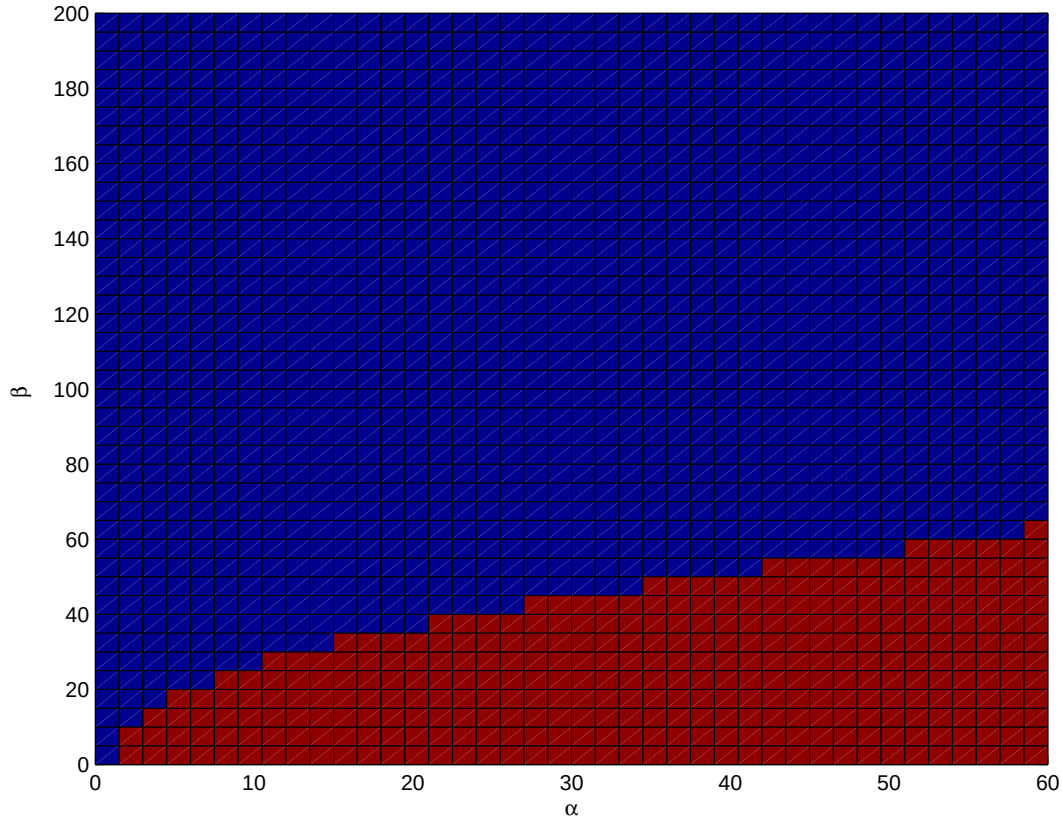

Figure 4.8: Remodelling parameters and stability of growth for $n_e = 0.6, n_{c,0} = 0.2$; the blue region shows values of remodelling parameters resulting in stable growth whereas red region shows those for unstable growth

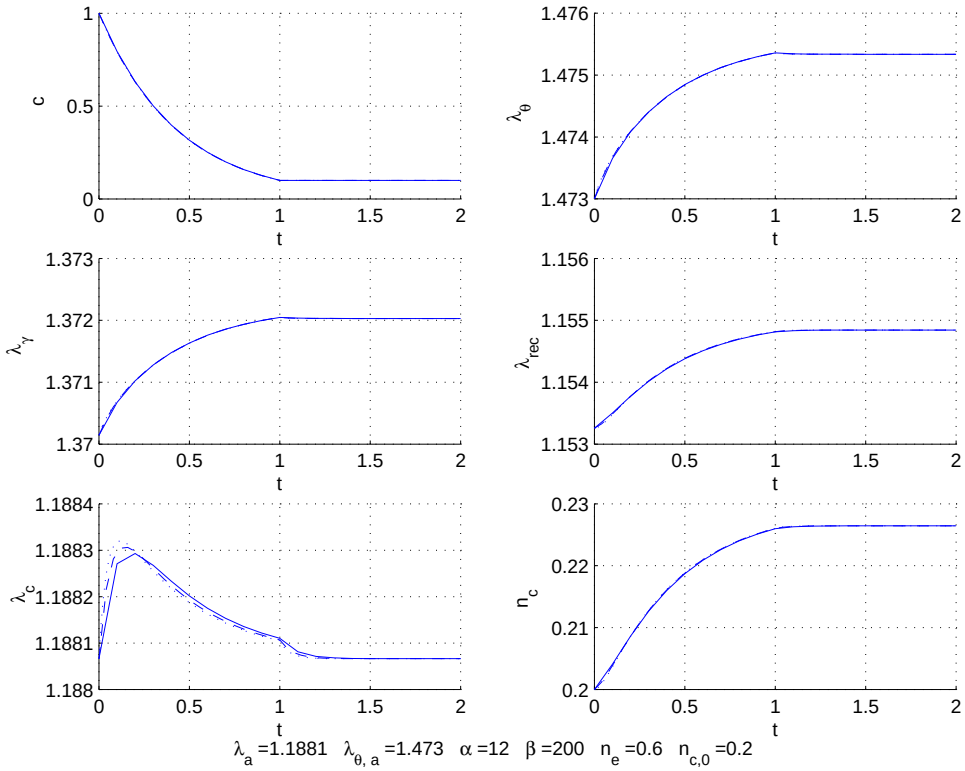

(a) Implicit Time Integration for $\Delta t = 0.1$ (—), $\Delta t = 0.04$ (- - -) and $\Delta t = 0.004$ (...)

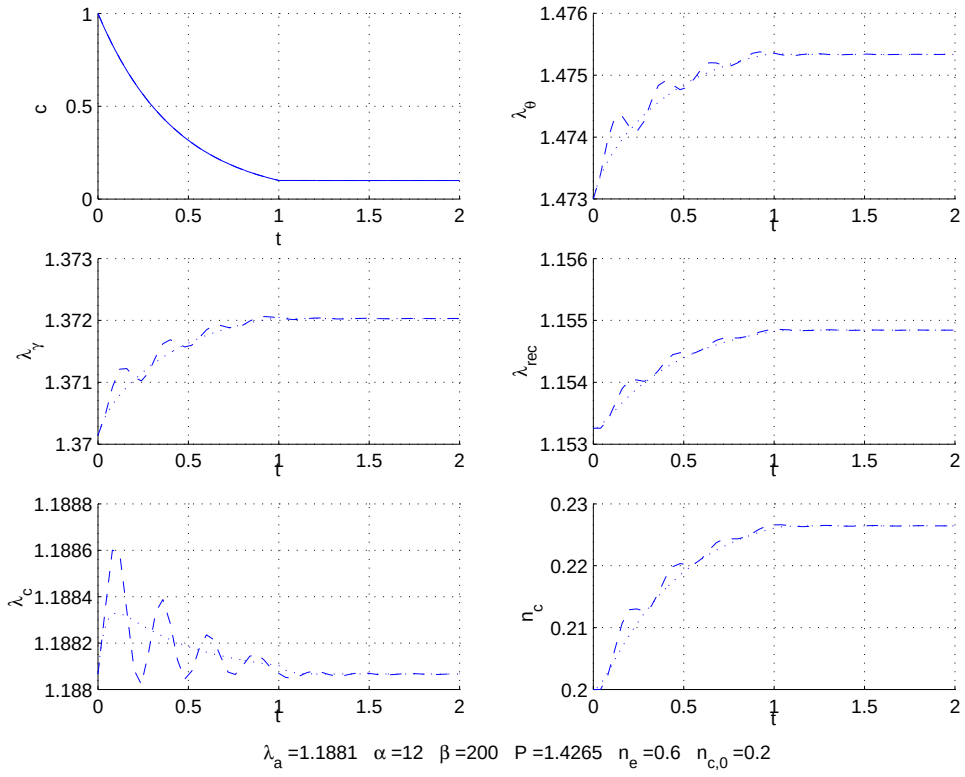

(b) Explicit Time Integration for $\Delta t = 0.04$ (- - -) and $\Delta t = 0.004$ (...)

Figure 4.9: Implicit versus explicit time integration I

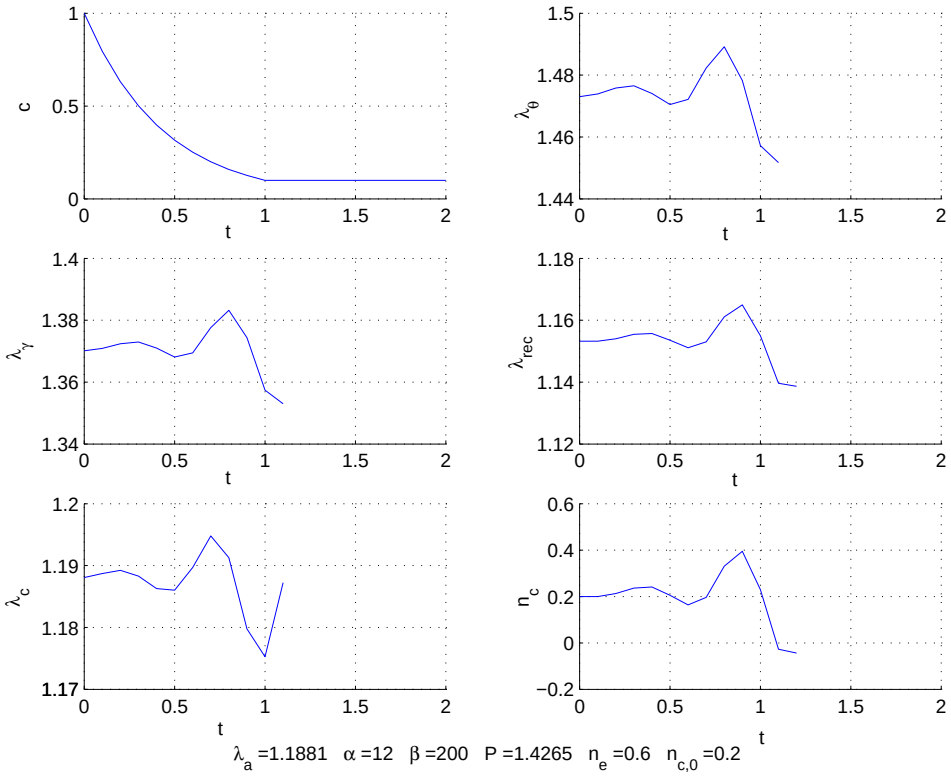

(a) Explicit Time Integration for $\Delta t = 0.1$

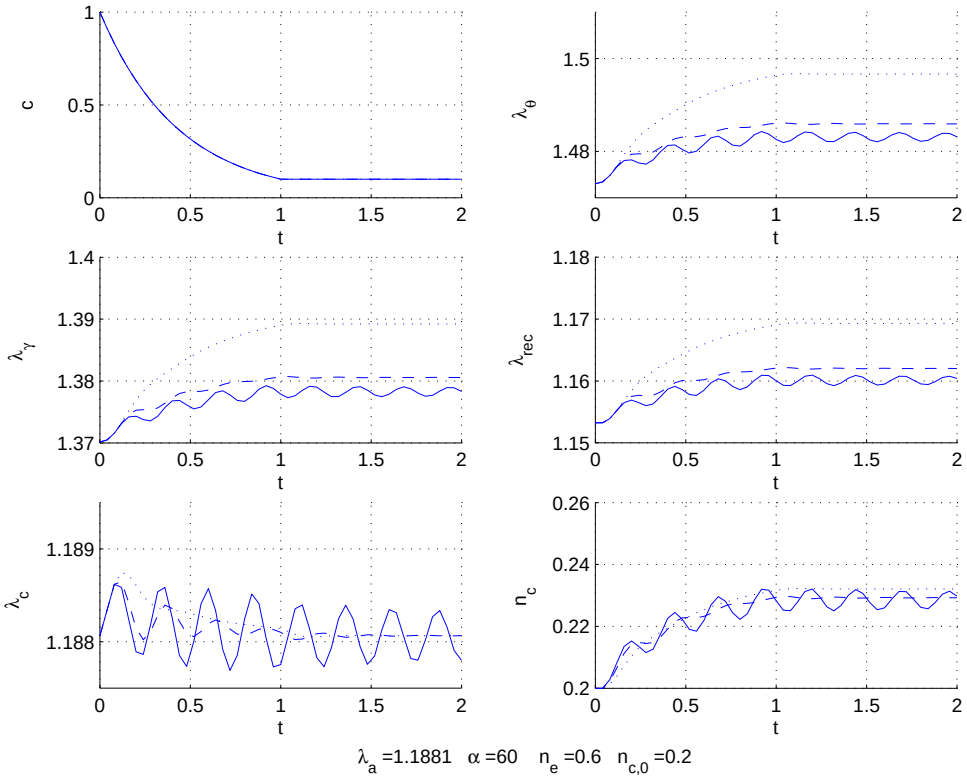

(b) Explicit Time Integration for $\Delta t = 0.04, \alpha = 60$ with $\beta = 120$ (...), $\beta = 200$ (- - -) and $\beta = 250$ (—)

Figure 4.10: Implicit versus explicit time integration II

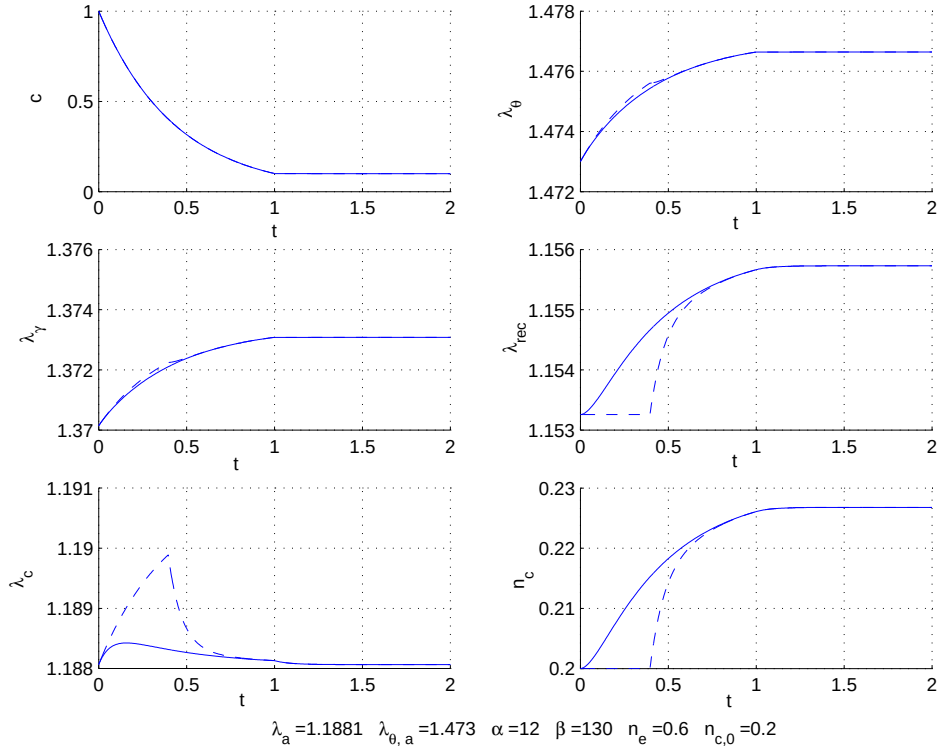

(a) Deformation: delayed response shown by dashed lines

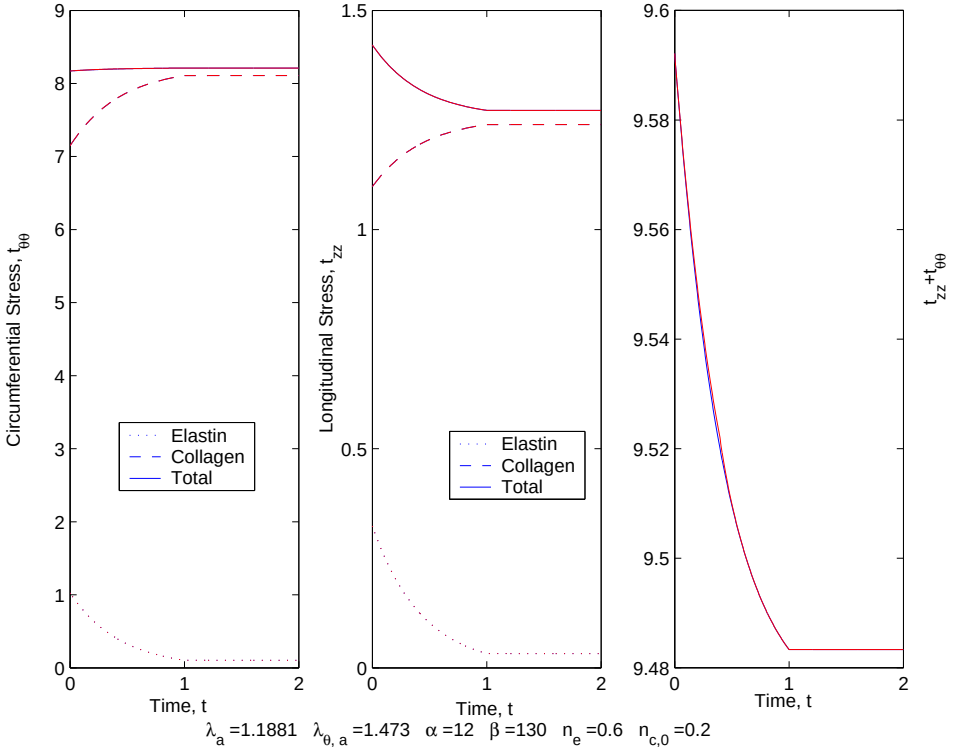

(b) Stresses scaled on C_e; total stress (—) is the sum of elastin stress(...) and collagen stress (- -); the plots for stresses overlap

Figure 4.11: Delayed remodelling for a stable growth; the remodelling is prevented for $t < 0.4$

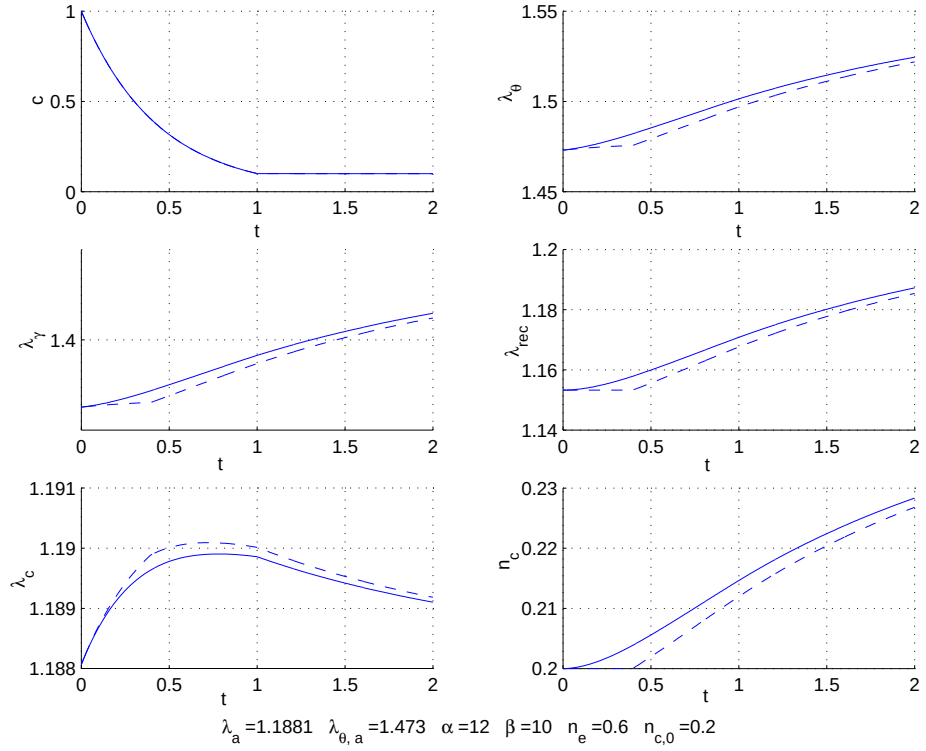

(a) Deformation: delayed response shown by dashed lines

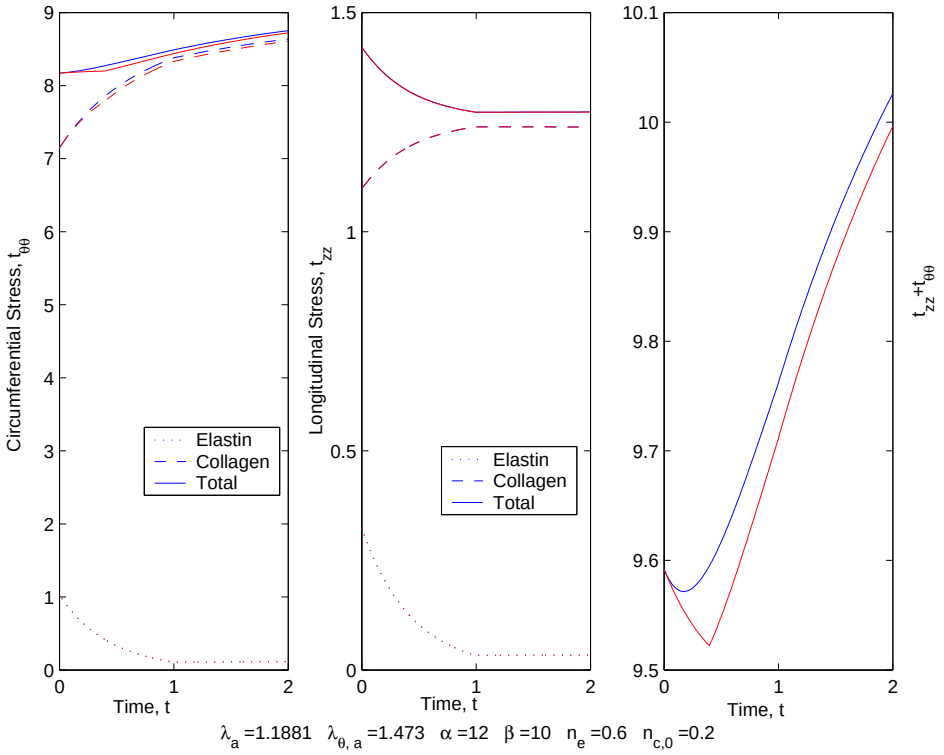

(b) Stresses scaled on C_e; total stress (—) is the sum of elastin stress(...) and collagen stress (- -), red lines indicate delayed response

Figure 4.12: Delayed remodelling for a non-stable growth; the remodelling is prevented for $t < 0.4$

Figures: Isotropic Cylindrical Membranes

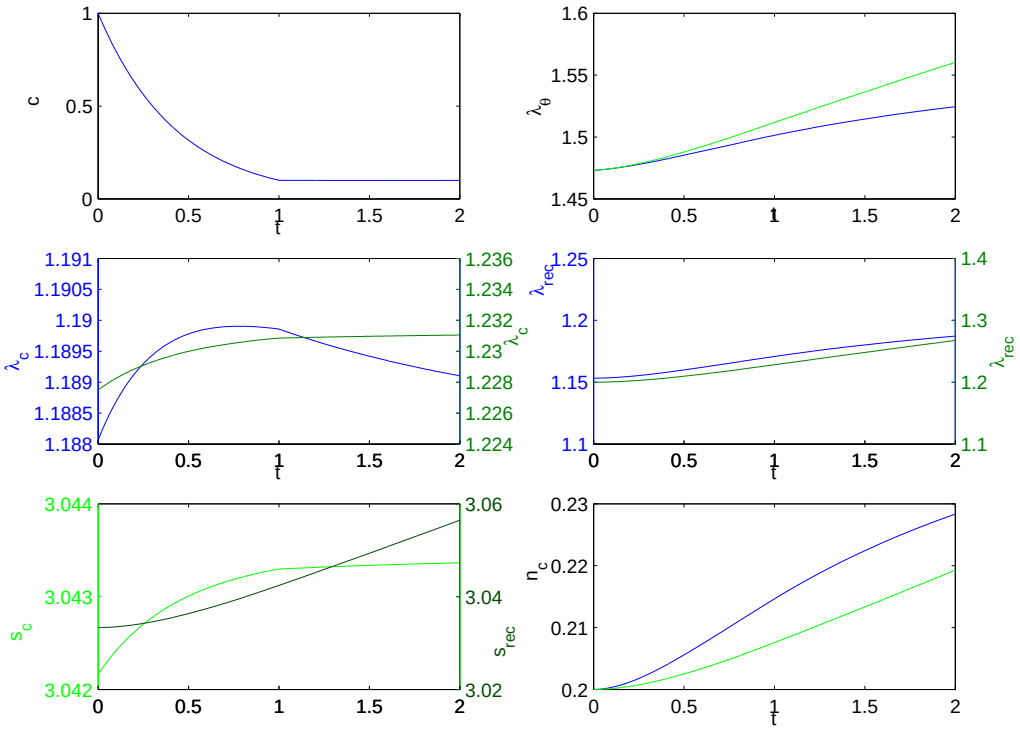

(a) Deformations; Attention: for the figures at the middle, multiple vertical axes are used. The axes on the left (blue) are for the anisotropic model and the ones on the right (green) are for the isotropic model.

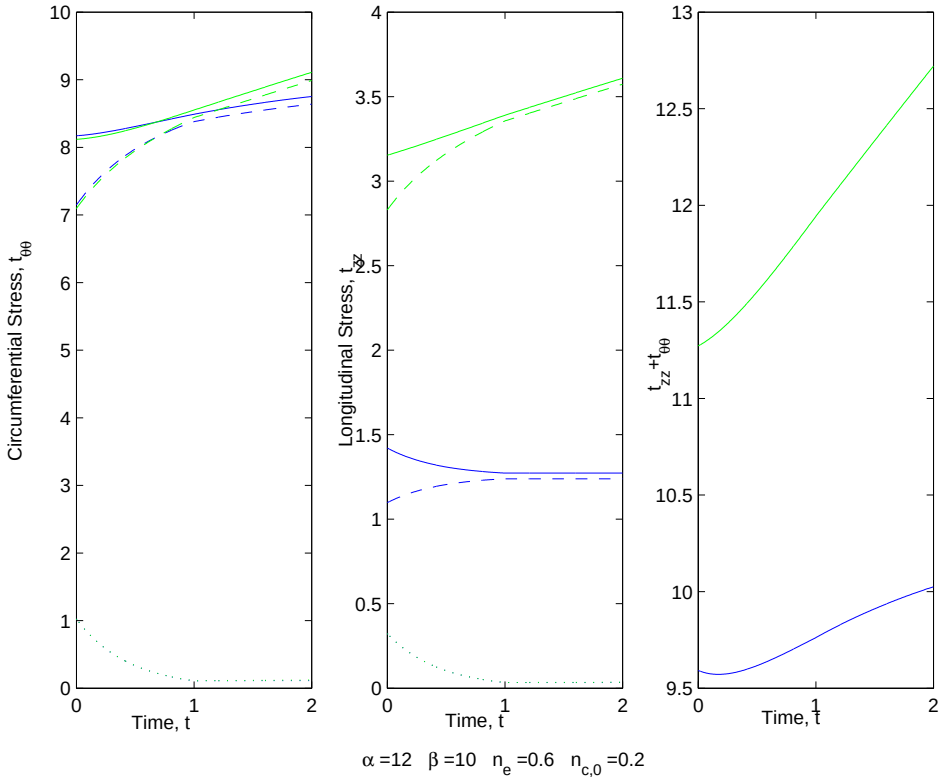

(b) Stresses;total stress (—) is the sum of elastin stress(...) and collagen stress (- -).

Figure 4.13: Comparison of isotropic (green) and anisotropic (blue) models with unstable growth

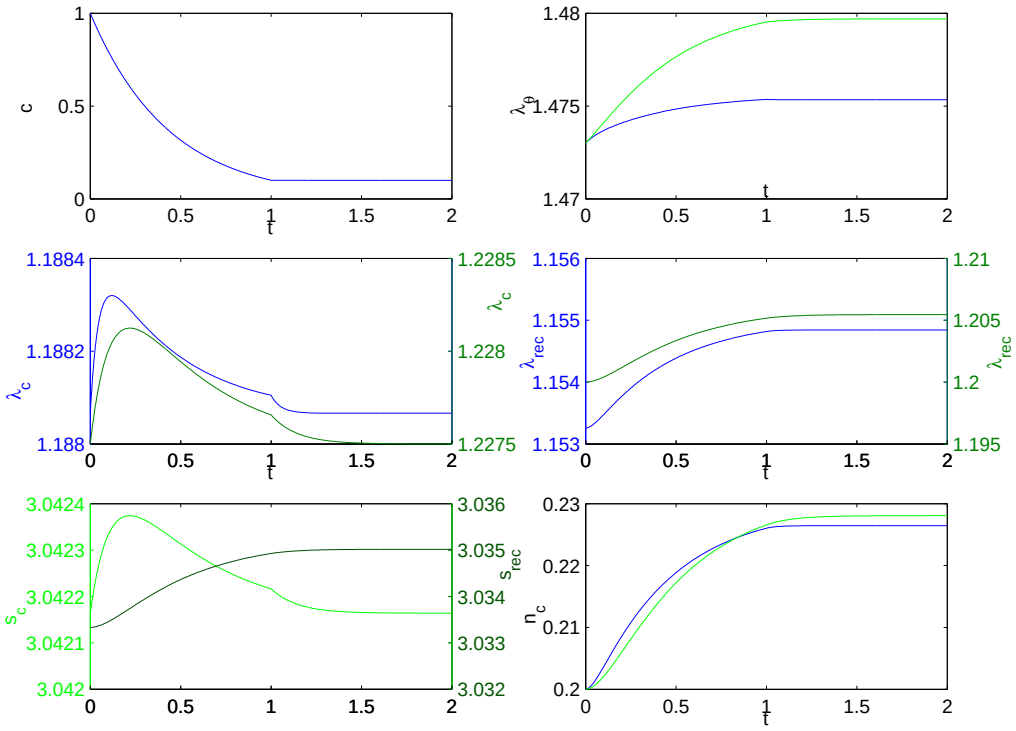

(a) Deformations; attn: double y-scales in some of the figures

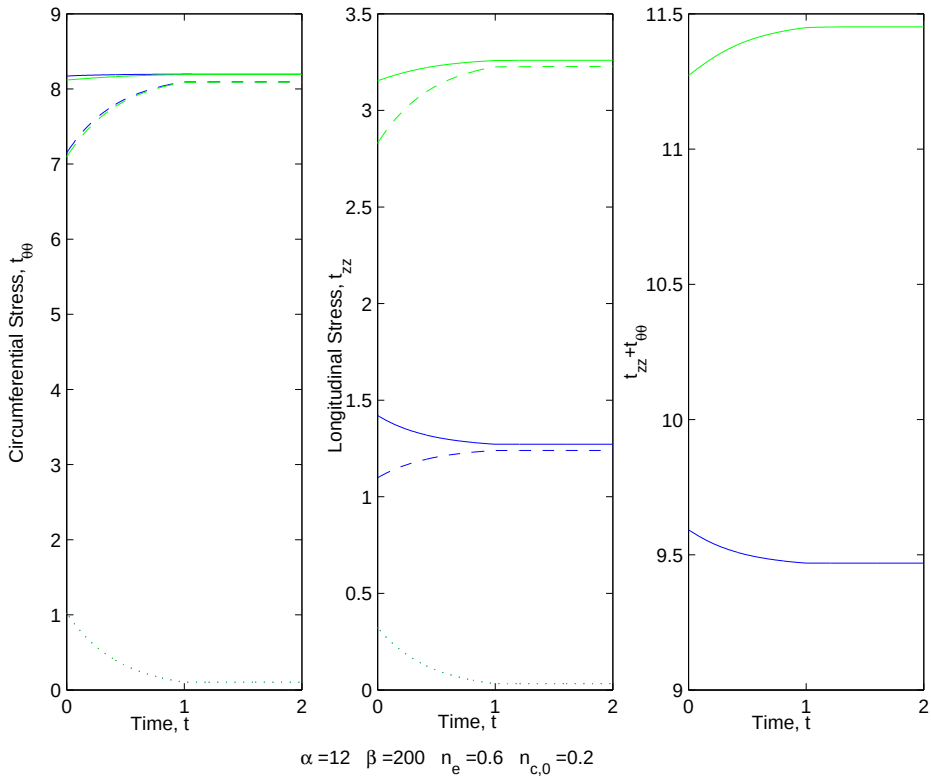

(b) Stresses; total stress (—) is the sum of elastin stress(...) and collagen stress (- -); circumferential stresses overlap

Figure 4.14: Comparison of isotropic (green) and anisotropic (blue) models with stable growth

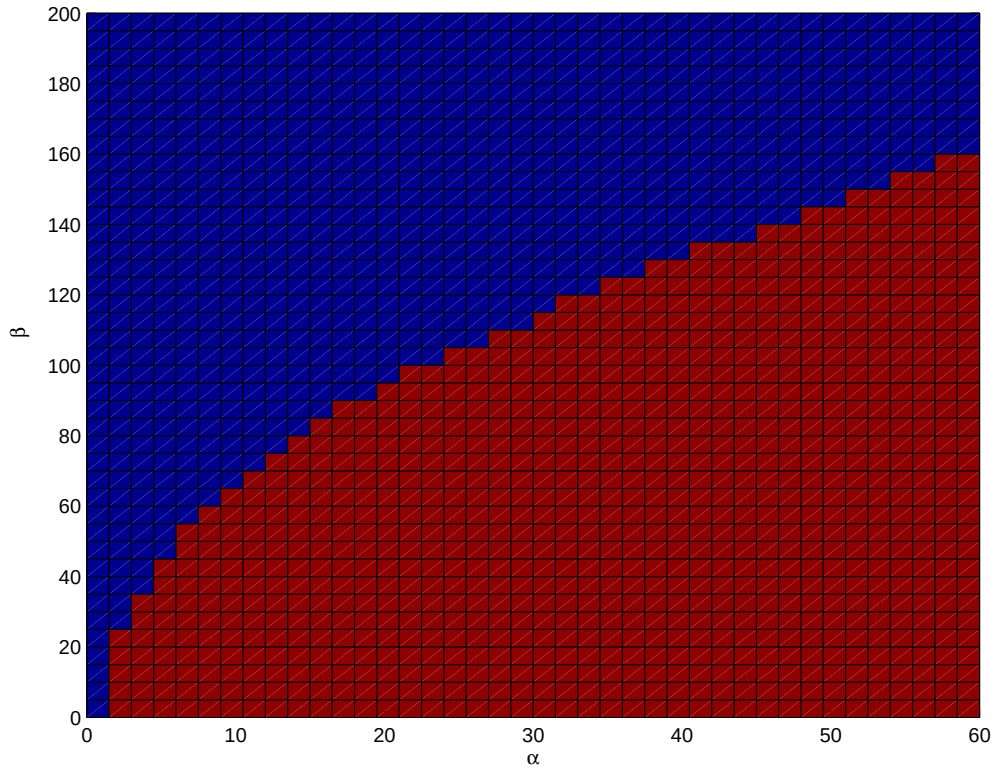

(a) $n_e C_e = 5\text{KPa}$, $n_c k_1 = 36\text{KPa}$ and $k_2 = 60, \lambda_{\theta,a} = 1.473$

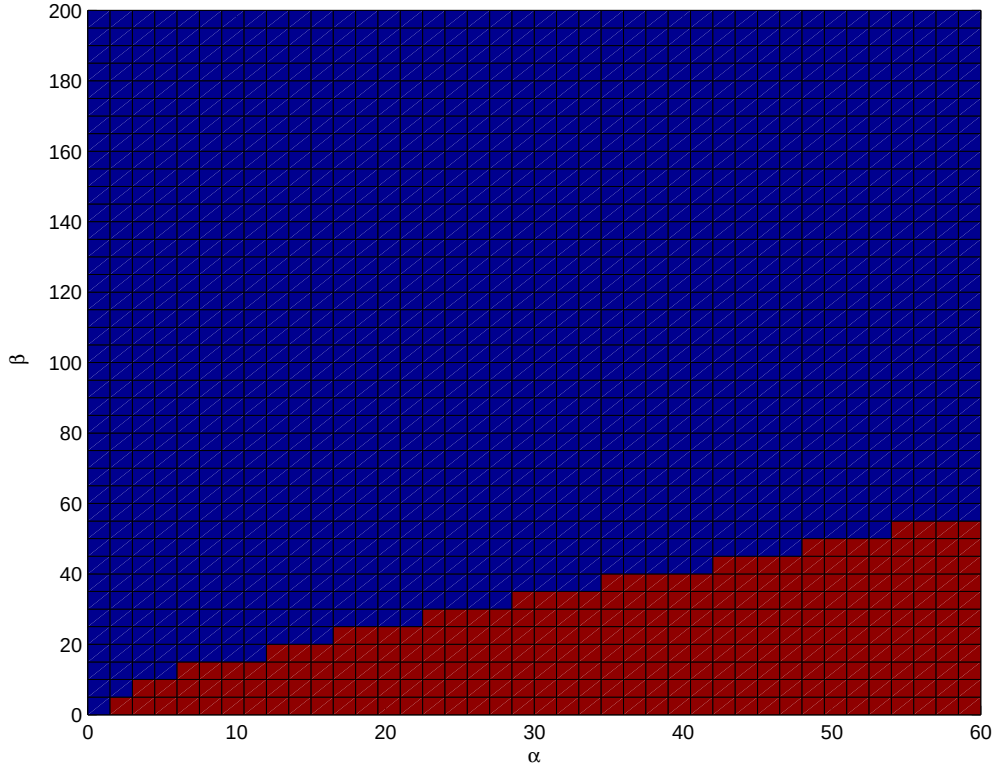

(b) $n_e C_e = 1.668\text{KPa}$, $n_c k_1 = 21.34\text{KPa}$ and $k_2 = 0.0675, \lambda_{\theta,a} = 2$

Figure 4.15: Remodelling parameters and stability of growth for the isotropic model with $n_e = 0.6, n_{c,0} = 0.2$; the blue region shows values of remodelling parameters resulting in stable growth whereas red region shows those for unstable growth

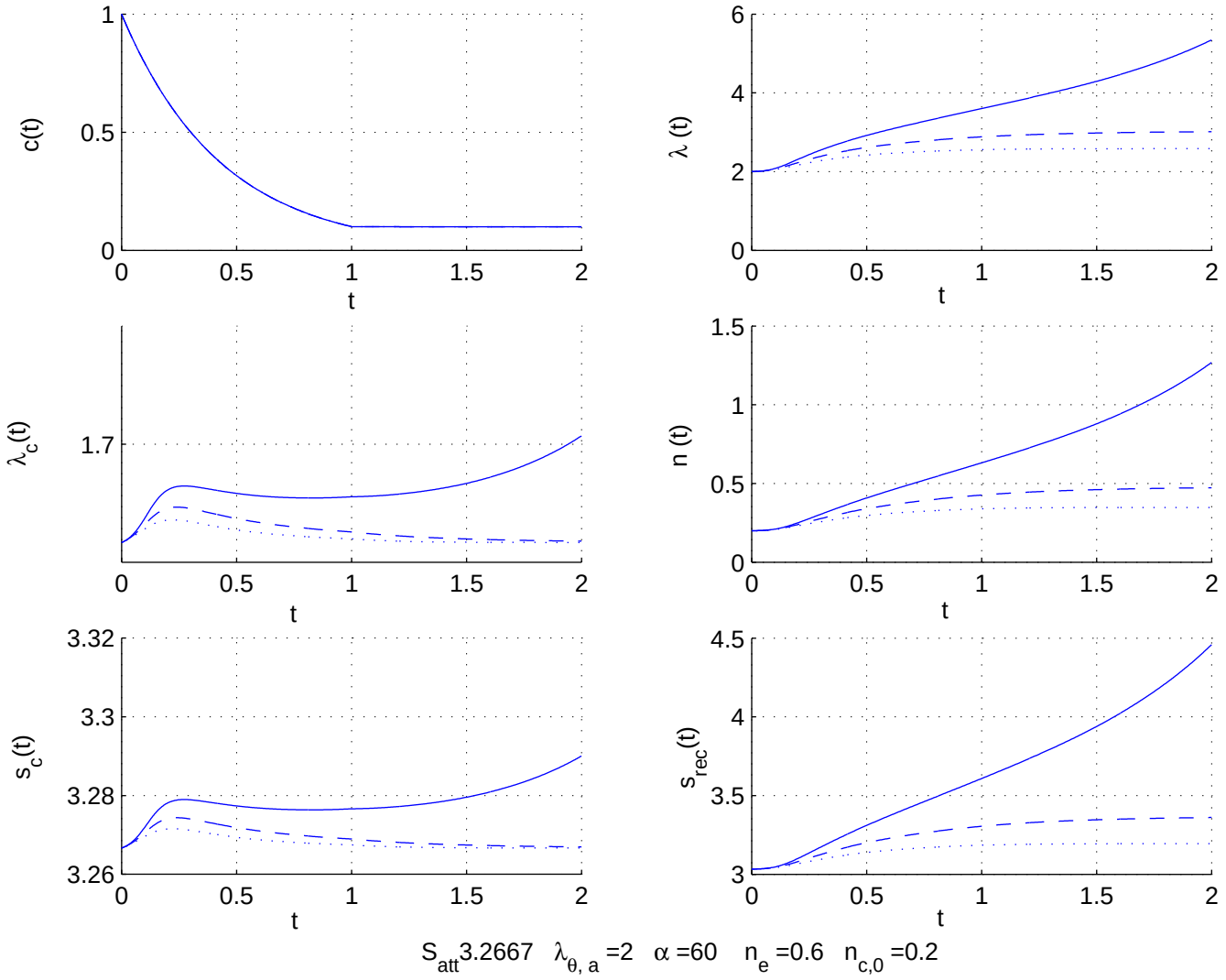

Figure 4.16: Growth for $n_e C_e = 1.668$KPa, $n_c k_1 = 21.34$KPa and $k_2 = 0.0675$: the solid lines are for $\beta = 40$, dashed lines for $\beta = 45$ and dotted lines for $\beta = 50$

Figures: Isotropic Spherical Membranes

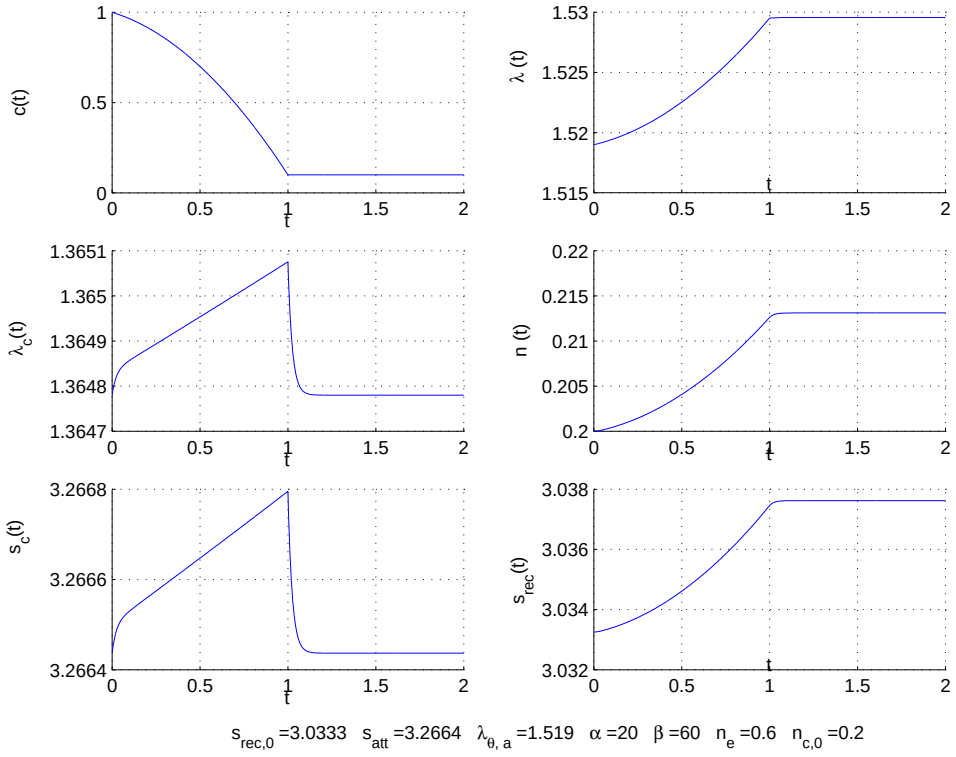

(a) Neo-Hookean Elastin

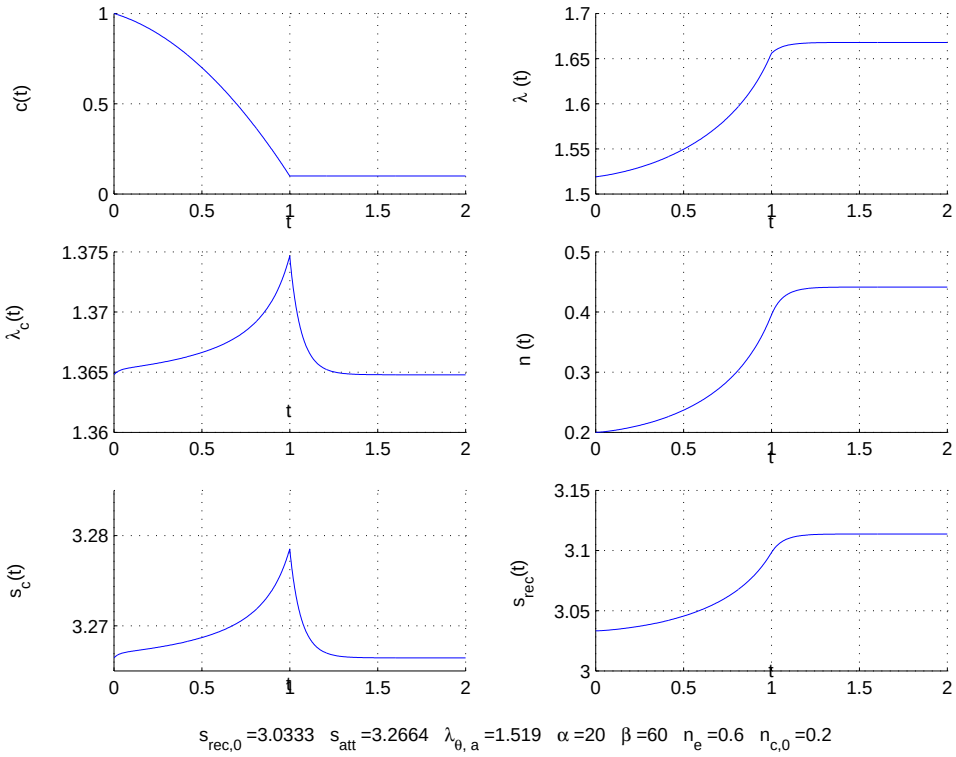

(b) Exponential Elastin

Figure 4.17: Growth of spherical membranes for concave degradation functions

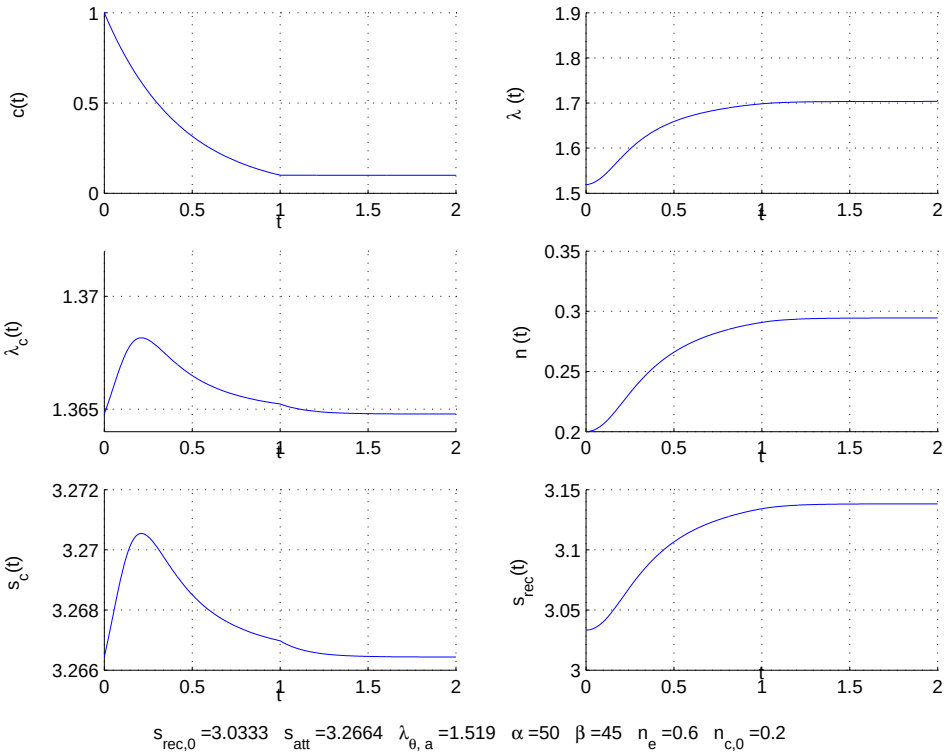

(a) Deformation

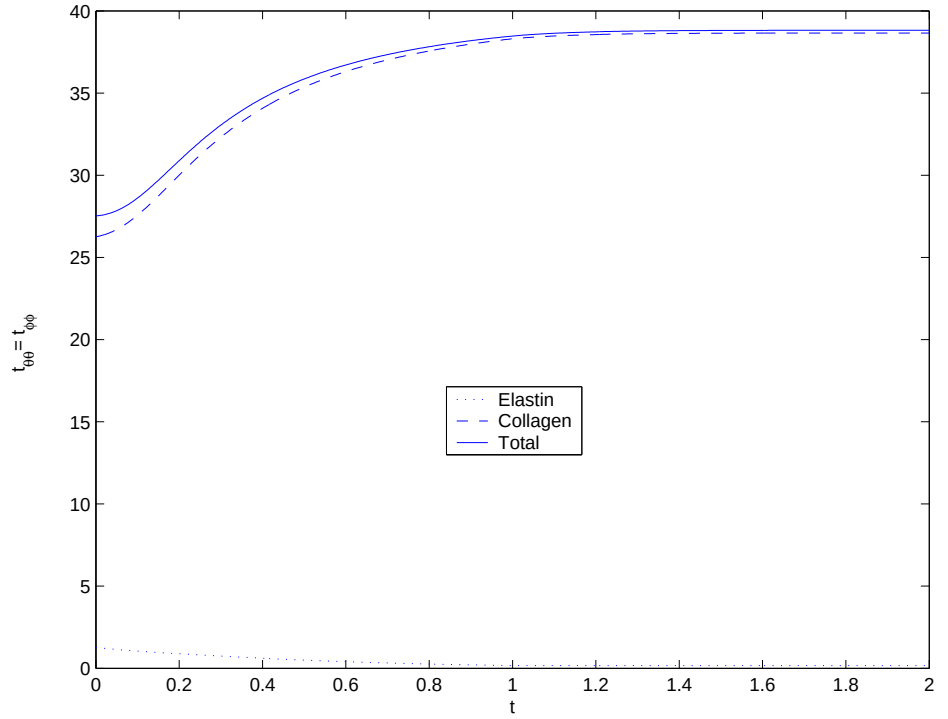

(b) Stresses scaled on C_e; total stress (—) is the sum of elastin stress(...) and collagen stress (- -)

Figure 4.18: Spherical membrane with neo-Hookean elastin and exponential collagen I: maximum stable growth; note that the numbers I and II in this figure and others to follow are just serial numbers.

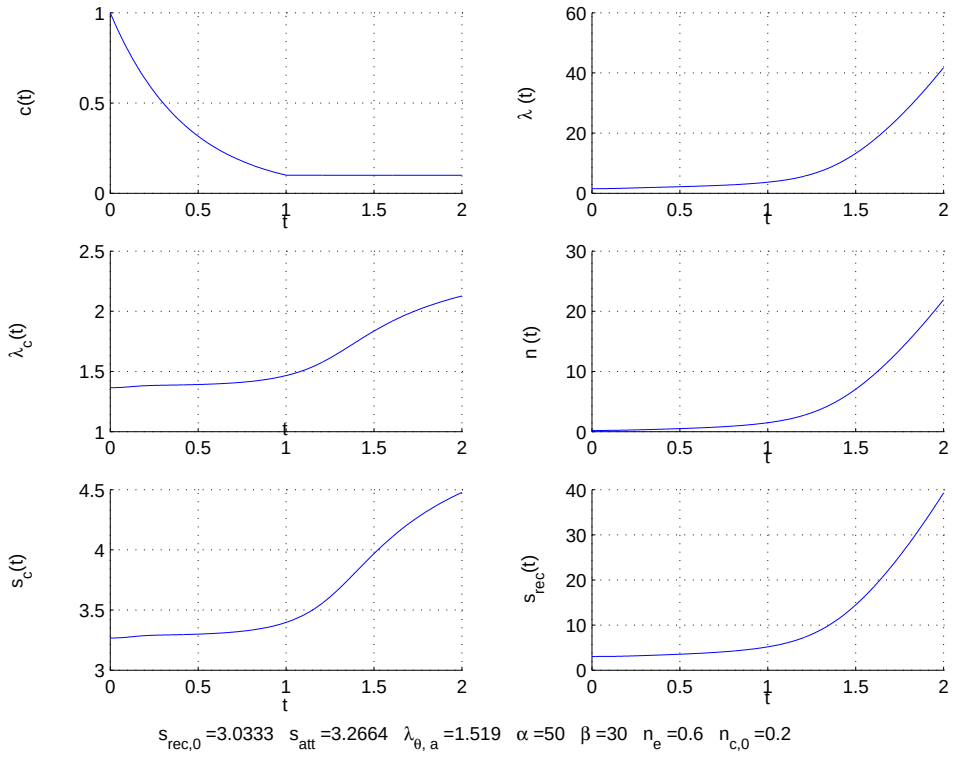

(a) Deformation

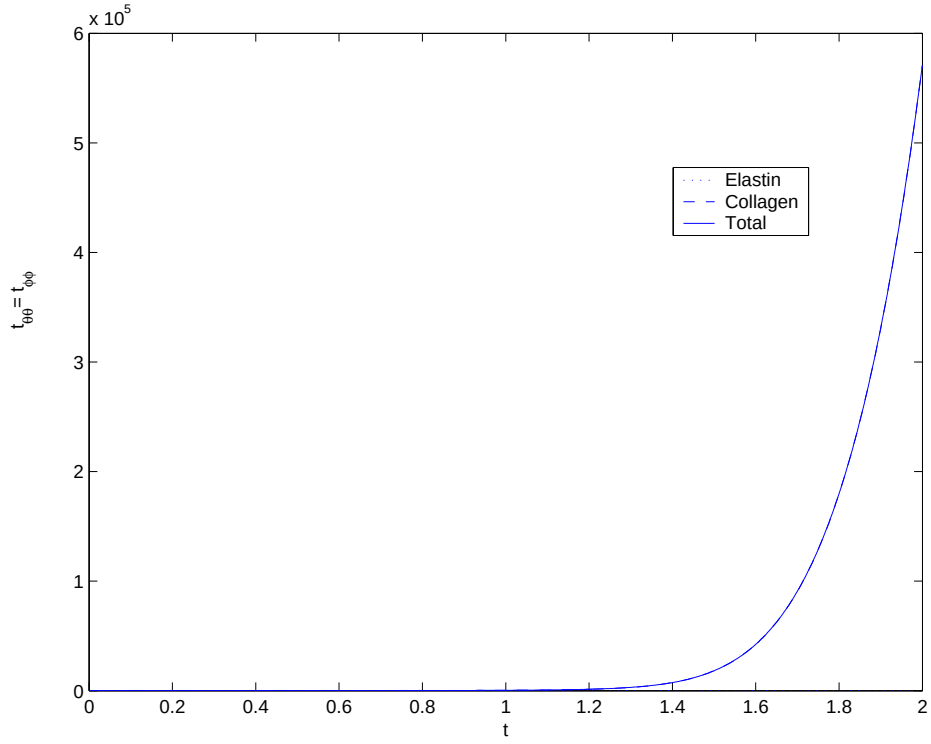

(b) Stresses scaled on C_e; total stress (—) is the sum of elastin stress(...) and collagen stress (- -)

Figure 4.19: Spherical membrane with neo-Hookean elastin and exponential collagen II: unstable growth

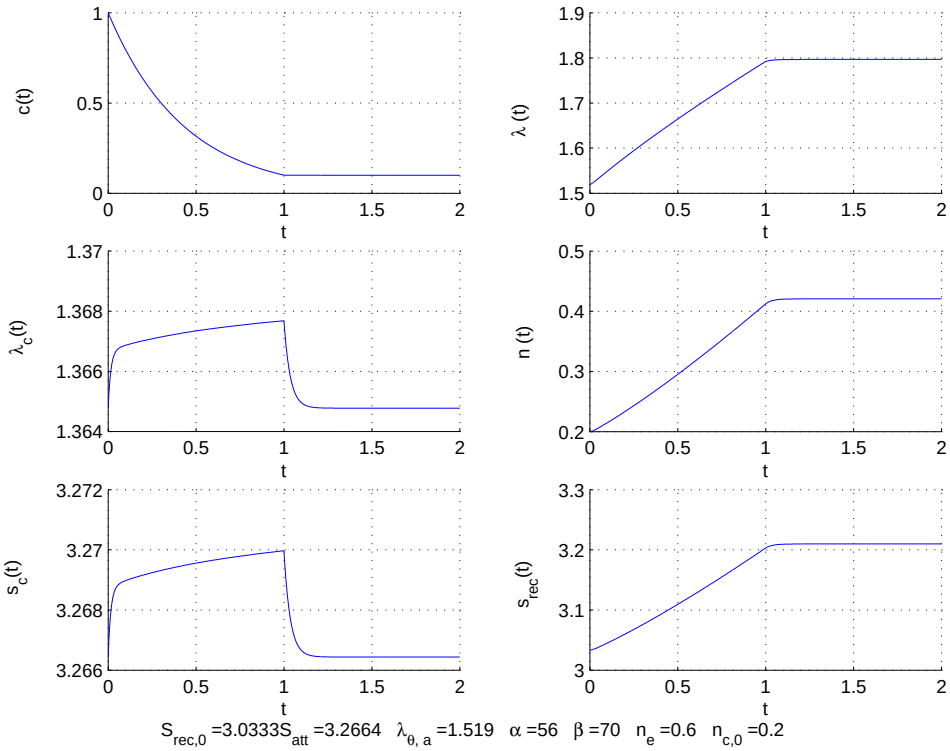

(a) Deformation

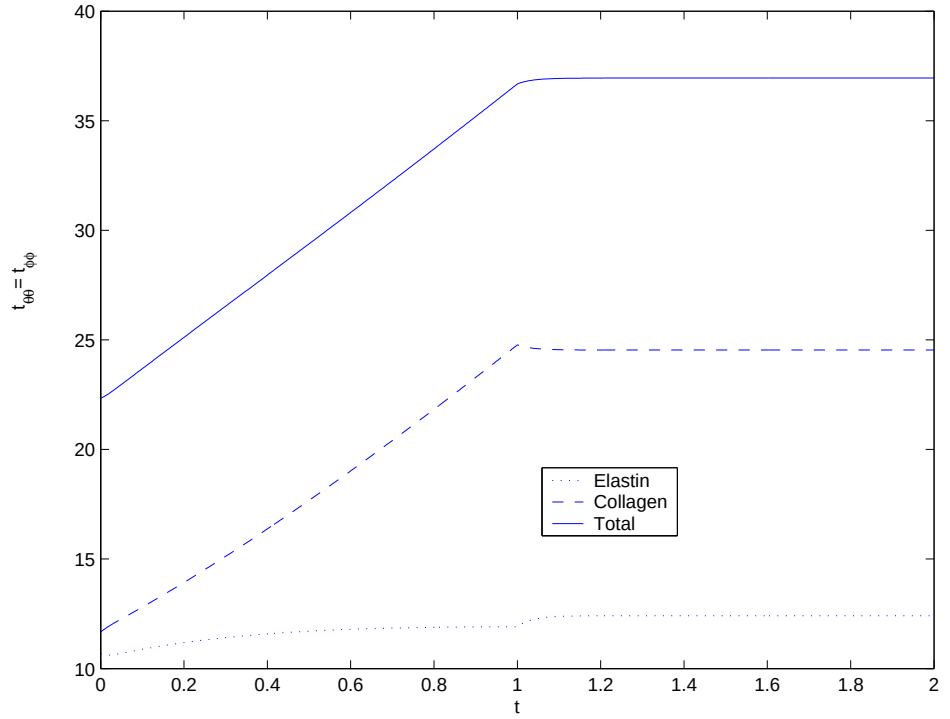

(b) Stresses scaled on k_1^e; total stress (—) is the sum of elastin stress(...) and collagen stress (- -)

Figure 4.20: Spherical membrane with exponential elastin and collagen I; maximum stable growth

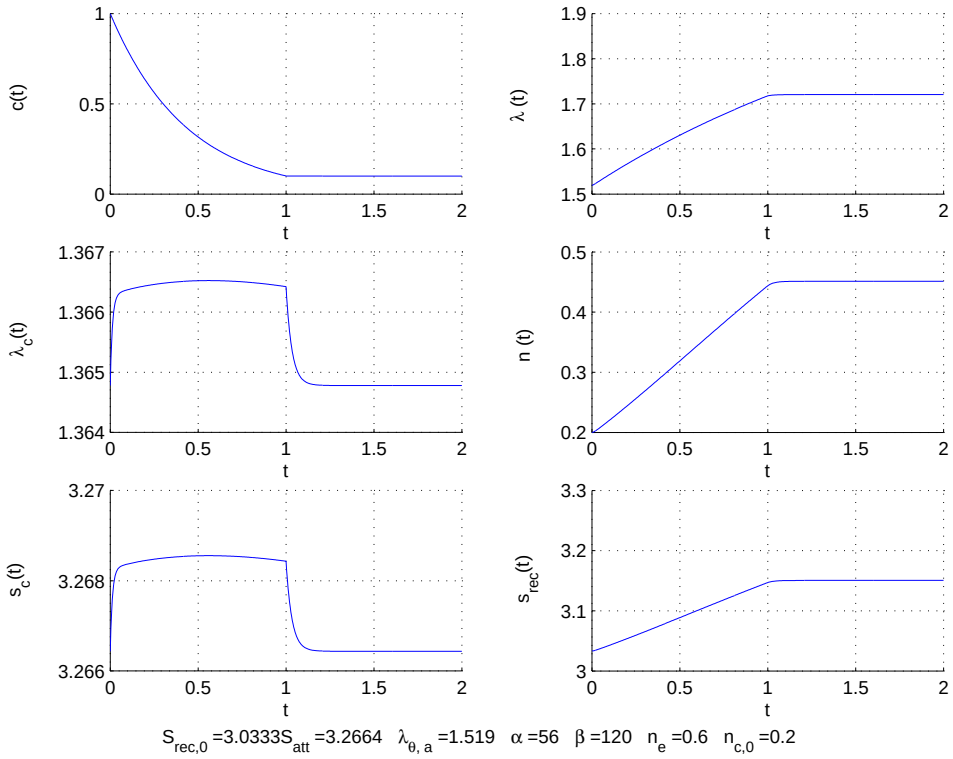

(a) Deformation

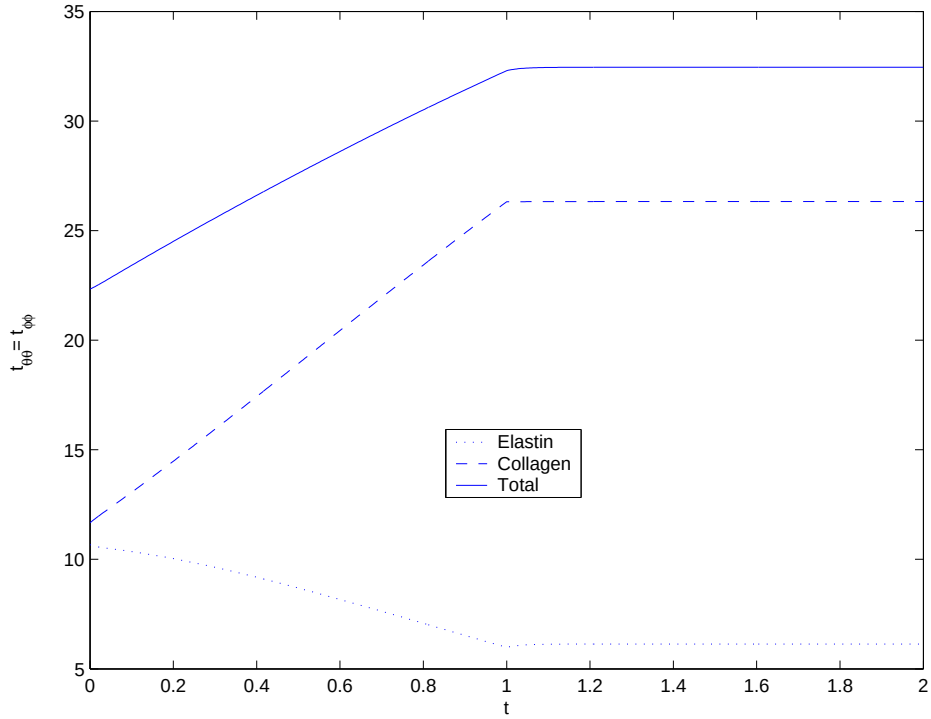

(b) Stresses scaled on k_1^e; total stress (—) is the sum of elastin stress(...) and collagen stress (- -)

Figure 4.21: Spherical membrane with exponential elastin and collagen II; stable growth

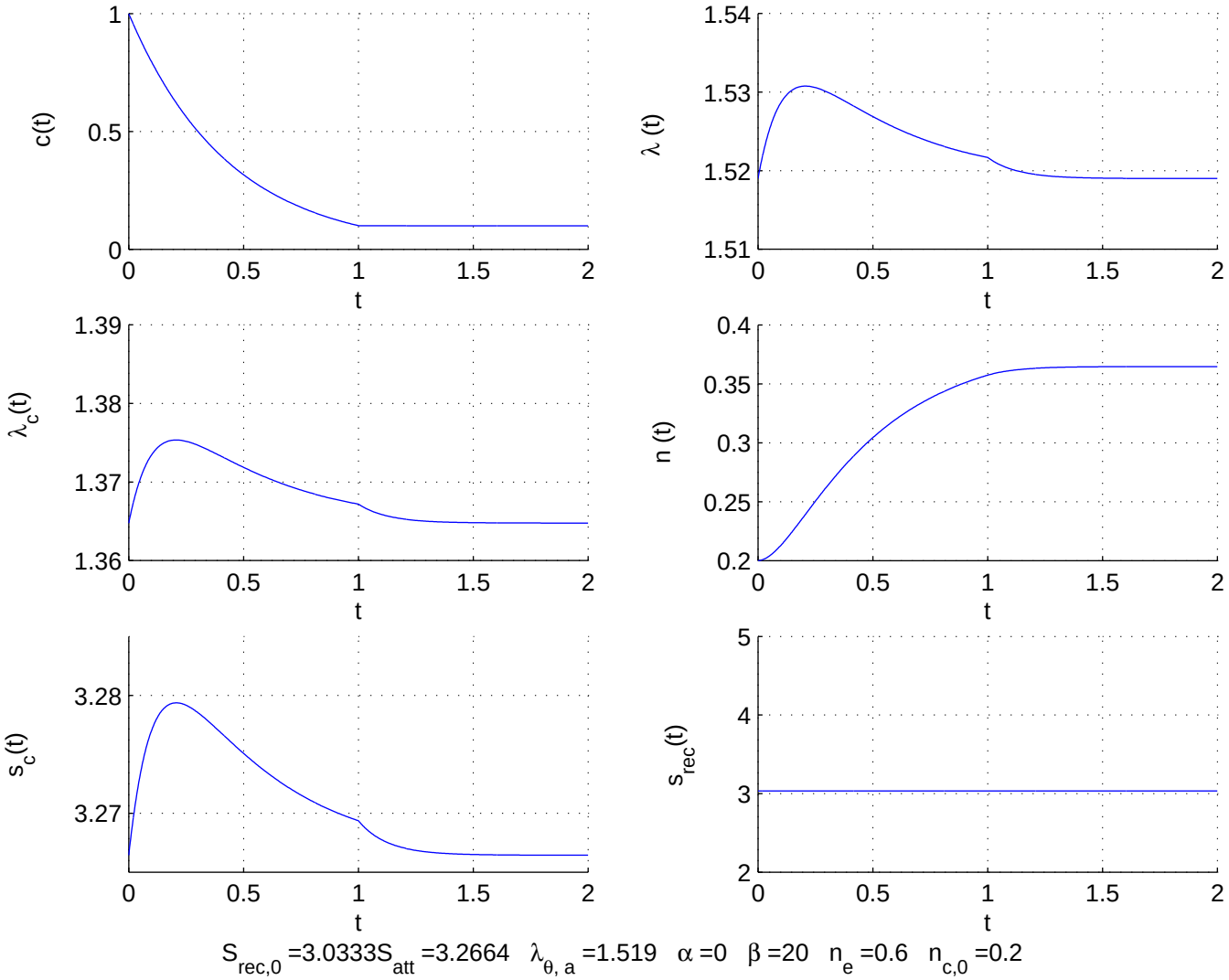

Figure 4.22: Tissue retraction for a thickening-only remodelling

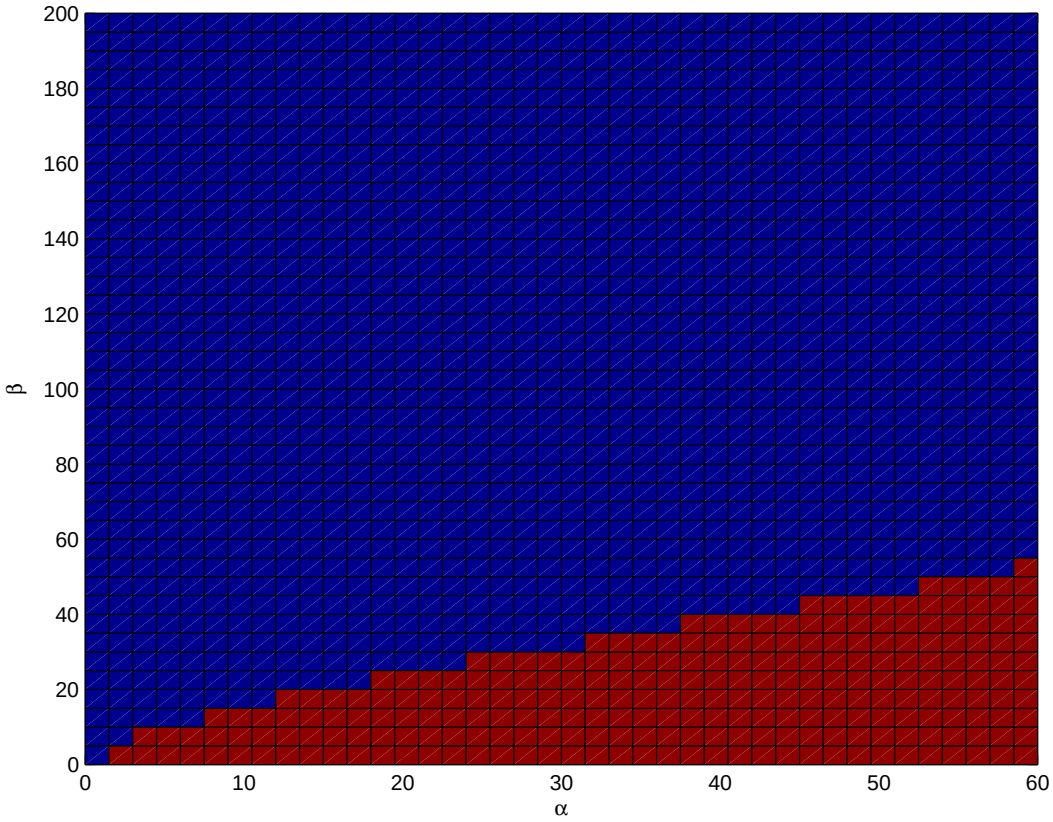

Figure 4.23: Remodelling parameters and stability of growth for a spherical membrane with neo-Hookean elastin and exponential collagen; the blue region shows values of remodelling parameters resulting in stable growth, whereas the red region shows those for unstable growth

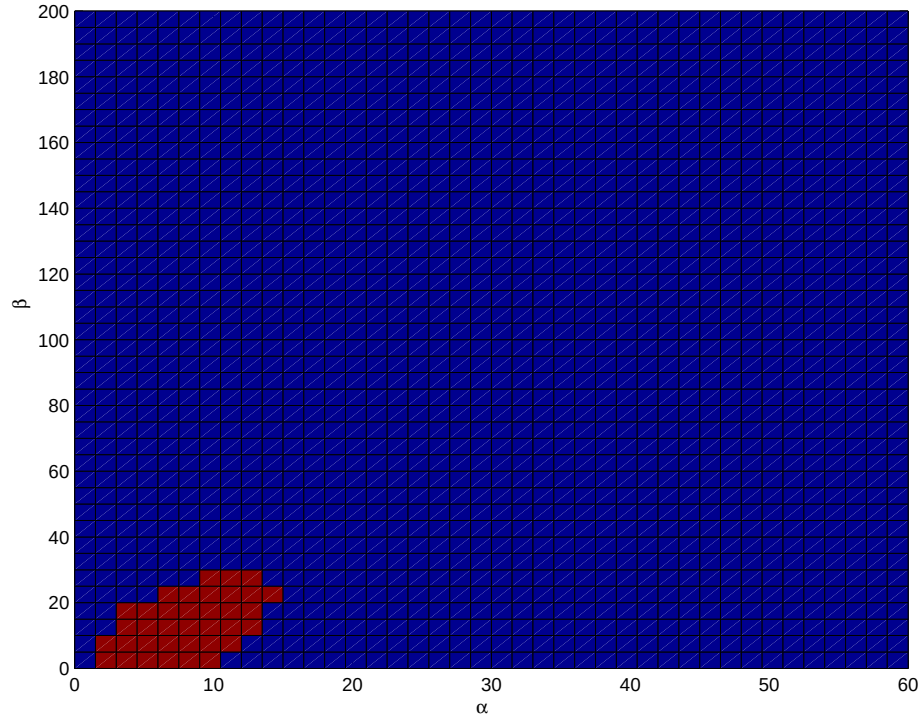

(a) Tissue stretch at attachment $\lambda|_{\lambda_c=\lambda_a} = 1.519$

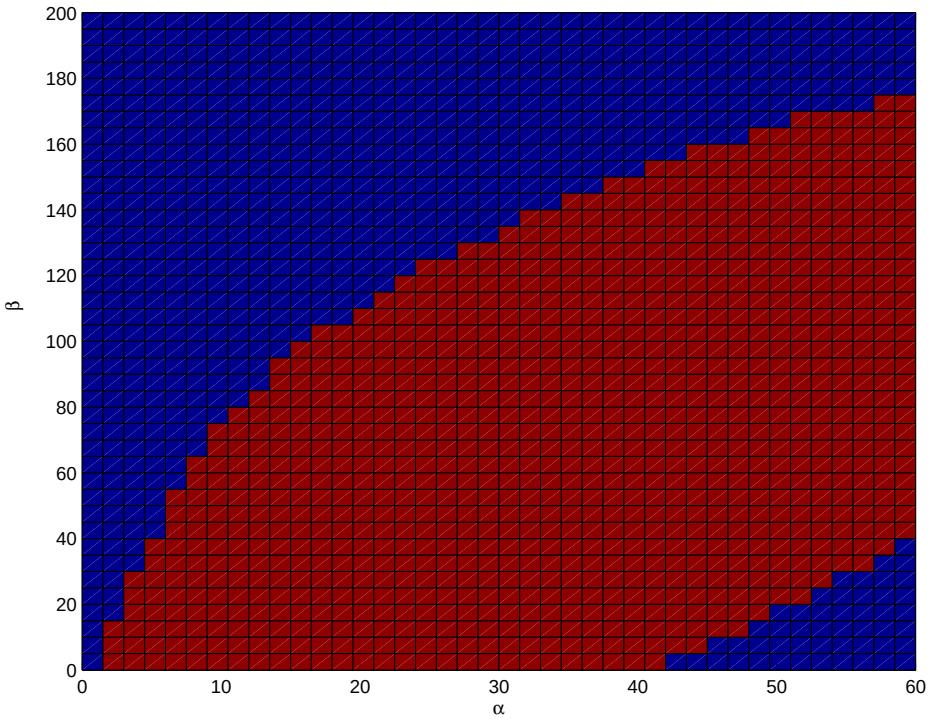

(b) Tissue stretch at attachment $\lambda|_{\lambda_c=\lambda_a} = 1.20$

Figure 4.24: Remodelling parameters and stability of growth for a spherical membrane with exponential elastin and collagen; the blue region shows values of remodelling parameters resulting in stable growth, whereas the red region shows those for unstable growth

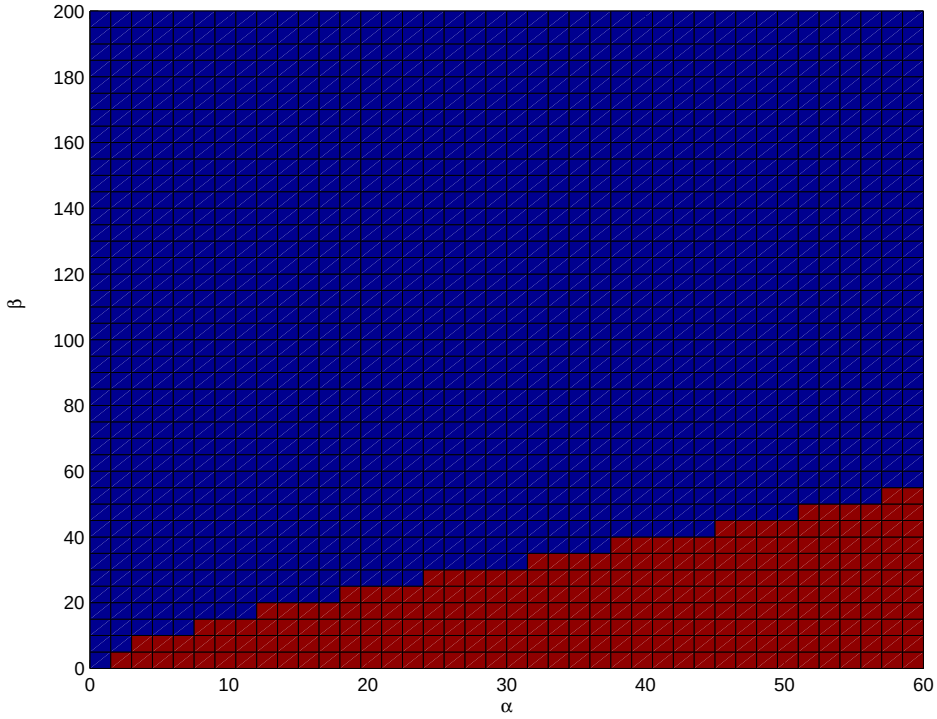

(a) Constrained linear thickening

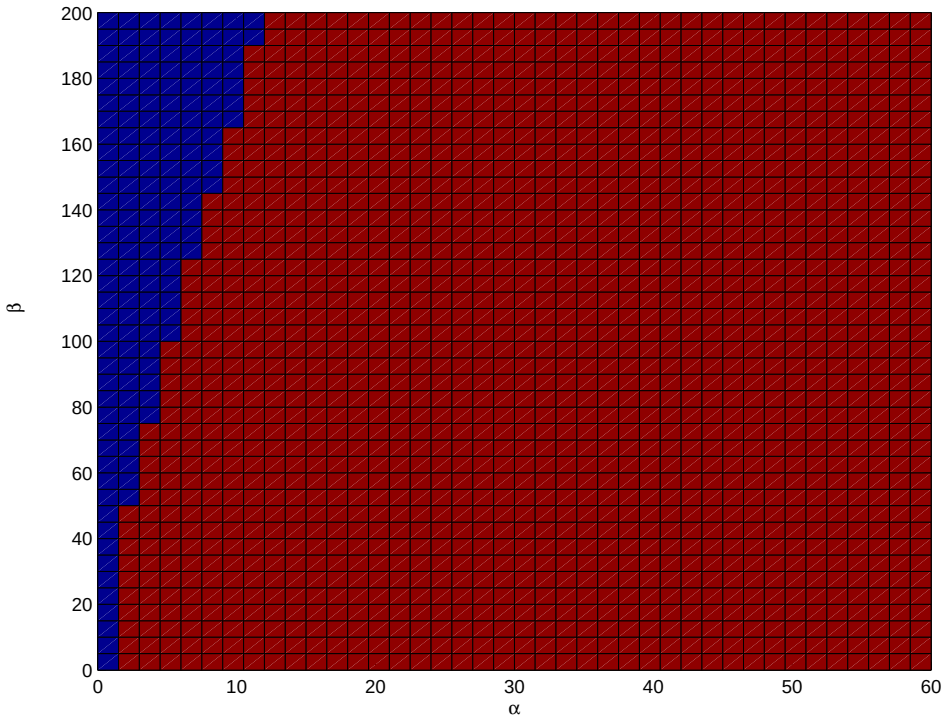

(b) Logistic thickening

Figure 4.25: Remodelling parameters and stability of growth for a spherical membrane with neo-Hookean elastin and exponential collagen with a tissue in-plane stretch at attachment of 1.519 and $n_e = 0.7, n_{c,0} = 0.2$; the blue region shows values of remodelling parameters resulting in stable growth, whereas the red region shows those for unstable growth

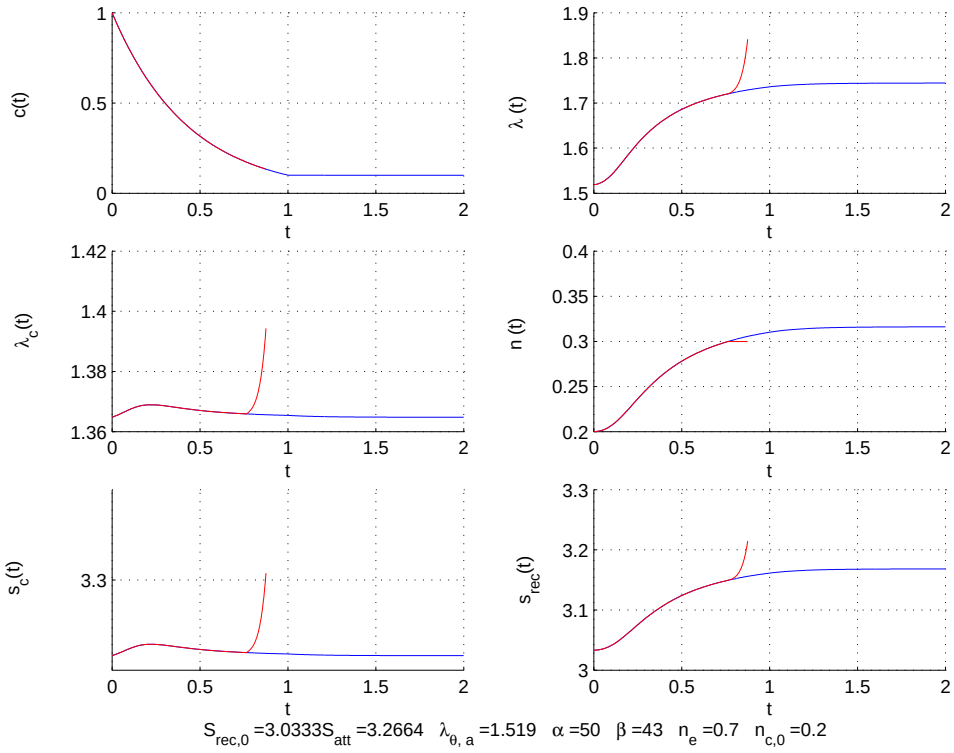

(a) Deformation

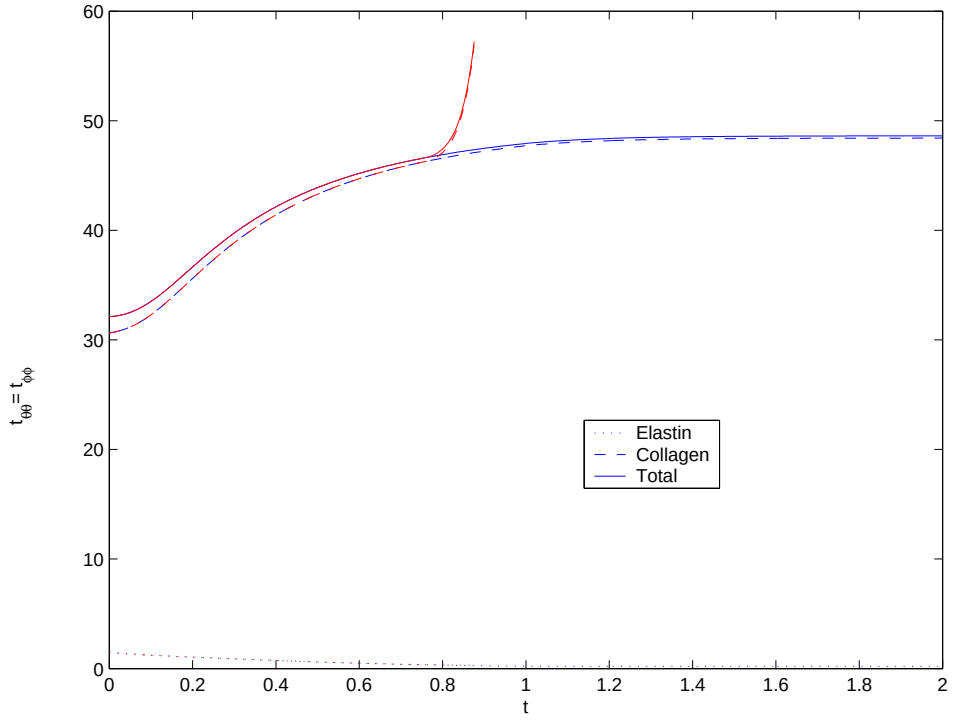

(b) Stresses scaled on C_1; total stress (—) is the sum of elastin stress(...) and collagen stress (- -)

Figure 4.26: Comparison of unconstrained (blue lines) and constrained (red lines) linear thickening for a spherical membrane with neo-Hookean elastin; the plot for the constrained thickening has been truncated because of high magnitudes. See Fig. 4.27 for the complete plot.

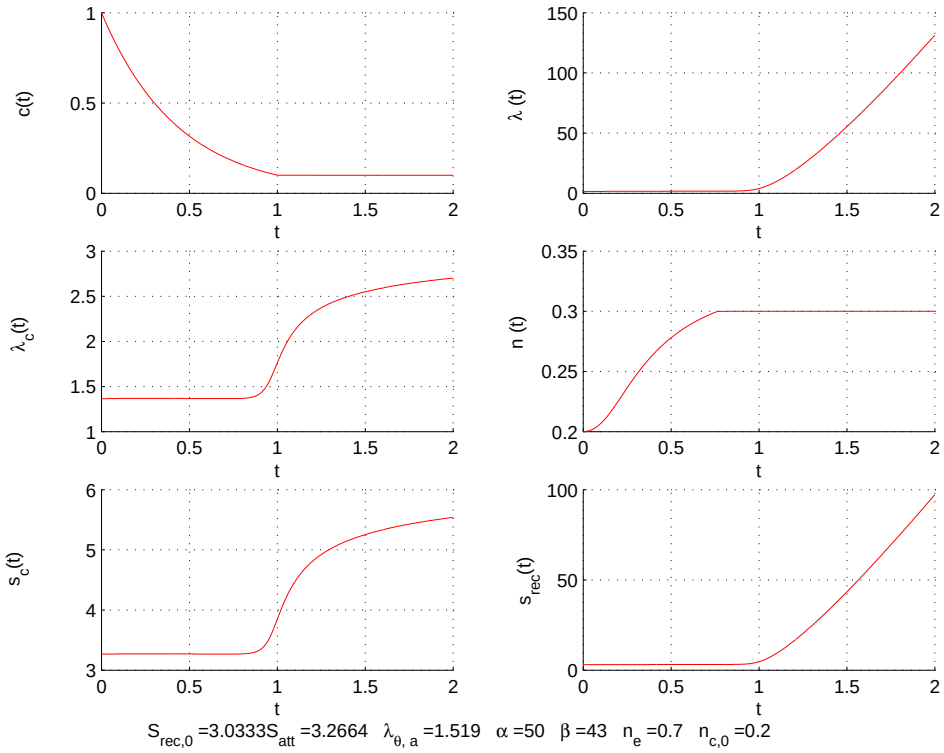

(a) Deformation

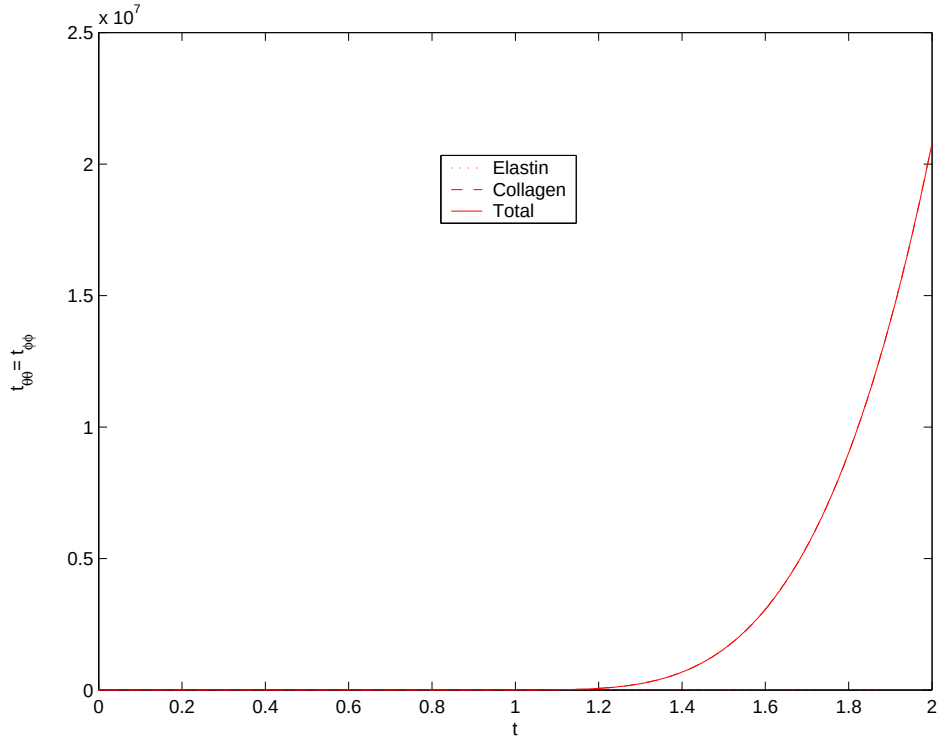

(b) Stresses scaled on C_1; total stress (—) is the sum of elastin stress(...) and collagen stress (- -)

Figure 4.27: Constrained linear thickening for a spherical membrane with neo-Hookean elastin

Chapter 5

On the Finite Element Simulation of Aneurysms

For the numerical simulation of the general model, i.e. a three-dimensional artery with localized elastin degradation given by (3.23), the finite element package Sepran was employed by Machyshyn [23]. An updated Lagrange finite element model for the nonlinear elasticity problem with no time dependence, i.e the equilibrium, constitutive and compatibility equations and boundary conditions for a constant load and constant material parameters was implemented in Sepran by Van Oijen [26]. A tissue model consisting of neo-Hookean elastin (3.17) and exponential collagen (3.21)-(3.22) was used by Van Oijen [26] using a mixed displacement-pressure formulation and a 27-node hexahederal. Machyshyn [23] incorporated the degradation equation (3.23) and remodelling equations (3.27)-(3.28).

A failure of the computation after a certain time was reported by Machyshyn [23]. The error message Sepran produced was that a "Zero or negative Jacobians" was encountered in a certain element. This lead to the conclusion that there is a mesh distortion and remeshing has to be carried out.

One objective of our work was to incorporate remeshing if indeed mesh distortion is the problem or to find out what the problem is otherwise.

What was happening was that a mesh, which was not that distorted as to cause zero or negative Jacobians, becomes suddenly distorted within one time step and the computations break down. In fact it was possible to carry out the computations with the previous mesh, i.e. the mesh at the time step prior to the one at which the computations crashed, if a different set of material constants are used. With this observation material instability became a suspect too. Material instabilities are common in hyperelastic models.

We carried out numerical simulations of models for which we know from a semi-analytic finite difference solution that material instabilities occur. We made a numerical simulation of pressurizing a cylindrical vessel made of a neo-Hookean material, which is known to have an almost horizontal load-displacement curve after a critical load that is dependent on the shear modulus of the neo-Hookean model, and inner and outer radii of the cylinder. Sepran reported "zero or negative Jacobians" at the load where the finite difference solution indicated material instability. A single element out of the the mesh was distorted.

In finite element simulations, material instabilities and numerical instabilities because of kinematic constraints such as incompressibility, can manifest themselves as mesh distortions [2, p. 6-18,19]. In many cases, numerical instability is apparent even in the early stages of

the analysis [2, p. 6-19]. Some finite element packages (ANSYS for example) issue a warning when a material may become unstable. Some other packages (such as MSC Marc) are able to continue computations through instabilities. Sepran, on the otherhand, does neither [†]. It thus becomes the responsibility of the analyst to track material instabilities and judge what the "zero or negative Jacobians" reports are due to.

At this point we would like to emphasize that mesh distortion caused by material instability does not mean that the finite element package employed is giving erroneous results. For example, a localized buckling results in one or few distorted elements and negative Jacobians will be encountered in element mapping of the next iterative step; what differs between packages is whether the mesh distortion only is reported or its associated cause is also reported. In any case remeshing is for mesh distortion resulting from large, non-uniform deformations and not for other causes.

A criterion widely used to trace instabilities is the Drucker stability postulate which states that the additional work done by an additional external agency must be positive. In a nonlinear finite element formulation using the Newton-Raphson method to solve the nonlinear algebraic equations at every load step, Drucker's requirement translates into requiring positive definiteness of the tangent stiffness matrix. When the tangent stiffness matrix is positive definite at a certain load step and non-positive definite at the next load step, the structure is considered to become unstable between the two load steps. However, this works only if all state variables are of the displacement type. For formulations in which Lagrange multipliers are carried along as degrees of freedom, which is what we have in our mixed pressure-displacement formulation, this requires eliminating the multipliers and this is often "messy" [9].

Another indication for the existence of a material instability is the degeneration of the convergence rate of the Newton-Raphson iteration. We observed that the Newton-Raphson iteration fails to converge at the time step in which the computations failed. Degeneration of the Newton-Rahpson iteration, however, does not necessarily mean material instability. We carried out numerical simulation of a neo-Hookean prismatic bar under uniaxial tension. The analytical solution of this problem is known and it does not exhibit material instabilities. Neither do we expect mesh distortions. However, the computation failed with Sepran issuing a "zero and negative Jacobians" message. We found out that an element in the mesh was extremely distorted. This failure should be because of numerical oscillations. Indeed we observed oscillations in the pressure term.

One can some times distinguish between material and numerical instability by using a damped Newton-Raphson iteration. If a damped iteration cures the problem, then it was because of numerical oscillations. If on the other hand it is a material instability, damping will not remedy it. Note that in a mixed pressure-displacement formulation numerical instabilities can occur because of the Lagrange multiplier (the hydrostatic pressure in our case) even though the material is stable.

We have carried out numerical experiments to test this hypothesis using models for which we know from analytical solutions whether material instabilities occur or not. For a prismatic neo-Hookean rod subjected to tension, which does not exhibit material instabilities, we were able to carry out the simulations to a larger load with damping than without. In a pressurized neo-Hookean cylinder, where material instabilities occur, damping did not help.

At this stage, we believe that the problem is not genuine mesh distortion. Other problems manifesting themselves as mesh distortion can not be remedied by remeshing [2, p. 6-18].

[†]Private communication with the Sepran author, Guus Segal

The constitutive equations implemented by Van Oijen [26] are done so using quadratic hexahedral. For small deformations, quadratic elements result in better accuracy over linear elements. For large deformations, however, quadratic elements should be avoided as they will easily become concave during deformation and result in negative Jacobians while mapping the element into the master element. Remeshing requires generating a new mesh and interpolating the solution from the old mesh to the new one. Remeshing subroutines currently available in Sepran do not support three-dimensional elements. Neither do the interpolation commands support hexahedrals. Guus Segal[†] recommends using tetrahedrals if interpolation is envisaged. Raoul van Loon [32] has implemented a remeshing scheme for a fluid-structure interaction problem using tetrahedral elements.

To carry out computations through material instabilities, one of the different methods called *continuation methods* has to be used. Among continuation methods, the one widely used in finite element packages is the *arc length algorithm*. Implementing this algorithm is beyond the scope of this work.

[†]Private communications

Chapter 6

Conclusions and Recommendations

We had roughly two objectives at the beginning of this work. The first was investigating different constitutive equations and remodelling laws. The second was remedying the crash in the computation that were faced by Machyshyn [23].

We carried out the numerical simulations for the first part using custom made Matlab codes. This was because the constitutive relations we wanted to investigate were not all supported on the available finite element package, Sepran. We could have implemented the constitutive equations into Sepran after obtaining the weak forms and carrying out the associated linearizations for all constitutive equations. But given the time constraints such an endeavor would be unrealistic. It was thus decided to consider simplified versions of the problem and compare the effects of constitutive and remodelling equations. To this end cylindrical membranes with homogenous deformations were considered.

The second objective was taken up with a significant bias on what was actually happening. The crash in the numerical simulation was considered to be because of large deformations and subsequent mesh distortion. After spending considerable time and effort investigating ways to circumvent mesh distortion we realized that the problem was not mesh distortion but material and/or numerical instabilities disguised as mesh distortion. Solving these instabilities is however far from trivial and could not have been done within the remaining time.

Another issue which cropped up during the work was that even for the constitutive relation which had been in use, the material constants were not properly determined. We therefore carried out statistical analysis using experimental data available in the literature.

In this chapter, we discuss the major conclusions of our work, limitations of the models implemented and recommendations for future work.

6.1 Conclusions

6.1.1 Constitutive, Degradation and Remodelling Equations

Among the material models we considered, the isotropic ones fitted the experimental data, specifically for cerebral arteries, much better than the anisotropic ones. This in no way means that cerebral arteries are isotropic. But considering the fit to the experimental data shown by the isotropic models and the absence of evidence, such as from a biaxial testing, against isotropic models, we conclude that isotropic models are at least as good as anisotropic models as a mathematical abstraction of the mechanical behavior of cerebral arteries. Finlay et al. [10] have shown from a morphological study of the apex of bifurcation of cerebral arteries

that collagen fibers are randomly oriented. This evidence also supports the case for isotropic models.

The ratio of the stress-free radius of the post-shifting curve to the pre-shifting radius in the experiment of Scott el al. [34] indicates a circumferential tissue stretch of 1.76 at attachment. We are not able to explain why the regression analysis with this value resulted in a poor fit. Wulandana and Robertson [47] carried out a joint regression analysis considering both the pre-shifting and post-shifting data and obtained a better fit using a circumferential stretch of 1.76 than what we have. We used only the pre-shifting curve.

Anisotropic models can result in situations in which the stress is higher in one direction than the other. We observed in the numerical simulation of cylindrical membranes that the stress in the circumferential direction can be an order of magnitude larger than the stress in the longitudinal direction. Apart from that, the growth magnitude and pattern did not exhibit significant differences between isotropic and anisotropic models.

How large the tissue deforms in the case of stable growth is determined by how much of the elastin strength is lost or equivalently by the minimum strength of the elastin with greater loss of elastin strength leading to larger growth. The shape of the growth curve, on the other hand, depends on the pattern of degradation. Using linear, convex and concave degradation functions, we observed from our numerical simulations that convex degradations lead to concave stable growth and concave ones result in convex stable growth. From the experimental evidence that stable cerebral aneurysms showed concave growth we infer that elastin degradation follows a convex path.

For a given degradation function, the growth can be stable or unstable depending the the remodelling parameters α and β. For a material model with neo-Hookean elastin and exponential collagen, a larger β/α ratio means smaller stable tissue stretch and stress where the smaller the ratio the larger the stresses and stretches and the higher the probability that the growth will be unstable. For models in which both constituents have exponential strain energy functions, the growth for convex degradation functions is unconditionally stable except for a small region of $\alpha - \beta$ plane.

Some investigators have suggested that the tissue may not start remodelling at the same time as the degradation [22]. We infer from our numerical simulation that for a stable growth, delayed remodelling does not affect the tissue size and stresses.

In this work we introduced the idea that the collagen should not be allowed to thicken indefinitely, i.e. the volume fraction of collagen n_c should be constrained to a certain maximum value. By so doing, we observed that the model can explain why vessels, which seem to be stabilizing, can grow at a very fast rate and may rupture.

For the model we selected as the most promising one, i.e. neo-Hookean elastin and exponential collagen, convex degradation, and remodelling with constrained thickening, the growth pattern is similar to what is clinically observed.

6.1.2 Remeshing and Instabilities

As opposed to what we assumed at the outset of this work, the mesh distortion observed was not due to large non-uniform deformation but to material and/or numerical instabilities. The implementation of algorithms to take care of material instabilities is quite involved and beyond the scope of this work. To avoid the numerical instabilities, which we presume to be because of the incompressibility constraint, one has to use a compressible material model.

While this report was being compiled, we learned that the group[†] involved in this research was moving into remodelling in which new collagen fibers are laid out at a constant stretch state. In that case, material instabilities may no longer be an issue.

6.2 Limitations in the Current Model

Blood vessels are subjected to longitudinal and non-uniform circumferential pre-stretches. We did not consider pre-stretches in this work.

In the equilibrium equations, Laplace formula in our case, we considered the wall thickness to change with the elastin stretch. A more realistic yet complicated model would have been to take into account the change in thicknesses due to both constituents.

We considered a blood vessel isolated from the supporting tissue. Aneurysm growth may be affected by extrinsic factors in its environment. Supporting evidence, however, is limited. Compact constrains established between the vessel and its environment could affect the aneurysm either positively or negatively, offering either protection against rupture or added propensity to rupture [45]. We used the simplifying assumption that the vessel is free from its environment except the blood pressure on the wall.

6.3 Recommendations

A lot remains to be investigated before we can confidently talk of a patient-specific predictive model of aneurysms. The most important of all, in our opinion, is a proper mechanical characterization of the artery. The experimental data available to date does not enable us to answer such important questions as whether the cerebral wall is isotropic or anisotropic.

Once a proper characterization of cerebral arteries is made, a suitable computational platform becomes necessary. We recommend the implementation of the arc length or other similar continuation methods to take care of material instabilities, if the current model is to be investigated further. It is also important to shift to linear elements from the quadratic elements now in use.

In addition to fiber elongation and thickening, fiber reorientation may also occur during remodelling. Incorporating that into the model is recommended. Here too the importance of experimental evidence is emphasized.

In this work, the collagen thickening was implemented as an involvement of inactive collagen which was already there. We have mentioned some experimental data which suggest new collagen is produced in aneurysms. We suggest inclusion of a mass balance equation in future models. We further recommend putting an upper limit on how much new collagen can be produced. Otherwise the tissue would always have an unlimited reserve of reinforcements and the models may not be able to predict rupture, which from a mechanical perspective is hypothesized to occur when the applied stresses exceed the capacity of the tissue. To say whether rupture is possible or not, proper failure theories should be used.

Once again, it goes without saying that unless supported by relevant experimental evidence a mathematical model remains yet another theory be it simple or complicated.

[†]Cardiac Mechanics, Department of Biomedical Engineering, TU/e

Appendix A

Nomenclature

In this report, scalars are denoted by italic characters (for example t for time), vectors are denoted by bold characters (for example $\mathbf{e}$ for a unit vector) and calligraphic characters are used for tensors (like $\mathcal{T}$ for stress).

The dimensions of physical quantities are expressed in terms of the fundamental dimensions mass (M), length (L) and time (T).

Table A.1: Operators

Symbol	**Description**
det	Determinant
div	Divergence
tr	Trace

Table A.2: Physical quantities represented by Greek letters

Symbol	**Description**	**Dimension**
α	Collagen recruitment rate	T^{-1}
β	Collagen thickening rate	T^{-1}
γ	Fiber orientation with respect to the circumferential direction	
λ_a	Collagen attachment stretch	
λ_c	Collagen stretch	
λ_{rec}	Collagen recruitment stretch	
$\lambda_{rec,0}$	Initial collagen recruitment stretch	
λ_θ	Tissue (elastin) stretch in the circumferential direction	
λ_θ, a	Tissue (elastin) stretch at attachment	
λ_ϕ	Tissue (elastin) stretch in the meridional direction	
τ_f	Fiber stress	$ML^{-1}T^{-2}$

Table A.3: Physical quantities represented by Roman letters

Symbol	Description	Dimension
$\mathcal{B}$	left Cauchy-Green stress stretch tensor	
$\mathcal{B}_c$	left Cauchy-Green stretch tensor for collagen	
$\mathcal{B}_e$	left Cauchy-Green stretch tensor for elastin (same as tissue)	
c	elastin degradation function	
$\mathcal{C}$	right Cauchy-Green stretch tensor	
C_e	Shear modulus of elastin	$ML^{-1}T^{-2}$
$C_{e,0}$	Initial shear modulus of elastin	$ML^{-1}T^{-2}$
$\mathbf{e_c}$	Unit vector in the direction of fibers in the deformed state	
$\mathbf{e_o}$	Unit vector in the direction of fibers in the reference state	
$\mathcal{F}$	Tissue (elastin) deformation gradient tensor	
$\mathcal{F}_c$	Collagen deformation gradient tensor	
$\mathcal{F}_{rec}$	Collagen recruitment tensor	
$\mathcal{F}_{rec,0}$	Initial collagen recruitment tensor	
h	Thickness of a membrane in the deformed state	L
H	Thickness of a membrane in the reference state	L
I	First invariant (trace) of the left Cauchy-Green stretch tensor	
I_c	First invariant (trace) of the left Cauchy-Green stretch tensor for collagen	
I_e	First invariant (trace) of the left Cauchy-Green stretch tensor for elastin	
$\mathcal{I}$	Identity Tensor	
k_1	Linear constant in an exponential strain energy density function	$ML^{-1}T^{-2}$
k_2	Exponential constant in an exponential strain energy density function	
n	Volume fraction of collagen (active and inactive)	
n_c	Volume fraction of active collagen	
n_e	Volume fraction of elastin	
n_p	Volume fraction of procollagen (inactive collagen)	
p	Hydrostatic pressure	$ML^{-1}T^{-2}$
P	Applied pressure	$ML^{-1}T^{-2}$
r	Radius of a membrane in the deformed state	L
R	Radius of a membrane in the reference state	L
s_a	Trace of the collagen deformation gradient at attachment	
s_{rec}	Trace of the collagen recruitment tensor stretch	
$s_{rec,0}$	Trace of the initial collagen recruitment tensor	
T	Tension	MLT^2
$\mathcal{T}$	Stress tensor	$ML^{-1}T^{-2}$
$\mathcal{T}_c$	Stress tensor for collagen	$ML^{-1}T^{-2}$
$\mathcal{T}_e$	Stress tensor for elastin	$ML^{-1}T^{-2}$
W	Tissue strain energy density	$ML^{-1}T^{-2}$
W_c	Collagen Strain energy density	$ML^{-1}T^{-2}$
W_e	Elastin strain energy density	$ML^{-1}T^{-2}$
$\mathbf{x}$	Position vector of a point in the deformed state	L
$\mathbf{X}$	Position vector of a point in the reference state	L

Appendix B

Glossary of Biomedical and Related Terms

Anatomy The study of structure and organization of living things. Gross anatomy involves structures that can be seen with the naked eye as opposed to microscopic anatomy (see *histology*) which involves structures seen under the microscope.
Adjective: *Anatomic, Anatomical*

Angiography X-ray examination of blood vessels following injection of a radiopaque (see *radiopaque*) substance.
Adjective: *Angiographic.*

Arteriosclerosis A degenerative change in the arteries, characterized by thickening of the vessel walls and accumulation of calcium with consequent loss of elasticity and lessened blood flow.
Adjective: *Arteriosclerotic.*

Congenital Pertaining to a condition present at birth, whether inherited or caused by the environment.

Distensibility The phenomena of expanding by stretching.

Endothelium A single thin layer of flat cells that line the interior surface of blood vessels, forming an interface between circulating blood in lumen (see *Lumen*) and the rest of the vessel wall.
Adjective: *Endothelial.*

Fundus A generic term referring to the portion of an organ opposite from its opening.
Adjective: *Fundic.*

Hemodynamics The study of the flow and properties of blood. Also called *hemorheology.*
Adjective: *Hemodynamic.*

Hemorrhage Escape of blood to extravascular space.

Histology The study of form of structures seen under the microscope. Also called microscopic anatomy.

Hydrophile A physical property of a material that can bond with water making it soluble in water and other polar solvents.
Adjective: *Hydrophilic.*

Hypertension A medical condition where the blood pressure is chronically elevated. While it is strictly called **arterial hypertension**, the word "hypertension" without a qualifier usually refers to arterial hypertension.
Adjective: *Hypertensive.*

Morphology The study of similarities and differences in the structure of organisms, also called comparative anatomy.

Lumen The interior of a vessel within the body.
Adjective: *Lumenal.*

Pathology A branch of medicine that studies the processes underlying disease and other forms of illness, harmful abnormality, or dysfunction.
Adjective: *Pathologic.*

Perfusion The injection or pumping of fluid through an organ or tissue.
Adjective: *Perfusive.*

Perivascular Relating to, occurring in, or being the tissues surrounding a blood vessel.

Physiology The study of how cells, organs, tissues or living organisms function under normal (healthy) conditions.
Adjective: *Physiologic, Physiological.*

Radiopaque Opaque to radiation; visible in X-ray photographs (opposed to *radiotransparent*).

Systole The contraction of chambers of the heart, driving blood out of the champer; also refers to the time period when the heart is contracting. The blood pressure is higher during this period.
Adjective: *Systolic.*

Bibliography

[1] Bruce Alberts, Dennis Bray, Julian Lewis, Martin Raff, Keith Roberts and James D. Watson (1994), *Molecular Biology of the Cell, 3rd edn.*, Garland Publishing, New York.

[2] ANSYS, Inc. (2005), *ANSYS Advanced Analysis Techniques Guide*

[3] A.M. Brown (2001), A step-by-step guide to nonlinear regression analysis of experimental data using a microsoft excel spreadsheet, *Computer Methods and Programs in Biomedicine*, 65: 191-200.

[4] T. Crawford (1959), Some observations on the pathogenesis and natual history of intracranial aneurysms, *J. Neurol. Neurosurg. Psychiat.*, 22: 259-266.

[5] P.B. Canham, H.M. Finlay, J.G. Dixon and S. Ferguson (1991), Layered collagen fabric of cerebral aneurysms quantitavely assessed by the universal stage and polarized light microscope, *Anat Rec* 231: 579-592.

[6] P.B. Canham, P. Whittaker, S.E. Barwick and M.E. Schwab (1991), Effects on circumferential order of adventitial collagen in human brain arteries, *Can J Physiol Pharmacol*, 70: 296-305.

[7] P.B. Canham, H.M. Finlay and S.Y. Tong (1996), Stereological analysis of the layered structure of human intracranial aneurysms, *J Microsc*, 183: 170-180.

[8] Han Soo Chang (2006), Simulation of the natural history of cerebral aneurysms based on data from the International Study of Unruptured Intracranial Aneurysms, *J Neurosurg*, 104: 188194.

[9] Carlos Fellipa (2005), *Qualitative Analysis of Critical Points*, http://www.colorado.edu/engineering/CAS/courses.d/, Lecture material for the Nonlinear Finite Element Methods course at the University of Boulder, Colorado

[10] H. M. Finlay, P. Whittaker and Peter B. Canham (1998), Collagen organization in the branching region of human arteries, *Stroke*, 29: 1595-1601.

[11] Tim Freestone, Robert J. Turner, Andrew Coady, Dan J. Higman, Roger M. Greenhalgh and Janet T. Powell (1995), Inflammation and matrix metalloproteinases in the enlarging abdominal aortic aneurysm, *Arterioscler. Thromb. Vasc. Biol.*, 15: 1145-1151.

[12] Y.C. Fung and J. Zhou (1997), The degree of nonlinearity and anisotropy of blood vessel elasticity, *Proc. Natl. Acad. Sci. USA* 94: 1425514260.

[13] Kozaburo Hayashi (2003), Mechanical Properties of Soft Tissues and Arterial Walls, *Biomechanics of Soft Tissues in Cardiovasular Systems*, 441: 15-64.

[14] C.M. He and M. R. Roach (1994), The composition and mechanical properties of abdominal aortic aneurysms, *J. Vasc. Surg.*,20: 6-13.

[15] M.T. Heath (2002), *Scientific Computing: An Introductory Survey*, The McGraw-Hill Companies, Inc., New York.

[16] R. Hermans (2002), *Blood Flow within Aneurysms: a Literature Study, Modeling and Numerical Simulation*, Technical Report, Technische Universiteit Eindhoven.

[17] R. Hermans (2004), *Modelling Aneurysm Mechanics towards a 3D-RA Based Clinical Application*, Final Report of the post-master program Mathematics for Industry, Technische Universiteit Eindhoven.

[18] G.A. Holzapfel (2003), Structural and Numerical Models for the (Visco)elastic Response of Arterial Walls, *Biomechanics of Soft Tissues in Cardiovasular Systems*, CISM 441: 109-184.

[19] G. A. Holzapfel, T. C. Gasser and R. W. Ogden (2000), A new constitutive framework for arterial wall mechanics and a comparative study of material models, *J. Elasticity*, 61: 1-48.

[20] J.D. Humphrey and P.B. Canham (2000), Structure, mechanical properties, and mechanics of intracranial saccular aneurysms, *Journal of Elasticity*, 61: 49-81.

[21] J.D. Humphrey and A.D. McCulloch (2003), The Cardiovascular System - Anatomy, Physiology and Cell Biology, *Biomechanics of Soft Tissues in Cardiovasular Systems*, CISM 441: 1-14.

[22] J.D. Humphrey (2002), *Cardiovascular Solid Mechanics*, Springer, New York.

[23] I. Machyshyn (2005), *Development of Cerebral Aneurysms, a Prediction Model*, Technische Universiteit Eindhoven.

[24] I. Machyshyn (2006), unpublished report, Technische Universiteit Eindhoven.

[25] The International Study Of Unruptured Intracranial Aneurysms Investigators (1998), Unruptured Intracranial Aneurysms Risk of Rupture And Risks Of Surgical Intervention, *The New England Journal of Medicine*, 339(24): 1725-1733

[26] C.H.G.A. van Oijen (2003), *Mechanics and design of fiber-reinforced vascular prostheses*, PhD-thesis, Technische Universiteit Eindhoven.

[27] R.W. Ogden (2003), Nonlinear Elasticity, Anisotropy, Material Stability and Residual Stresses in Soft Tissue, *Biomechanics of Soft Tissues in Cardiovasular Systems*, CISM 441: 65-108.

[28] Ortega-Azurdy, E. Vinken and E. Chtcherbakov (2001), *Simulating Blood Flow within Aneurysms*, Technical Report, Technische Universiteit Eindhoven.

[29] J.T. Powell, A.R. Brady, S.G. Thompson, F. Gerald, R. Fowkes and R.M. Greenhalgh (2004), Abdominal Aortic Aneurysm Expansion: Risk Factors and Time Intervals for Surveillance, *Circulation, Journal of the American Heart Association*, 110: 16-21.

[30] Sander de Putter (2002), *Simulating Blood Flow in Cerebra Saccular Aneurysms*, Technical Report, Technische Universiteit Eindhoven.

[31] Sander de Putter (2006), *On Patient-Specific Wall Stress Analysis in Abdominal Aortic Aneurysms*, PhD Thesis, Technische Universiteit Eindhoven.

[32] Raoul van Loon (2005), *A 3D method for modelling the fluid-structure interaction of heart valves*, PhD-thesis, Technische Universiteit Eindhoven.

[33] M.R. Roach and A.C. Burton (1957), The Reason for the Shape of the Distensibility Curves of Arteries, *Canad. J. Biochem. Physiol.*, 14: 681-690.

[34] S. Scott, G. Ferguson and M. R. Roach (1972), Comparison of the elastic properties of human intracranial arteries and aneurysms, *Canadian Journal of Physiology and*

Pharmacology, 50: 328-332.

[35] L.N. Sekhar and R.C. Heros (1981), Origin, growth, and rupture of saccular aneurysms: A review, *Neurosurger.*, 8: 248-260.

[36] W.E. Stehbens (1972), *Pathology of Cerebral Blod Vessels*, C.V.Mosby Co.,St. Louis.

[37] H.J. Steiger, R. Aaslid, S. Keller and H.J. Reulen (1986), Strength, elasticity and viscoelastic properties of cerebral aneurysms, *Heart Vessels* 5: 41-46.

[38] H.J. Steiger (1990), Pathophysiology of develeopment and rupture of cerebral aneurysms, *Acta Neurochir Suppl*, 48: 1-57

[39] W.E. Stehbens (1981), *Structure and Function of the Circualation*, Plenum Press,New York.

[40] L.A. Taber (2004), *Nonlinear Theory of Elasticity: Applications in Biomechanics*, World Scientific Publishing, Singapore.

[41] M. Toth, G.L. Nadsay and I. Nyary (1998), Sterically inhomogenous viscoelastic behavior of human saccular aneurysms, *J Vasc Res* 35: 345-355.

[42] K.A. Vardulaki (1998), Growth rates and risk of rupture of abdominal aortic aneurysms, *British Journal of Surgery*, 85: 1674-1680.

[43] R. P. Vito and S. A. Dixon (2003), Blood Vessel Constitutive Models-1995-2002, *Annu. Rev. Biomed. Eng.*, 5: 413-39.

[44] P. N. Watton, N. A. Hill and M. Heil (2004), A Mathematical Model for the Growth of the Abdominal Aortic Aneurysm, *Biomechan. Model Mechanobiol.*, 3: 98-113.

[45] David O. Wiebers, David G. Piepgras, Fredric B. Meyer, David F. Kallmes, Irene Meissner, John L. D. Atkinson, Michael J. Link and Robert D. Brown (2004), Pathogenesis, Natural History, and Treatment of Unruptured Intracranial Aneurysms, *Mayo Clin Proc.*, 79(12): 1572-1583.

[46] R. Wulandana (2003), *A Nonlinear and Inelastic Constitutive Equation for Human Cerebral Arterial and Aneurysm Walls*, PhD Thesis, University of Pittsburgh.

[47] R. Wulandana and A.M. Robertson (2005), An inelastic multi-mechanism constitutive equation for cerebral arterial tissue, *Biomech. Model. Mechanbiol.*, 4: 235-248

[48] ADAM Inc. (2004), *Illustrated Health Encyclopedia.*